Effect of microstructural changes in copper during the electrochemical conversion of CO_2 to hydrocarbons

by

Manas Tripathi

to obtain the degree of Master of Science
at the Delft University of Technology,
to be defended publicly on Monday, January 31st, 2022 at 1:30 PM.

T̃U Delft

Acknowledgement

Abstract

Excess CO_2 in the atmosphere has been a troublesome problem for humanity for the last few decades now. Academics, governments and industries are working together to tackle this problem to avert a global warming disaster. Research on many technologies is in progress to tackle global warming, with carbon capture being one exciting solution. The process of converting this captured carbon dioxide into something useful has gained momentum in research and academia since the 1980s. Out of the many catalysts worked upon to convert the excess CO_2, copper has gained particular limelight because of its exceptional ability to reduce CO_2 into valuable products such as methane, formic acid, ethane, methanol, to name a few.

The literature study associated with this project identified a knowledge gap between the present literature and the understanding of the microstructural impact on CO_2 reduction. The thesis project studied the effect of microstructure changes on the electrochemical properties of copper and its subsequent impact on CO_2 reduction capabilities to bridge the knowledge gap. Sigma- Aldrich copper of purity 99.999% was selected for this thesis work, and four samples: as received, electropolished, and two annealed samples were prepared. Optical microscopy and XRD measurements were used for microstructural characterization, and it was found that annealed samples lost their rolling direction, and their grain sizes increased. Evaluation of electrochemical behaviour through CV and EIS results indicated the formation of a complex triple passivation layer on the copper samples. Through evaluation of EIS results, we found that the electropolished sample had the most robust Cu_2O layer.

From the CO_2 reduction experiments, it was found that as-received samples had the highest F.E. for CO_2 reduction, and non-electropolished samples had a high F.E. for hydrogen production. The performance of the electropolished sample stood out with a high F.E. of 46.3% for hydrocarbon production. The reason for this behaviour was, possibly, the presence of robust Cu_2O layers that prevented the sample from catalyst poisoning and helped form a strong bond with CO* (carbon monoxide free radical).

The thesis opened up avenues for further research. By further investigation of factors like grain orientation and grain boundary density combined with XPS results, the understanding of the complex nature of passive layers formed on copper during CO_2 reduction can be improved, which will ultimately help develop better catalysts.

List of acronyms and chemical formulae

Al_2O_3	Aluminium Oxide
CE	Counter Electrode
Cu	Copper
CO_2	Carbon Dioxide
CO	Carbon Monoxide
CH_4	Methane
$COOH*$	Carboxyl intermediate
$CHO*$	aldehyde intermediate
CHE	Computational Hydrogen Electrode
$COH*$	alcohol intermediate
$*CO$	Carboxyl intermediate
CO_2RR	Carbon dioxide Reduction Reaction
C_2H_4	Ethylene
Cu_2O	Cuprous Oxide
CuO	Cupric Oxide
CV	Cyclic Voltammetry
CZA	Copper Zinc Aluminium
DFT	Density Functional Theory
$FeCl_3$	Ferric Chloride
$HCOO^-$	Formate anions
HCl	Hydro Chloric Acid
H_2O	Hydrogen oxide
$EBSD$	Electron Backscatter Diffraction
$ECSA$	Electrochemical Surface Area
EIS	Electrochemical impedance spectroscopy
$F.E.$	Faradic Efficiency
GC	Gas Chromatography
H_2	Hydrogen
$KHCO_3$	Potassium Bicarbonate
$N(CH_3)_3$	Trimethylamine
NP	Nano Particles
RE	Reference Electrode
RHE	Reference Hydrogen Electrode
R_ct	Charge transfer resistance
$SECM$	Scanning Electrochemistry Microscopy
SEM	Scanning Electron Microscopy
SHE	Standard Hydrogen Electrode
STY	Space Time Yield
STM	Scanning Tunneling Microscope
WE	Working Electrode
XPS	X-ray Photoelectron Spectroscopy
XRD	X-ray Diffraction
ZnO	Zinc Oxide

Contents

List of Figures

List of Tables

Introduction

1.1. Why tackling CO_2 is a necessity?

Over the last century, global greenhouse emissions have increased manifolds, leading to severe consequences such as global increase of temperature, increased forest fires, air pollution and many other global-scale catastrophes.[9]

The major greenhouse gases are Carbon Dioxide (CO_2), Methane (CH_4), Nitrous oxide (NO_2) and other fluorinated gases (example: chlorofluorocarbons, hydro-chlorofluorocarbons, and halons). According to data available on Climate Watch, the World Resources Institute [1], CO_2 is the most significant contributor to greenhouse emissions. It can be observed from Figure 1.2 that CO_2 contributes around three quarters to the global greenhouse emissions.

Global greenhouse gas emissions by gas

Greenhouse gas emissions are converted to carbon dioxide-equivalents (CO_2eq) by multiplying each gas by its 100-year 'global warming potential' value: the amount of warming one tonne of the gas would create relative to one tonne of CO_2 over a 100-year timescale. This breakdown is shown for 2016.

Our World in Data

F-gases (HFCs, CFCs, SF$_6$) 2.1%

Carbon dioxide (CO_2) 74.4%

Methane (CH_4) 17.3%

Nitrous oxide (N_2O) 6.2%
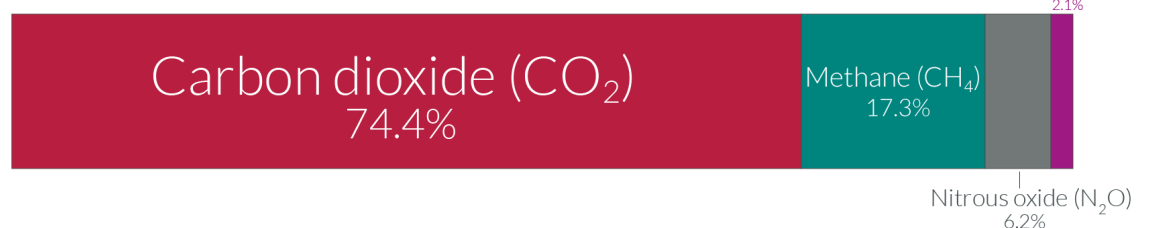
OurWorldInData.org – Research and data to make progress against the world's largest problems.
Source: Climate Watch, the World Resources Institute (2020).
Licensed under CC-BY by the author Hannah Ritchie.

Figure 1.1: Share of CO_2 in total Greenhouse Emissions.(2016) Source: Climate Watch, the World Resources Institute

This is a matter of great concern as CO_2 emissions have constantly increased over the last century and now have reached unsustainable levels. Even though the recent shift to renewable energy sources like wind energy, solar energy etc. have led to downward trends in CO_2 emissions, the current level of CO_2 in the atmosphere is responsible for global warming, air pollution and other indirect effects like food shortage, water shortage, etc. [17]

Several methods to reduce the level of CO_2 from the atmosphere has been undertaken. Methods like afforestation and usage of renewable energies are some of the most researched and worked out procedures to systematically reduce CO_2 emissions in the world. However, they are not effective in converting excessive carbon dioxide into a usable product. Electrochemical CO_2 reduction reactions(CO_2RR) have successfully demonstrated that carbon dioxide can be converted to hydrocarbons such as methane, ethylene, and ethanol.[14, 22] The challenge lies in developing commercially viable processes. The catalysts used for CO_2 reduction deactivate in 5-150 hours which is not suitable for industrial use. Moreover, the F.E. of products obtained is not optimum to scale to industrial production. Faradic efficiency(F.E.) is the ratio of charge used to form a particular product in an electroreduction experiment for the total charge supplied. Furthermore, the electrolytic cell design used for CO_2RR is complex due to problems like leakage and mixing of gases, making it challenging for industrial usage adaptation. Due to the complex developmental process of production of hydrocarbons, it is still easier to use conventional methods like drilling, fracking, and gas injection from the earth's surface as they are well researched.[10]

CO_2 electroreduction has been studied on several metals as catalyst of the reaction. They can be categorized as a function of the main product generated.

- The first category consisting of metals like gold, silver, zinc, palladium, gallium, nickel and platinum primarily produce carbon monoxide as their reaction product. [14]

- The second category consisting of metals like lead, mercury, indium, strontium, cadmium, thallium primarily produce formates or formic acid as their main products. [14] [18]
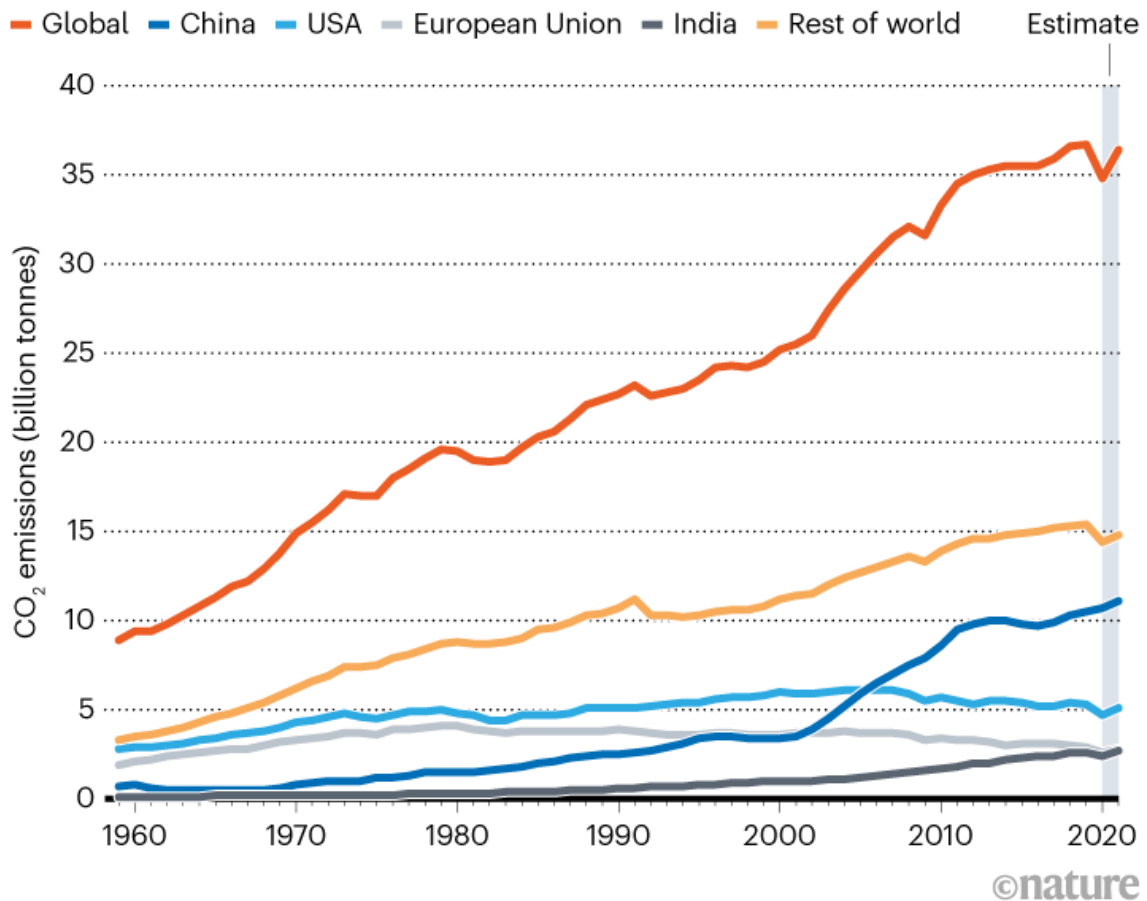
Figure 1.2: Global increase in CO_2 Emissions. Source:Global Carbon Project.

- The third category is copper, which has been studied in great detail because of its exceptional ability to produce C_2 hydrocarbons along with producing carbon monoxide and other products.[14, 22] Due to this versatility, it has been studied further in this study and the reason for the immense interest in the material will be further discussed in the next section.

1.2. Copper: an interesting material choice

The main reason for selecting and studying copper is its versatility to produce critical chemical compounds like C_2H_4, CH_4 and CH_3OH. A study done by *Kuhl et al.* [22] provided evidence that as far as 16 products can be obtained with CO_2 electroreduction on copper. The main products are hydrogen, methane, formate, carbon monoxide and ethylene.

Copper can be used as a potential catalyst to reduce CO_2 at less energy expense. Numerous works have been done to utilize renewable energy sources to drive this electroreduction. CO_2 Electroreduction on copper is done by using copper as the working electrode. As the reaction product yield at the laboratory level is insufficient, CO_2 electroreduction is not established at an industrial scale. Another reason is the low catalyst deactivation time making it unfeasible to scale CO_2 electroreduction to an industrial scale. Due to these reasons, lab-scale experiments are prevalent.

Copper has a high F.E. for various hydrocarbons. *Hori et al.*[14] reported a faradic efficiency of 25.5% for C_2H_4 at -1.44 V vs RHE at room temperatures for copper electrode. Other electrode metals like Pd, Cd and Ni were incapable of producing C_2H_4 and primarily formed CO and formates.

Another interesting feature of copper is its ability to reduce CO_2 at intermediate overpotentials. Overpotential is defined as, the additional potential required to drive a chemical reaction at a specific rate. It is desired that this additional potential is not high to facilitate the reaction. Copper can form CO at -1.44 V vs RHE and methane at -1.02 V vs RHE overpotentials when compared to metals like Au which catalyzes CO_2 into CO at -1.14 V vs RHE and Pb which catalyzes CO_2 into formate ions at -1.63V vs RHE.[14]

1.3. Report outline

The report starts with a brief introduction (**Chapter 1:Introduction**) to the problem of global warming and how copper can play a crucial role to solve the problem.

Chapter 2:Theory, discusses the mechanism of CO_2 reduction in brief and elaborates on the various factors which affect the CO_2 reduction properties of copper. The chapter concludes with a small discussion of how varying grain sizes would impact the CO_2 reduction properties of copper.

Chapter 3:Experimental methods describes the experimental techniques utilised for the characterisation of copper samples and to study their electrochemical and CO_2 reduction properties.

Chapter 4:Results and discussion analyses the experimental results obtained during this thesis work and critically analyse all the results obtained.

Chapter 5:Conclusions provides a brief summary of most important findings from this thesis study.

Chapter 6:Future recommendations provides suggestions for further continuation of this study and discuss the specific areas where improvements can be made to make this study more relevant.

<div align="right">

2

</div>

<div align="right">

Theory

</div>

2.1. Factors affecting CO_2 reduction

2.1.1. Grain Boundaries and Grain size

Huang et al.[16] worked on copper mesh taking inspiration from traditional grain refinement methods like normalizing and quenching, studying the impact of grain refinement at nano-scale. They used multiple facile redox reactions to reduce the size of the copper mesh continuously. The size of copper grains varied from 23.1nm to 13.7nm. The researchers observed that copper mesh with the smallest grain size had more catalytic activity than other samples.

The sample with the smallest grain size of 13.7nm had the highest current density and highest Faradic Efficiency (78%). Thus, the grain refinement not only helped in increased catalytic activity but also helped in increased selectivity of CO_2 reduction towards CO production. The reason for increased selectivity was hypothesized as the formation of porous structures on copper mesh, which increased catalytic surface area. Electrochemical Active Surface Areas(ECSA) of the smallest grain size had the highest active surface area of 78.9 cm^2 compared to other samples with larger grain sizes. Smaller grain sizes provided more surface area(larger number of grain boundaries) for forming porous structures on copper's surface, which acted as an active catalysis site and increased the ECSA. The calculation of ECSA supported the hypothesis that increased surface area due to decreased grain size led to a surge in active catalytic sites, increasing selectivity and high F.E.

Electrochemical Impedance Spectroscopy (EIS) measurements also showed that charge transfer resistance, R_ct of the smallest grain size copper sample was the lowest. Having low R_ct helped in enhancing charge transfer capability. *Huang et al.*[16] also discussed the presence of oxides in the initially prepared sample, which lost the oxide component during successive reduction reactions. The authors concluded the impact of the presence of oxides to be negligible as XRD and XPS measurements after the reduction reactions found a trace amount of oxides and did not play a role during the CO_2 reduction experiments.

Yang et al.[55] developed high-density grain boundaries on copper oxide nanoparticles along with producing micro-strains in the nano-structures.For this study, firstly CuO samples were synthesised by putting copper powder in porcelain boats and heating it to anneal the sample at 500 °C. Cu Fast cooled (Cu-FC) was synthesized by quenching it in liquid nitrogen, Cu Medium cooled (Cu-MC) quenching in water for 20 minutes and Cu Slow cooled (Cu-SC) letting it cool in the air till it reached room temperature. A comparison was made regarding the effect of different cooling rates. The average sizes of the CuO-SC, CuO-MC and CuO-FC nanoparticles were found out to be 40.5, 35.8 and 35.3 nm, respectively. Small sizes of the fast cooled sample were attributed to Ostwald Ripening processes where fast cooling led to the limited growth of the grain sizes. SEM and TEM analysis of the samples revealed that fast cooled sample had a higher grain boundary density and SXRD results further consolidated the presence of higher micro-strains as well. Electroreduction experiments conducted on these samples showed that fast cooled sample had the highest faradic efficiency of 35.7% for ethanol production. Another interesting observation was that the C_2 to C_1 product ratio was highest for fast cooled sample and it can be an interesting observation for modifying copper sample at a micro-scale.

The study concluded by acknowledging the C_2 product selectivity and high faradic efficiency of fast cooled sample to the high density of grain boundaries and higher micro-strains induced in the sample, which acted as an active site for catalysis. This study showed that annealing and quenching could make substantial changes in the nanostructure of copper, and it can serve as a precedent for further experimental investigation. *Yang et al.*[55] also considered a variation of the electrochemical surface area and found it as 1.1, 1.93 and 1.74 for CuO-SC, CuO-MC and CuO-FC, respectively. As the differences were not staggering, the authors did not attribute the better performance of the fast cooled sample to the excess surface area. Thus, *Yang et al.*[55] found that grain boundary density and varying micro-strains were the leading reasons instead of size for the change in F.E. of hydrocarbon production.

Study done by *Huang et al.* and *Yang et al.* offered contradictory evidence regarding the oxides present on copper samples. The presence of oxides was deemed insignificant by *Huang et al.*[16] as XRD results showed that they were present in a minimal quantity. *Yang et al.*[55] on the other hand, discussed CO_2 reduction on copper oxides and thus does not present a comparison with regards to pure copper samples. The oxides presented a different catalytic surface than a pure copper sample, and their reaction mechanisms differed from a pure copper surface. It impacted the product output of CO_2 reduction experiments in studies done by *Yang et al.*[55]. As bulk copper is expected to form oxides due to unavoidable exposure to oxygen, studying their impact on bulk copper samples will be necessary.

Another difference between findings of *Huang et al.* and *Yang et al.* was the difference in ECSA in the copper samples. *Huang et al.* found that copper samples with small grain size had increased ECSA, and that is why they had higher catalytic activity. *Yang et al.* did not find a significant difference between ECSA for the prepared copper samples of varying grain sizes. As

Huang et al. studied copper mesh, and *Yang et al.* worked with copper oxide nanoparticles, varying composition and materials react differently as catalyst materials. Thus a direct comparison between them does not yield conclusive results.

Study on copper nanowires performed by *Zhang et al.*[54] discussed CO$_2$ electroreduction on Cu nanowires, prepared by electrochemical deposition. It was found that reducing grain size of the Cu nanowires helped in increasing catalytic activity, methanol selectivity and methanol space time yield (STY). The researchers found that smaller grain size samples were less susceptible to the effect of sintering on the sample. Sintering at a nanoscale was defined as the merging of Cu nano-particles during the elecroreduction process. XRD analysis combined with SEM analysis confirmed that the Cu nano-particles grew in size after undergoing an electroreduction of 130 hours. A possible explanation of the decrease in performance of samples with bigger grain size was given as the gas channel blockage, which happened at the initial phases of the CO$_2$ hydrogenation step.

(a) Before   (b) After
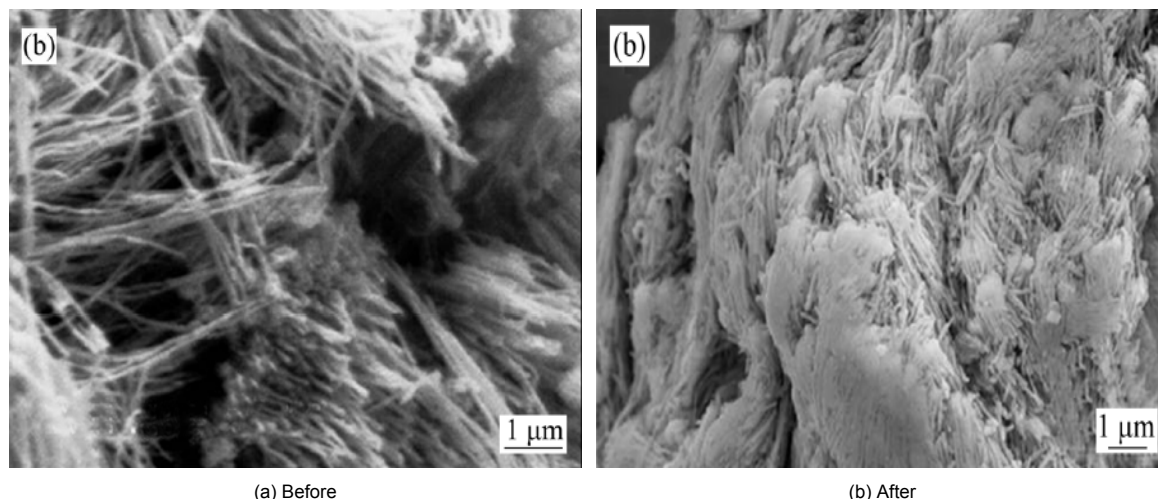
Figure 2.1: SEM image comparison of the Cu Nanowire fibers. [54]

Bigger grain sizes lead to an increase in this phenomenon and thus reduce the overall performance of Cu nanowires. The continuous migration of Cu atoms and sintering on the nanowire surface is why this blockage happened. The study suggested that the best way to tackle the issue was to use Cu nanowires with refined grain sizes as the Cu sample with the smallest grain size of 26 nm showed the best catalytic activity and can catalyse the reduction of CO$_2$ till 130 h. The grain size measured after electroreduction for 130 h with this sample was found to be 67 nm, thus confirming the agglomeration and clustering of Cu particles on the nanowires. Though this study gave a brief idea on how reducing the grain sizes of nanowires can be done and how it can be beneficial, the lack of numerical results made this research paper a weak reference. The study gave strong conclusions but lacked statistics to back them up. However, this study again supported the idea that reducing grain size might be beneficial for improving the catalytic activity of the Cu sample. The paper does not discuss the variation in ECSA of the samples and only talks about the variation in grain sizes.

Nano-structures are different from bulk materials as nano-structures have higher surface area over volume ratio and have quantum effects emergence at such a small size. Thus, a direct co-relation can not be made in properties of nanostructures and bulk samples. Using the works discussed in this section as a premise, similar work will be attempted for copper at a micro-scale and it will be interesting to observe how the variation in grain size, grain boundary density, ECSA will impact the electrochemical properties of bulk copper and its subsequent CO$_2$ reduction capabilities.

2.1.2. Grain Orientation

The following section discusses the impact of different crystal orientations of copper catalysts on CO$_2$ electroreduction. Studies found that grain orientation plays a major role in electroreduction product selectivity.[12, 33]

CO$_2$ electroreduction on single crystal Cu(s)-[n(111)X/(111)] and Cu(s)-[n(110)X/(100)] electrodes by *Hori et al.*[15] found a unique product of CH$_3$COOH. The researchers created spherical single crystal copper using copper stick lead from 99.9% pure copper using a graphite crucible.

The researchers concluded that the variations in products obtained by electrochemical reaction were due to surface reconstruction of (110) surface. Introduction of steps of (100) and surface reconstruction of (110) to (430) was speculated. A highly varying product distribution was observed for different crystal orientations. (111) facet of Copper favoured methane(CH$_4$) formation and (110) facet supported the formation of products like CH$_3$COOH and other C$_2$ products. This observation was later backed up by the DFT study done by *Luo et al.*[30] which demonstrated that (111) facet favours the COH* intermediate pathway and (100) favoured the CHO* intermediate pathway which resulted in selective product formation.

Keerthiga et al.[21] studied pure Cu electrode and focused on (110) and (220) electrodeposited copper facets. Samples of pure Cu were subjected to chronoamperometric deposition at different concentrations of CuSO$_4$ bath. They prepared two samples: one in a low concentration which showed a deposit thickness of 1 μm and the sample prepared in higher concentration had a deposition thickness of 5 μm. X-Ray diffraction technique using Halls method showed that texture coefficients of pure Cu showed orientation towards (111) facet and electrodeposited samples showed orientation towards (220) facet.

Electroreduction experiments were conducted in a KCl solution over a period of three hours. Maximum Faradic Efficiency (F.E.) of 28% for methane was observed on pure Cu electrode compared to 26% for sample prepared in low concentration and 20% for electrode prepared in high concentration respectively. F.E. of 43% was observed for the formation of ethane on Cu/Cu-L, compared to 10% on pure Cu electrode and 28% on Cu/Cu-H electrode. The study cited *Hori et al.*[15] groups observation that

(n-110) facets favour formation of C_2 products. It is for this reason Cu/Cu-L favoured the formation of ethane and methane by (111) facet as steps of (111) surface formed on it. These steps and roughened surfaces acted as points where $\cdot CH_2$ steps formed and were able to dimerize further and protonate to form ethane.

Kas et al.[20] focused on Cu_2O thin films with different grain orientations which were deposited on commercially available copper plates. The crystalline morphology of the films was controlled through the amount of charge passed through the electrode. Films with varying deposition thickness were obtained. The crystalline phase of the films was found out with the use of X-Ray Diffraction. The XRD results indicated that films with [100], [110] and [111] directions were obtained. Electrochemical reduction of CO_2 on the experimentally obtained thin films gave unique results. Ethylene was found to be the major product, irrespective of the facets undergoing experiment over a potential range of -0.2 V to -1.2 V *vs* RHE. Online Electrochemical Mass Spectrometry showed that CO_2 reduction did not occur on Cu_2O surface but rather on in-situ produced metallic copper nano-particles. The high selectivity of ethylene was distinctively different from polycrystalline and oxide derived nano-particles for copper. Previous studies done on polycrystalline copper suggested that methane is the major product formed[11] and ethane was found out to be the major product on oxide derived copper nanoparticles [27].

The CO_2 reduction carried out on increasing thickness of [110] oriented Cu_2O films resulted in product variations with the change of thickness. This suggested that product selectivity for thin films is a function of film thickness rather than being strongly dependent on the preferential orientation of the films. With increasing potential (range of -0.2 V to -1.2 V *vs* RHE) it was found that products change from methane to ethane (more inclined to C_2 products) at higher potential CO (carbon monoxide) being constant and production of ethylene continuously decreasing. For the observed results the researchers hypothesized that increasing film thickness, increased surface roughness, which in turn led to higher surface area and differences in local pH values. This gave the *CO intermediate more stability for reduction to take place and thus C_2 products are formed. It was also concluded that for Cu_2O thin films product selectivity is majorly affected by film layer thickness related pH changes and not by facet orientation.

Cu_2O has been discussed here as the first oxidation step of copper is always into cuprous oxide(Cu_2O).[8, 36] Electrochemically, Cu_2O and Cu react in a similar fashion as pure Cu always forms Cu_2O in the presence of oxygen, and the way Cu_2O reacts to CO_2 can act as a precedent for pure copper samples.

Martinez-Lombardia et al. [31] studied the consequences of different crystallographic orientations on the electrochemical activity of pure copper and found that different grain boundary orientations had different chemical activity when put in the same conditions. The researchers firstly modified the crystal structure using rolling reduction and then polished the samples. After polishing the sample, the samples were passivated by polarizing it. Using EBSD, two regions rich in <001>//ND and <111>//ND orientation adjacent to the passive layer were selected and SECM was conducted. The researchers established that the passive layer adjacent to <111>//ND had a higher thickness of the Cu_2O layer and was more protective. In the active state, even though the highest current density was obtained for <111>//ND oriented copper grain, it was argued based on surface energy and energy work function that <111>//ND oriented grains should show the highest corrosion resistance. It was also concluded that different grain boundaries had different electrochemical and corrosion resistance. Thus, this study focused on how the reactivity of certain grain orientation is affected by neighbouring grain orientations with varying orientations.

On the basis of study done by *Keerthiga et al.*[21] and *Hori et al.*[15] it can be concluded that product selectivity of the electrochemical reduction of CO_2 depends on facets of Cu electrode for nano-crystalline and single-crystal materials. According to *Kas et al.*[20] the primary factor affecting the product selectivity in thin films is the film thickness and the grain orientation of grain boundaries adjacent to the thin films. The work done by *Martinez-Lombardia et al.* [31] gives an insight into this behaviour by observing that different Cu grains had different electrochemical properties in terms of current density and passivity due to surface energy bearings. For this thesis work, poly-crystalline copper electrodes will be considered, based on the studies reviewed in this section it is hypothesized that preferential orientation of copper electrodes might dominate the product selectivity.

Factors like higher grain boundary density, as established previously during discussion of *Yang et al.*[55] also influence the product selectivity. The presence of higher grain boundary density along with high micro-strain led to the formation of C_2 products easily as they provided more energetically favourable active catalytic surfaces for the formation of *CHO intermediate, which provided a pathway for C_2 products. As *Yang et al.* performed the study on copper oxide, it is important to note that a relation is drawn between pure copper sample and copper oxide samples. As during CO_2 reduction, pure copper always forms copper oxide,it would be useful to characterize the presence of copper oxide during experimentation with bulk copper sample.

2.1.3. Surface Preparation

It is important to discuss the methods through which the samples can be prepared because they eventually affect the efficiency and product selectivity of CO_2 reduction.

Tang et al.[47] studied CO_2 electroreduction on three different samples to study the impact of various methods of sample preparation. First sample was a copper electrode prepared by manually polishing the sample. Second sample was a copper electrode prepared by depositing Cu nanoparticles on the copper surface which resulted in nanoparticles ranging from 50-100 nms. The third sample was a copper electrode sputtered with Argon ions.

Cyclic voltammetry carried out on all three samples under Cu_2O and N_2 environment found that current density was higher on the roughened surfaces(Sample B and Sample C) than the electropolished Sample A. Out of the three samples, Sample B had the roughest surface. F.E. of reaction products was calculated and it was found that Sample B with nanoparticles had the highest F.E. for CO and C_2H_4. Figure 2.3 shows the F.E. of various products obtained via CO_2 electroreduction. it was observed that Sample A showed a high selectivity to hydrogen which was not the intended product. It was also observed that except CH_4 and C_2H_6, the nanoparticle sample B, showed the best results. To further elaborate on the reason how surface morphology affected the product distribution and efficiency of the samples, the authors performed a DFT (Density Functional Theory) study. The DFT results suggested that the presence of stepped (211) sites on Sample B and Sample C showed higher activities than terrace (111) and (100) as the free energy of adsorbed hydrogen intermediate (H*) was in close proximity to the initial and final states of the reaction. Study done by other researchers also corroborated the hypothesis made by the present work. [37, 44] Thus, it could be concluded that a surface which provided a rougher surface with more active catalytic sites would yield a higher F.E. for the hydrocarbons.

A study done by *Lopes et al.*[29] did a similar analysis on copper catalyst to investigate the effect of annealing on poly-crystalline Cu samples. The researchers took three samples of 99.9% Goodfellow samples. From the SEM images(Figure 2.4) it was observed that the sample annealed in H_2 had a slightly rough surface, and sample annealed in air had many tube-like

(a) Sample prepared by electropolishing

(b) Sample prepared by depositing Cu nanoparticles
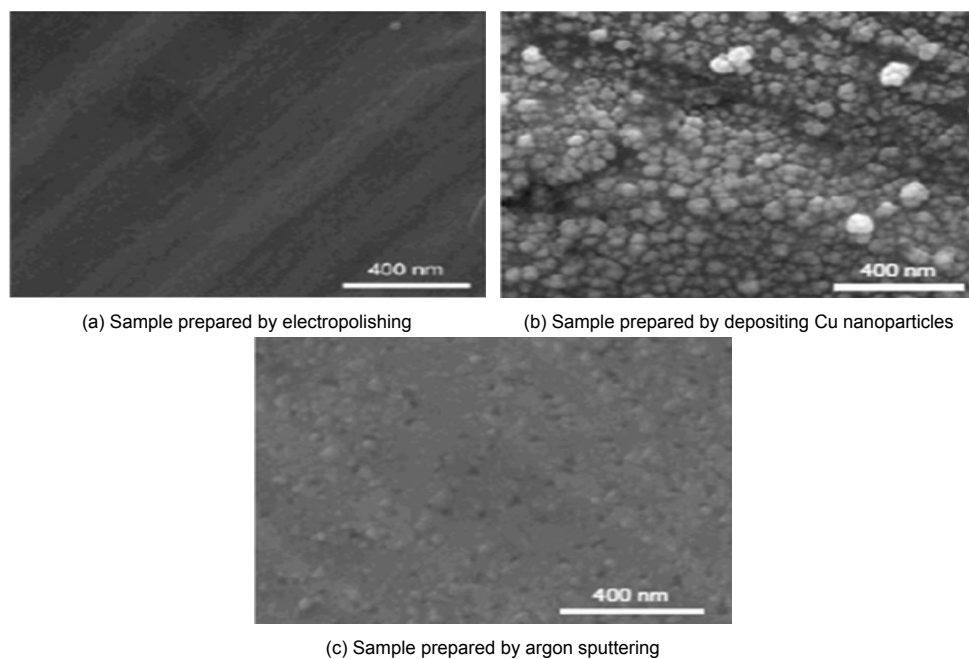

(c) Sample prepared by argon sputtering

Figure 2.2: SEM images of prepared samples. [47]

structures forming on the surface. The electropolished sample was relatively smooth. XPS and XRD analysis of these samples was performed to analyze the chemical composition and Cu oxidation states on the sample. It was realized that the annealed samples showed the presence of Cu_2O and CuO layers on their surface. The electropolished sample had a relatively smaller peak on XPS spectra for the CuO layer. It was probably because of the oxidation due to little exposure of copper samples to air after electropolishing. Relating the XPS spectra to a previous study[38], the authors established that sample annealed in air had a metallic Cu phase with Cu_2O as the interlayer and CuO phase as the upper layer. The sample annealed in hydrogen also showed minor traces of Cu_2O and CuO in the XPS spectra. The sample annealed in air was found to have an oxide layer in order of several micrometer thicknesses. *Lopes et al.*[29] did not quantify the thickness of oxide layer on different samples but concluded that XRD measurements are not very reliable when it comes to detecting the presence of oxygen on the copper surface, if oxygen was present in a trace quantity.

Cyclic voltammetry (CV) was conducted in 0.1 M of $KHCO_3$ saturated with CO_2. Comparison of CV results showed that electropolished and hydrogen annealed copper sample had similar behaviour in terms of reduction onset potential and cathodic currents. On the other hand, air-annealed copper sample showed lower reduction onset potential and almost four times higher cathode current than Cu-p and Cu-H_2. The author attributed this increase of the cathodic currents on air-annealed copper sample to a high roughness factor compared to other two samples. To further quantify the CO_2 electroreduction performance of these samples, chronoamperometry experiment at 0.65 V for 16h was conducted on the three samples. The only liquid product obtained was formate anions($HCOO^-$). The air-annealed copper sample showed a F.E. of approx. 30%, while the Cu-H_2 and Cu-p showed a F.E. of 10% and 16% respectively. Authors speculated that this result showed that surface roughness is not the only factor that increases the F.E. Presence of oxidation layers of Cu_2O and CuO must have played a role too. Another interesting result mentioned in this study was that F.E. of reaction products could be improved by optimizing the electrolyte solution. Cu-Air showed a F.E. of 46% for formate anions($HCOO^-$) at similar conditions with a 0.5M concentration of $KHCO_3$.

Finally, the researchers discovered that the air-annealed sample performed excellently throughout 64h when run into a four-cycle of 64h. It was one of the highest deactivation times ever demonstrated by a polycrystalline Cu. The researchers hypothesized that this high deactivation time was due to the stabilization of Cu^+ ions, which led to the formation of roughened surfaces with low coordination sites, which were due to annealing the sample in air. The oxygen atoms were able to bind to these low coordination sites better, which led to the formation of very stable layers of Cu_2O and CuO on the surface, providing a stable higher surface area for CO_2 electroreduction.

Thus, from this section, we can conclude that, the performance of Cu as a catalyst depends on a variety of factors. It is not straightforward and one major problem with all the research done here is that there is no fixed guideline according to which researchers conducted these experiments. *Tang et al.*[47] in their study found that rough copper surface which had a presence of oxide layers on its surface led to higher F.E. efficiency for hydrocarbon production. *Lopes et al.*[29] in their work found that when copper samples had the presence of oxide layers on the surface the deactivation time of copper electrode and F.E. for formation of formate ions increased. From both these studies it can be hypothesized that better performance of copper electrodes can be attributed to the morphological changes it goes through when oxide layers are formed on its surface. Cu_2O and CuO layers increased the ECSA and also formed a stable protective layer on the copper electrode surface which increased its protection against catalyst poisoning. Both *Lopes et al.*[29] and *Tang et al.*[47] found that electropolished copper electrode had the least surface roughness and comparatively less F.E. for hydrocarbons. Absence of thick oxide layers on the surface resulted in lower ECSA and thus reduced the F.E. of copper sample.

Researchers working with catalysis background prefer to work with electropolished sample as it ensures less impurity on the surface of the catalyst and helps in understanding the unaltered behaviour of copper samples during CO_2 reduction. Several researchers are working on studying the impact of oxide layers and presence of certain impurities on copper surface but due to
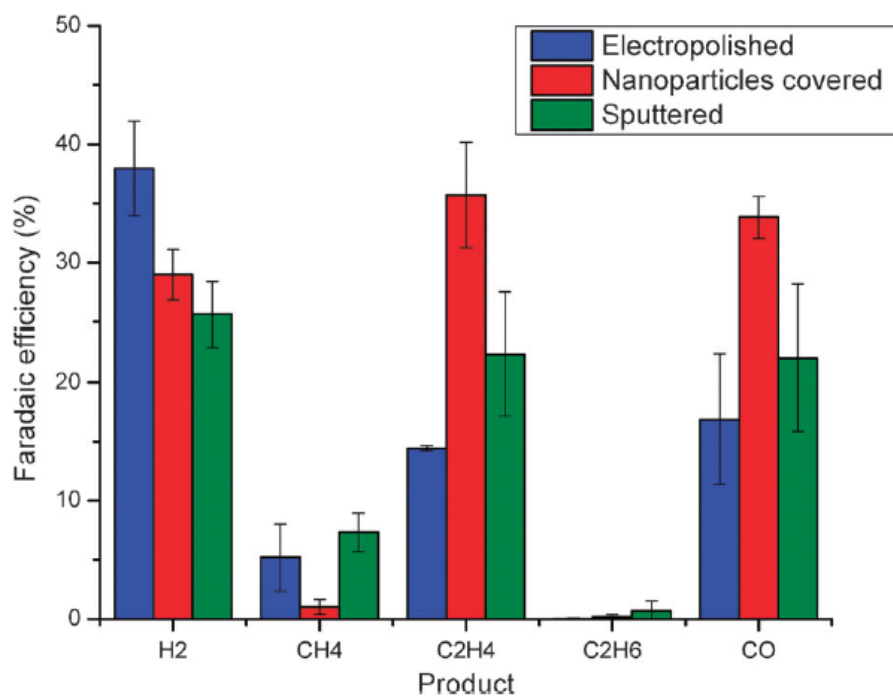
Figure 2.3: Faradic efficiency comparison of CO_2 electroreduction on the 3 samples.

(a) Sample prepared through electropolishing

(b) Sample annealed in H_2

(c) Sample annealed in synthetic air
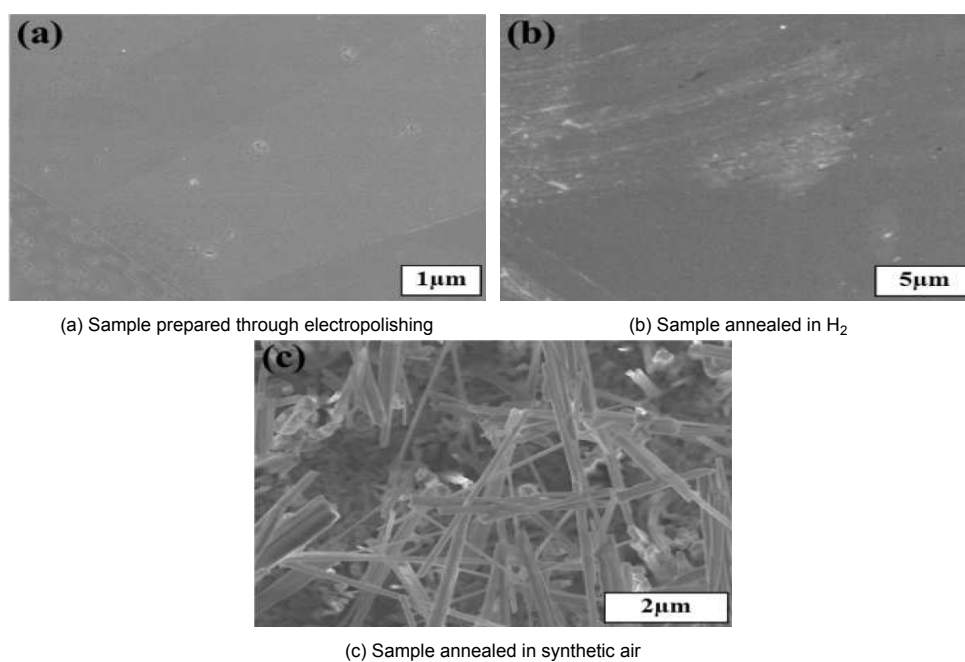
Figure 2.4: SEM images of prepared samples. [29]

lack of fixed guidelines along which all the research is conducted, a very reliable conclusion is yet to be drawn. Thus, this thesis work would aim to bridge the gap by studying the difference between these approaches of sample preparation as it certainly plays a part in CO_2 reduction.

2.1.4. The problem of catalyst deactivation

Catalyst deactivation can be defined as the loss of catalytic activity over time. It is a major problem because replacing catalyst in industry alone causes a loss of many billion dollars [52].

Like any other catalyst, copper also faces the problem of deactivation through several mechanisms during CO_2 electrore-

duction. *De Wulf et al.*[6] reported that total Faradic Efficiency (F.E.) of copper electrode reached 65% for CH_4 and C_2H_4 over 20 minutes and slowly reduced to 0% over a time period of 120 minutes. This means that copper deactivates in dangerously low times and this poses a major question over its usability to make the whole process of CO_2 electroreduction viable.

Study done by *Hori et al.*[13] took inspiration from their previous works on CO_2 electroreduction and studied the copper deactivation during the process. The researchers in their earlier studies [14][15] found that the Faradic Efficiency (F.E.) of the copper electrode decreases with time for all the carbon products. In this study the researchers first listed all the possible causes for catalyst deactivation and then with experiments tried to find the most probable cause.

- Presence of heavy metal impurities in reagent chemicals : Presence of heavy metals even in low amounts can be a possible cause of deactivation as, heavy metals can reduce and settle on the copper electrode, thus impeding its catalytic behaviour.

- Presence of organic substances in electrolyte: Substances like surface active reagents can be adsorbed on copper electrode and deactivate it

- Deposition of reaction intermediate or reaction products on copper electrode can also be a possible reason for the deactivation.

The study dealt with all the three above mentioned methods step by step. To study the impact of presence of organic substances in electrolyte, the researchers performed electroreduction in untreated electrolyte solutions and electrolyte treated with pre-electrolysis. The "pre-electrolysis" is the procedure of scavenging the electrolyte solution with a large cathodically polarized electrode. Platinum black was used in this case. When electrolysis was performed in both the electrolyte solutions, electrodes in pre-electrolysis treated solution performed better and were deactivated in about 120 minutes. On the other hand, electrodes in untreated electrolytes were deactivated in around 40-60 minutes. The presence of trimethylamine ($N(CH_3)_3$)in the electrolyte was determined as the cause of the poor performance of the untreated electrolyte.

To study the effect of heavy metal impurities in the electrolyte solution, $FeSO_4$ and $ZnSO_4$ were intentionally added to the solution and their impact was studied. It was found that Zinc and Iron reacted with CO_2 and deposited themselves on Copper electrode, which further inhibited the catalyst activity of copper. The catalytic activity of the electrode deteriorated severely after 60 minutes of operation. The researchers hypothesized that Fe atoms interacted with Cu by forming a surface alloy which ultimately damages the catalytic activity of copper. In contrast, Zn, blocked the catalytic sites of copper due to steric effect and still reduced CO_2 into CO. It was also found that to reverse the deactivation effect anodic polarization of the electrode at -0.05V versus SHE helped extensively.

Prasnikar et al.[40] studied the impact of steam on copper, zinc, aluminium (CZA) catalyst by aging the catalyst at varying gas compositions and doing a post-mortem analysis of the different electrodes. The researchers took eight commercially available samples and analyzed their activity in a parallel packed bed reactor setup with varying gas compositions of CO_2, H_2, H_2O and N_2. Techniques like XPS, SEM mapping, XRD and N_2 physisorption were used to study before and after samples and to determine the possible deactivation mechanisms on the sample. CZA samples of HiFuel W230 series from Alfa Aesar was used for this study.

It was demonstrated that, presence of steam increased the sintering of Cu and Zn particles. Sintering led to the increase in size of Zn and Cu particles, ultimately reducing their catalytic ability. The increase in grain sizes led to decrease in number of grain boundaries due to the amalgamation of different particles which led to a decreased catalytic surface. Another explanation for increase in size of copper was found to be hydroxylation of the surface or decreased contact between Cu, ZnO and Al_2O_3 surface which led to reduced inter-metallic interaction and thus a higher sintering rate.

The presence of zinc led to formation of ZnO precipitate on copper. As ZnO selectively reducesCO_2 into CO, formation of ZnO precipitates led to selective catalysis of CO_2 into CO and thus affected the activity of copper to reduce CO_2 into additional hydrocarbons. Another important conclusion of this work was determining the impact of Al_2O_3 particles. Al_2O_3 particles evenly covered both available sites of copper and zinc and decreased the mobility of electrons to the Cu sites. This led to poor catalytic performance of the CZA electrode. Though, Al_2O_3 was important for the structural stability of CZA catalyst, from this study it was understood that it ultimately acted as a double edged sword. Thus, from this study it can be concluded that even in pure copper samples, sintering would happen and it will be detrimental to the performance of the catalysts.

Review study carried out by *Popovic et al.*[39] mainly focused on the deactivation mechanisms in Nanoparticle Cu (Cu NP) electrodes and the shortcomings in studying these deactivation methods. The paper outlined the essential characteristics of why Cu nanofilms have garnered more attention compared to polycrystalline Cu. The most important reasons being higher surface area, more active catalytic sites, higher number of grain boundaries and porosity. *Nitopi et al.*[33] conducted a review study which illustrated that the major reason for degradation of Cu NP electrodes was the fragmentation and clustering of nanoparticles due to applied potential which ultimately leads to coalescence. This was similar to the issues reported in previous works outlined in this report, and thus it showed that even at nano-scale problem of coalescence existed. The paper concluded with suggestions to improve the study of deactivation mechanisms in Cu catalysts and outlined steps like developing advanced electron microscopy tools, improving testing methods for faster analyzing speeds and finally making a link between catalyst degradation mechanisms and the electrolyzer design. Another interesting feature outlined by this study was that the highest catalytic activity observed by Cu electrode was 150 hours, for ethylene production with gas diffusion electrodes.[7] Polymer-based gas diffusion electrode was used to increase the stability and working time of the electrode. Though, it had its drawback that catalytic activity was compromised slightly, but still the faradic efficiency of the electrode was reported to be 70%. Apart from this the rest of the copper-based electrodes remained active between 5 to 15 hours.

From the above-discussed works, it can be surmised that catalyst deactivation is a significant problem for CO_2 electroreduction. As *Hori*[12] mentioned in his work that the usual deactivation time for copper-based electrodes was between 5 to 15 hours, it proved that the current state of the art for copper-based electroreduction is not feasible for industrial usage. The primary reasons for this deactivation were realised to be the sintering of Cu particles and nano-particles, due to which copper particles agglomerated and active surfaces on the electrode decreased over time. Another important cause for deactivation was the presence of trace impurities like Fe or Zn ions and organic impurities like trimethylamine, which caused catalyst poisoning and thus reduced the activity of Cu electrodes. One feasible solution suggested by *Hori et al.*[13] was the "pretreatment" of electrolyte solution before using it for the electroreduction process.

Even though catalyst deactivation does not have a direct relevance to this thesis work as operation period of CO_2 reduction will not exceed 1 hour, it has been discussed here because it is one of the biggest reasons CO_2 reduction has not been scaled up to the industrial level till now.

2.2. Thesis research goals

From an intensive literature review of the current state of art research available on this topic, the following knowledge gaps were identified:

- Lack of co-relation between microstructural and electrochemical properties of copper.
- Minimal scientific data is present directly linking annealing of copper samples and its impact on electrochemical properties of copper.
- Lack of equivocal scientific outlook relating the electrochemical properties of copper to its impact on CO_2 reduction.
- Lack of a standard protocol to study microstructural changes in copper samples and relate it with the changes in its CO_2 reduction properties. [39]

One hypothesis was formulated from the literature review that small grain sizes of the nanoparticles yielded higher F.E. for hydrocarbons. As smaller grain sizes led to the higher active catalytic surface area, availability of higher ECSA contributed to more active surfaces for CO_2 to react and form a higher number of *CO intermediates.[16, 54] As annealing increases the grain size of the sample, this thesis work will test this hypothesis on a bulk copper sample.

The goal of this thesis research is to reduce the existing knowledge gap and provide a scientific approach towards the following research questions:

- How does the microstructure of copper change after annealing?
- How does change in grain size due to annealing impact the electrochemical properties(oxidation and reduction products, product formation potential) of copper?
- Does electropolishing influence the electrochemical properties of copper?
- How do annealing and electropolishing affect the CO_2 reduction properties of copper?

The research approach used for the thesis is as follows:

A literature survey was done to formulate research questions and select an experimental method to investigate those questions. After selecting the experimental methods, experiments were methodically performed with pre-determined parameters to accumulate data regarding the research questions. Subsequently, the experimental results were validated by repeating them with the same parameters to check their reproducibility. Once the reproducibility of the experimental data was determined, data was analysed, and their results were compared with the data obtained for other samples. After interpreting the data, conclusions were drawn from the results obtained, and future recommendations were suggested.

3

Experimental Methods

For the thesis work, it was important to select the right experimental techniques which can give the best evaluation of processes and can outline the experimental scope of the work. During the literature survey, crucial experimental techniques which were used by the authors mentioned in their work was outlined. This particular section talks about experimental techniques selected for this thesis and explains the experimental conditions.

3.1. Annealing and characterization techniques

3.1.1. Annealing of the copper samples

Annealing was performed on copper samples to modify their microstructure. Annealing temperatures of 350°C, 450°C, and 500°C were selected, keeping in mind the re-crystallization temperature of copper, which is 200°C[2]. To study the impact of time on grain growth, different annealing periods of 3hr, 6hr and 9hr were employed. All samples were annealed in a sealed steel package filled with argon gas to avoid oxidation during annealing.

Once the samples were annealed for the specified time, they were cooled in the sealed steel package outside the furnace at room temperature for 1hr. After the samples achieved room temperature, they were retrieved by cutting the steel package. After the samples was retrieved, they were washed in an ultrasonic bath with ethanol.

3.1.2. Optical Microscopy

The samples under consideration were pure Cu samples(Sigma Aldrich) of 99.999% purity with a dimension of 25mm X 25mm X 1mm. For the first part of experimentation, samples were mechanically polished to get a scratch-free surface. Initially, samples were hot mounted to aid in grinding and polishing. Further literature study found that pure copper had a re-crystallization temperature of 200°C. As the hot mounting machine heated the sample at 180°C for about 10 minutes, there was a possibility of altering the original structure. Figure 3.1 shows that even at temperatures low as 43°C, re-crystallization starts in the cold-rolled pure Cu, and there was a possibility of changing the initial structure at a slow rate. All the samples were cold mounted using an epoxy resin to avoid unwanted alteration of original grain directions, which prevented the use of excess temperature and pressure on as received copper samples.
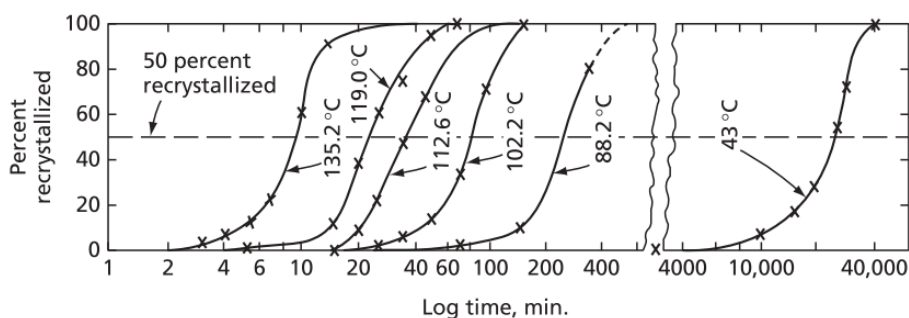
Figure 3.1: Isothermal transformation curves for pure copper cold-rolled 98%.[2]

Sanding was performed on a rotating disc machine starting from a grit size of P80 to P2000 sanding papers. After sanding, the samples were immersed in an ultrasonic bath for 20 minutes to clean the sanding residue. Afterwards, they were dried, and mechanical polishing was done on 3μ and 1μ cloth with diamond abrasive suspension. A separate sample was electropolished in 85% o-Phosphoric acid at +2.1 V vs RHE against a carbon rod. [26]. Electropolishing was done to study the impact of electropolishing on its electrochemical properties and its subsequent impact on CO_2 reduction. In the catalysis community, it is a common practice to perform CO_2 reduction on electropolished surfaces to remove oxide and other trace impurities.

11

Once samples were mechanically polished, the samples were etched to make the grain boundaries visible. Etchant solution utilized was 8gFeCl$_3$ + 25cm^3 HCl+100ml H$_2$O. To etch the samples, they were immersed in the etchant solution using forceps for 40 seconds and were immediately washed with ethanol to avoid over-etching. The samples were dried afterwards. After etching the samples, they were observed under an optical microscope to check for the grain sizes and grain boundaries.

For calculating grain sizes, microscopic images of the sample were taken using the Keyence microscope. Further, using ImageJ software, grain sizes were calculated. From a stitched image of the sample, 18 distinct grain boundaries were measured along their length, and an average was calculated. Hi-resolution images from the microscope helped in distinguishing the grains. Each grain boundary was selected when it made a clear distinction from the other grains.

3.1.3. XRD measurements

X-Ray Diffraction (X-Ray Diffraction) was used to verify the purity of the copper samples and characterize the planar crystal orientations of the samples.

The working principle of XRD is based on the diffraction from incident crystals. Considering the use of monochromatic X-rays that are elastically scattered and diffracted from the electron clouds around the nuclei of the atoms, the Laue condition, shown in Equation 3.1 , allows to understand when it is possible to observe a constructive interference for reflection by an arrangement points. These points correspond to hypothetical atoms lying on the crystal lattice planes. This condition must be fulfilled to have diffraction:

$$\mathbf{R}.(\mathbf{k} - \mathbf{k'}) = 2\pi\mathbf{m}$$
(3.1)

Where $\mathbf{k}$ and $\mathbf{k'}$ are the wave vectors of the incoming (incident) and outgoing (diffracted) beam, respectively, $\mathbf{R}$ is the Bravais lattice vector of the crystal and $\mathbf{m}$ the Miller indices of the family of crystal lattice atomic planes.

An analogous equation, which can be seen in Equation 3.2, has been developed to explain the Laue condition from a geometrical point of view. This is denoted as Bragg's law and it expresses the condition for constructive interference for specular reflection by planes.

$$2d_{hkl}sin\theta = n\lambda$$
(3.2)

In Equation 3.2 d_{hkl} is the interplanar distance between the diffraction crystal lattice family of planes identified by a specific set of Miller indices (h k l), μ is the incident angle, i.e. the angle correspondent to diffraction intensity maxima (peaks) that are created in the diffraction pattern as consequence of constructive interference, n is a positive integer related to the diffraction order and thus to the Bragg peaks and λ is the wavelength of the incoming X-rays. Figure 3.2 shows the schematic of Braggs equation

For phase identification, Bruker D8 Advanced diffractometer Bragg-Bentano geometry with graphite monochromator and Vantec position sensitive detector was used. A coupled θ-2θ scan with step size of 0.030°2θ was employed.

For texture measurement, Bruker D8 Discover with Eulerian Cradle and parallel beam geometry was used to do the XRD measurements. A Phi Scan from 0-355°was performed with plotting of steps at 2θ= 50.73°, 59.30°, and 88.84°.
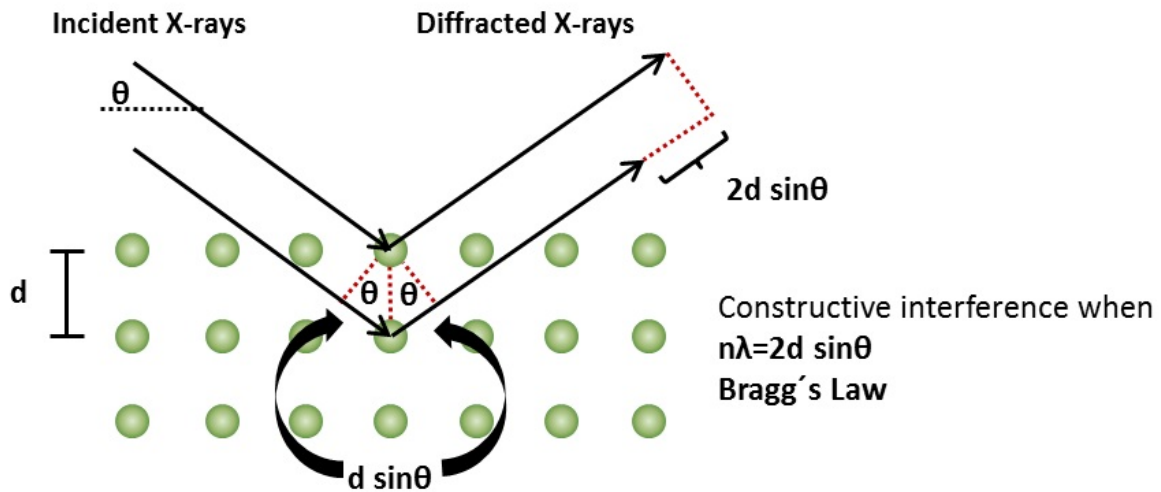
Figure 3.2: Schematic representation of Braggs equation.[3]

3.2. Electrochemical experiments

For the evaluation of electrochemical changes during CO$_2$ electroreduction methods of Cyclic Voltammetry(CV) and Electrochemical Impedance Spectroscopy(EIS) was used. In the electrochemical cell shown in Appendix A, copper was used as the working electrode, Ag/Agcl was used as the reference electrode, and a platinum mesh was used as the counter electrode. A VSP-300 (Biologic) potentiostat was used to perform CV and EIS experiments. The experiments were performed after a N$_2$ bubbling of 1 hour to push out the presence of oxygen dissolved in the KHCO$_3$ solution. During the experiments, N$_2$ was constantly supplied on top of the setup to maintain inert conditions. The reason KHCO$_3$ was chosen for electrochemical experiments was to study the effect of the most commonly used electrolyte in CO$_2$ reduction. KHCO$_3$ acts a good carrier of CO$_2$ and has proven

to improve CO$_2$ results by ensuring a continuous flow of CO$_2$ facilitated by breaking down of HCO$_3^-$ molecule into hydrogen and carbonate ions. [56]

3.2.1. Cyclic Voltammetry

Cyclic Voltammetry(CV) is an electrochemical technique where a potential is applied to the sample within the range of interest and the resulting current is measured. Cyclic voltammetry experiment gives crucial information about oxidation and reduction processes that can take place in the metal/electrolyte system in the selected potential window. For the particular case of CO$_2$ electroreduction, it has been used to predict the potentials where oxidation and reduction products are produced during the process and thus helped in narrowing down the effective potential range. For the thesis work a voltage range of -0.18 Volt vs RHE to 1.2 Volt vs RHE was chosen. The applied potential was increased from -0.18 V to 1.2 V vs RHE during forward sweep and then reversed to -0.18 V vs RHE during the backward sweep with steps of 5 mV/s. Voltage range chosen was to incorporate all reduction reaction products copper undergoes in CO$_2$ reactions with KHCO$_3$ solution.

CV experiments were repeated at least three times to assure the reproducibility. Each trial was conducted on a freshly prepared copper sample. Every trial had three cycles of forward and backward sweep and the third cycle was considered for analysing results. The cyclic voltammetry experiments were performed on scan rate of 5 mV/s.

3.2.2. Electrochemical Impedance Spectroscopy

EIS experiment is performed by measuring the alternate current as a response to an applied sinusoidal potential wave over a range of frequencies. EIS is a non-destructive technique, and the measurements are performed in-situ, which allows for repeated measurements on the same sample. EIS data is studied by fitting the data to an electrical circuit. The electrical circuit elements should describe the physical elements of the metal/electrolyte interface. [49]

For this thesis, EIS experiments are carried out to characterize the electrochemical properties of the copper/electrolyte interface before and after CO$_2$ reduction. EIS measurements can help in gauging the resistance and porosity of oxide layers formed on the copper sample in KHCO$_3$ sample. Thus, EIS techniques could help in quantifying and improving the CO$_2$ electroreduction process by generating information about what is happening on the samples in-situ.

EIS experiments were conducted from a frequency range of 7 MHz to 1 mHz. A wide range was utilized to study the behaviour of copper material and the possible passive layer structure it forms on reaction with KHCO$_3$. EIS experiments were repeated two times to assure the reproducibility. EIS spectrum analyzer software was used to analyse the EIS data.
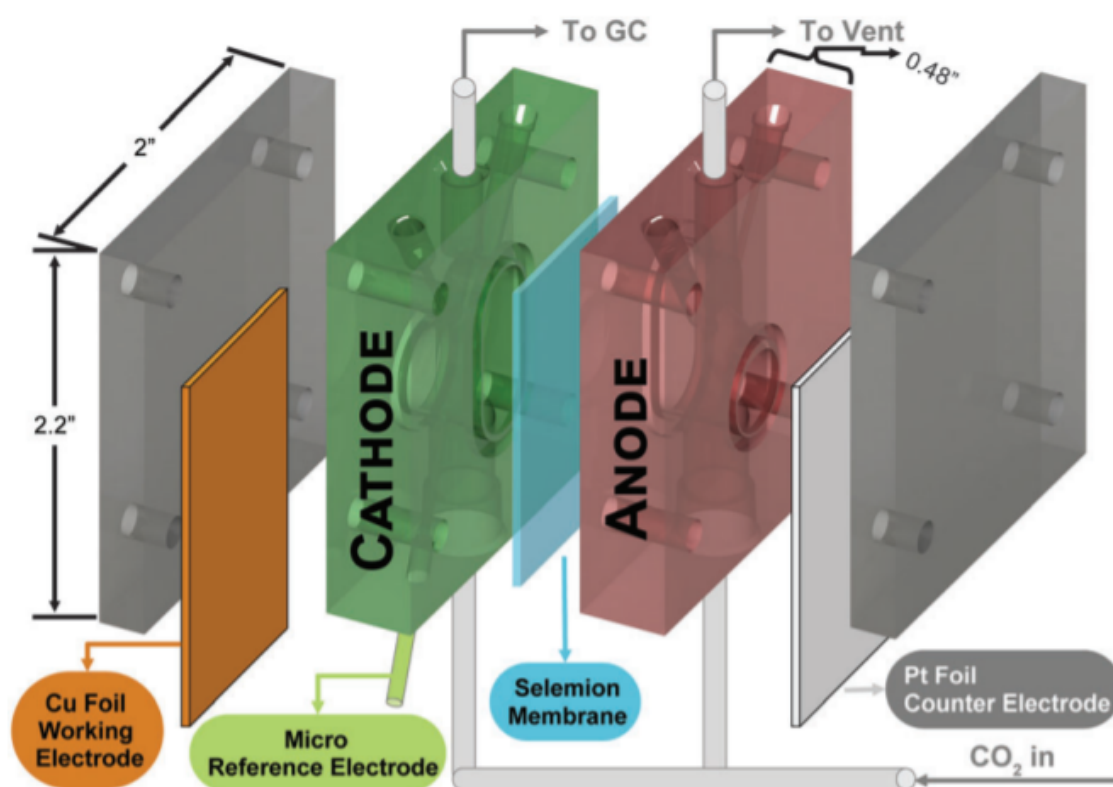
3.3. CO$_2$ reduction

Figure 3.3: Schematic representation of setup used for CO$_2$ reduction.[28]

The setup used for CO$_2$ reduction was similar to the setup used by *Lobaccaro et al.*[28] at Lawrence Berkeley National

Laboratory.

The setup consisted of two poly-carbonate compartments separated by a semi-permeable membrane. Cu foil was placed in the cathode chamber and it was purged with CO$_2$. The micro reference electrode Ag/AgCl (Innovative Instruments, USA) was used. Another outlet went from cathode chamber to Gas Chromatography (GC) to analyze the products of CO$_2$ reduction.

Selemion membrane was placed between the cathode and anode chamber. Selemion membrane allows the flow of certain anions which help the progression of CO$_2$ reduction. Platinum counter electrode was placed in the anode chamber and it was next to the cathode chamber. Anode chamber was connected to the vent as H$_2$ gas was produced there. Figure 3.3 shows the schematic of the setup used for CO$_2$ reduction for this thesis work.

To conduct CO$_2$ reduction on copper, chronoamperometry was performed at E = -1.0 V vs RHE. One hour of CO$_2$ reduction was conducted and the respective products were analyzed. Gaseous products were characterized using an online gas chromatography and liquid products were identified using High-Performance Liquid Chromatography (HPLC). The experiments were repeated twice to verify their reproducibility.

Results and Discussion

4.1. Micro-structure characterization

4.1.1. Microcopy results

Figure 4.1 shows the optical images of as-received samples. Both the Figure 4.1a and Figure 4.1b represent a different surface region of the sample. Copper grains showed elongated shape following the rolling direction. [42]. Study conducted by *Guo et al.* also showed similar effect on microstructure of uni-directional cold rolled copper samples.[53] The average grain size was found to be 1596μm with a standard deviation of 510μm.

(a)   (b)
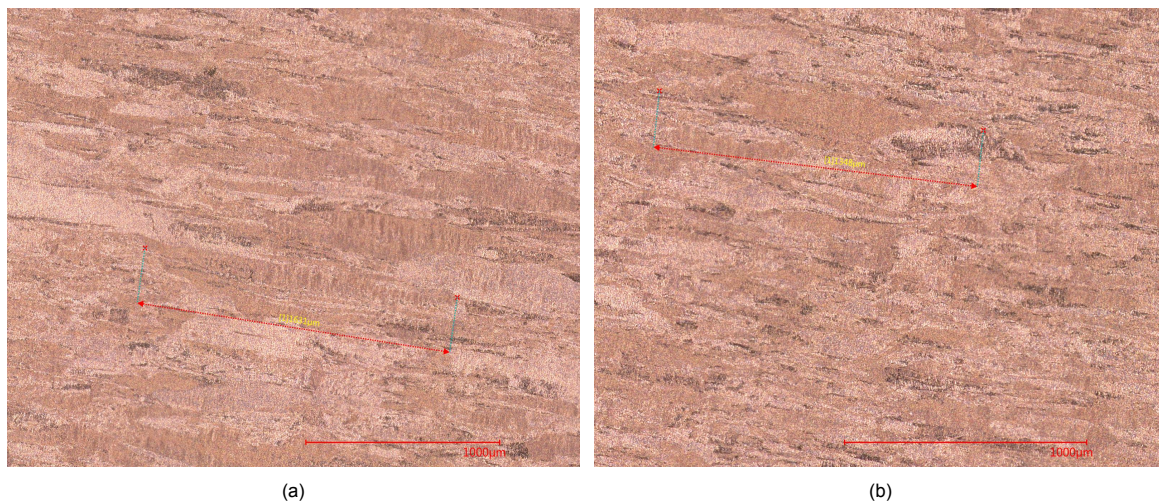
Figure 4.1: Microscopic pictures of As received Copper

Figure 4.2 shows the optical images of electropolished Cu samples. Figure 4.2a and Figure 4.2b represent different areas of the sample. On calculating the average grain size of electropolished copper, it was found to be 1689μm with a standard deviation of 649μm. The electropolished sample looked similar to the as-received sample in terms of comparison with its grain size and grain direction. The rolling direction was evident on the microscopic image and hence the two structures were found to be comparable.

Figure 4.3a and Figure 4.3b show two different region of the Cu sample annealed at 350°C for six hours. Grain coalescence and grain elongation were two significant effects of annealing observed on the Cu samples. After annealing, the Cu sample showed significant enlargement in grain size. The sample also lost the rolling direction texture completely as evident from the microscopic images. The average grain size was found to be 2943μm with a standard deviation of 1639μm. The deviation amongst the size of grains was immense and a plausible reason could be the uneven heating of the sample during annealing which leads the grain growth in a very random fashion. The reason for grain agglomeration is explained later in this section.

Figure 4.4 presents the optical images of Cu samples annealed at 450°for six hours. Similar to the sample annealed at 350°C, it also exhibited grain elongation and loss of rolling direction. The average grain size was found to be 3794μm with a standard deviation of 1608μm. The sample had a very high value of standard deviation of grain size. From the optical images (Figure 4.4) it was observed that the grains elongated in random directions and it became harder to distinguish different grains.

Figure 4.5 shows the images of Cu samples annealed at 500°for 6 hours. Like the other annealed samples it also exhibited grain elongation and grain coalescence. The average grain size was found to be 3868μm with a standard deviation of 1284μm. The grain size did not grow dramatically compared to the annealed sample of 450°. One significant feature was the reduction in the standard deviation values of the grain size.
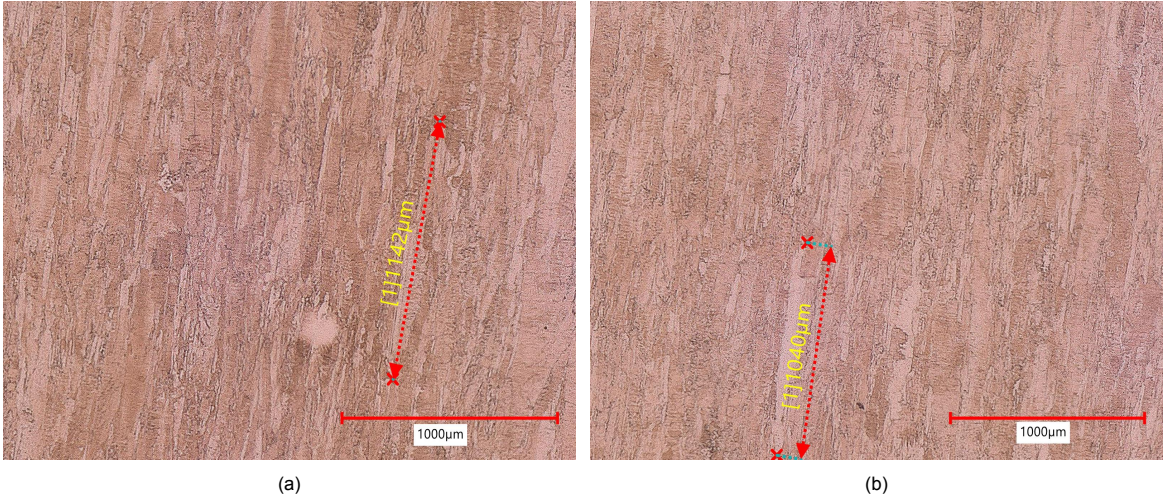
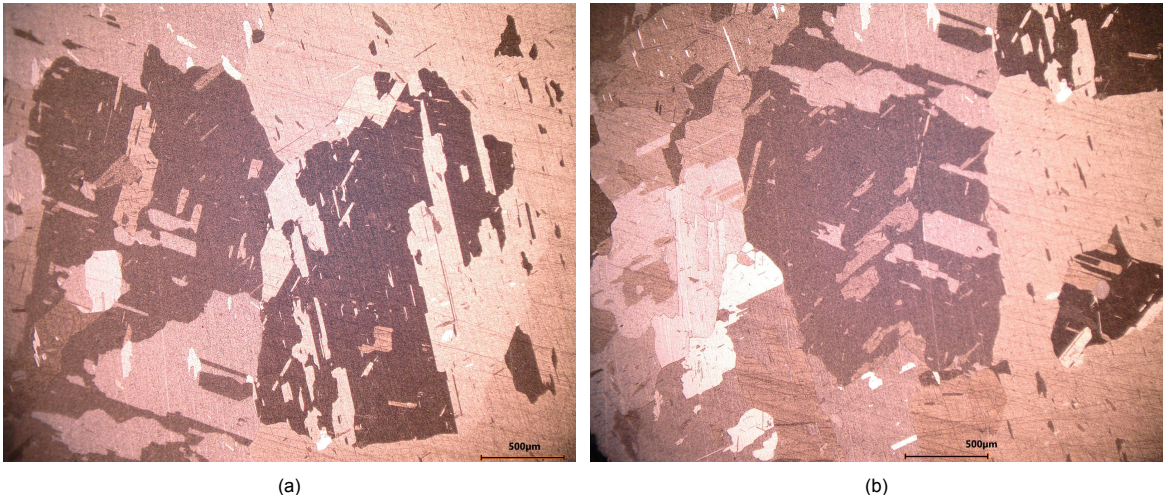Figure 4.2: Microscopic pictures of Electropolished Copper

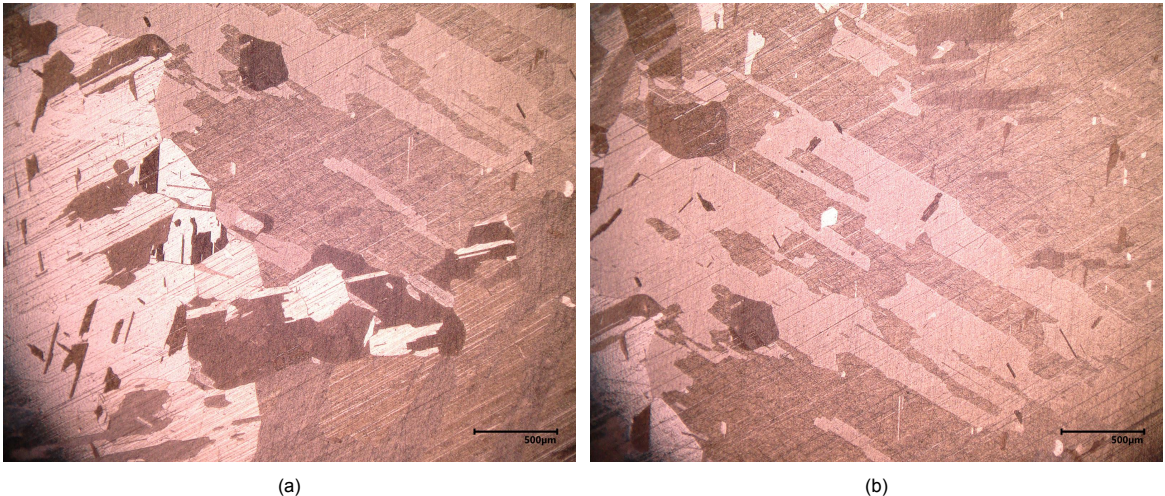Figure 4.3: Microscopic pictures of sample annealed for 350°for 6 hours

Figure 4.4: Microscopic pictures of sample annealed for 450°for 6 hours

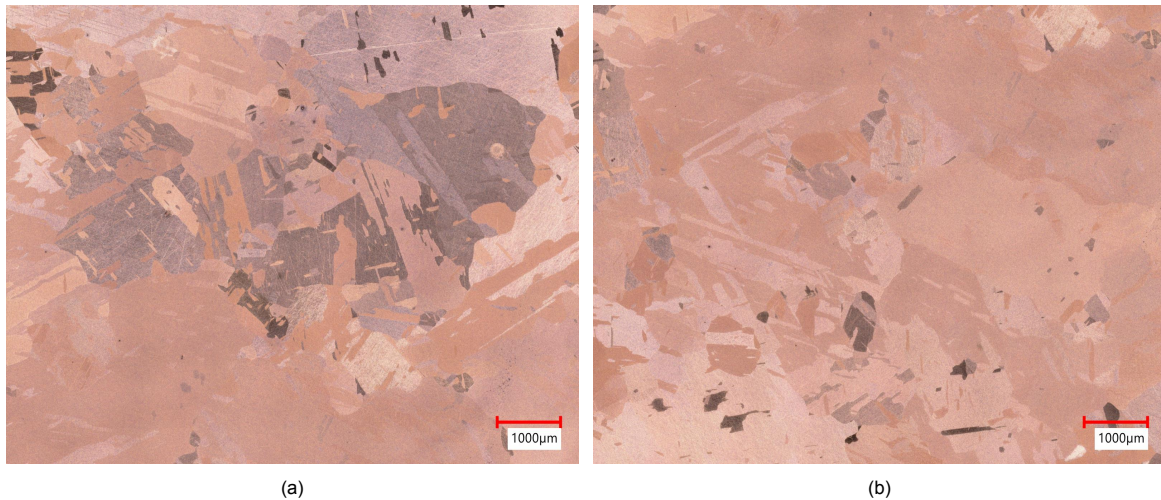<div align="center">(a)   (b)</div>

Figure 4.5: Microscopic pictures of sample annealed for 500 degrees for 6 hours

Other set of samples annealed at 500°for 3 and 9 hours exhibited grain elongation and grain coalescence as well. Figure 4.7, Figure 4.5 and Figure 4.8 show the microscopic images of samples annealed at 500°C for three, six and nine hours respectively. It was observed that significant growth in grain size stopped after 450°. One notable feature observed in sample annealed at 500°for 9 hours was the reduction of standard deviation in the grain size.

The results of grain sizes and their standard deviation have been tabulated in the Table 4.1.

Table 4.1: Calculated Grain sizes and their standard deviation

Sample	Measured Grain size	Standard deviation
As received	$1596\mu m$	$510\mu m$
Electropolished	$1689\mu m$	$649\mu m$
Annealed (350°,6h)	$2943\mu m$	$1639\mu m$
Annealed (450°,6h)	$3794\mu m$	$1608\mu m$
Annealed (500°,6h)	$3868\mu m$	$1284\mu m$
Annealed (500°,3h)	$2850\mu m$	$1054\mu m$
Annealed (500°,9h)	$3955\mu m$	$987\mu m$

From the calculated grain sizes, it was evident that there was an increase in the grain size of the annealed copper samples. The mechanism behind grain growth were microstructural phenomena such as grain coalescence and re-crystallization. Annealing provided the heat energy required to drive these processes.[48]

The coalescence of grains and grain elongation can be explained in terms of free surface energy. Figure 4.6 gives a stepwise explanation of how grain coalescence works. In the example provided, three grains with shared boundary engulfed into a single large grain and have comparatively less free surface energy than the initial configuration of three grains neighbouring each other. [4]

Possibly, the microscopic structure during annealing underwent a three-step process. The first step was the recovery phase, which happens below the re-crystallization temperature. During the recovery phase, physical and mechanical changes caused due to the deformation of metal is recovered to its non-deformed phase. In terms of energy, the energy of deformed metal is released, and the effect of cold work is slowly reversed.

The second step was re-crystallization. During re-crystallization, metals start forming new grains and lose their original grain structure. During re-crystallization, the deformed grains of the crystal structure are replaced by stress-free new grains.[4]

The third and final step was grain growth which happens due to the surface energy of grain boundaries. The process was driven to reduce the surface energy and reduce the grain boundary area. The orientation these new grains took depended on the grains coalescing together to form the new grain boundaries. The phenomenon through which grain growth happens is called geometrical coalescence. During geometrical coalescence, grains with similar orientations are grouped to reduce the surface energy of the overall system. During the final step, the grains elongate. Thus, the annealed samples changed their orientation and grew to achieve the least free surface energy configuration.

As previous studies suggested that cold rolled samples recrystallize at lower temperatures, all the samples considered for this study completely recrystallized and went on to the third stage of annealing and showed grain growth.[4, 46] The experimental values observed in the Table 4.1 confirm this hypothesis. It is very hard to differentiate the steps of recovery, re-crystallization and the third stage of grain growth as it will require intermittent quenching steps and it will be unrelated to direct purview of the study. The relative orientation of these grains were similar and energy needed to move these grains was provided by heat of annealing process.

Microscopy results showed a linear trend for grain growth for annealed samples of 350°C and 450°C samples. Annealing did not result in significant grain growth after 450°C, and thus the four samples: as-received, electropolished, 350°C annealed
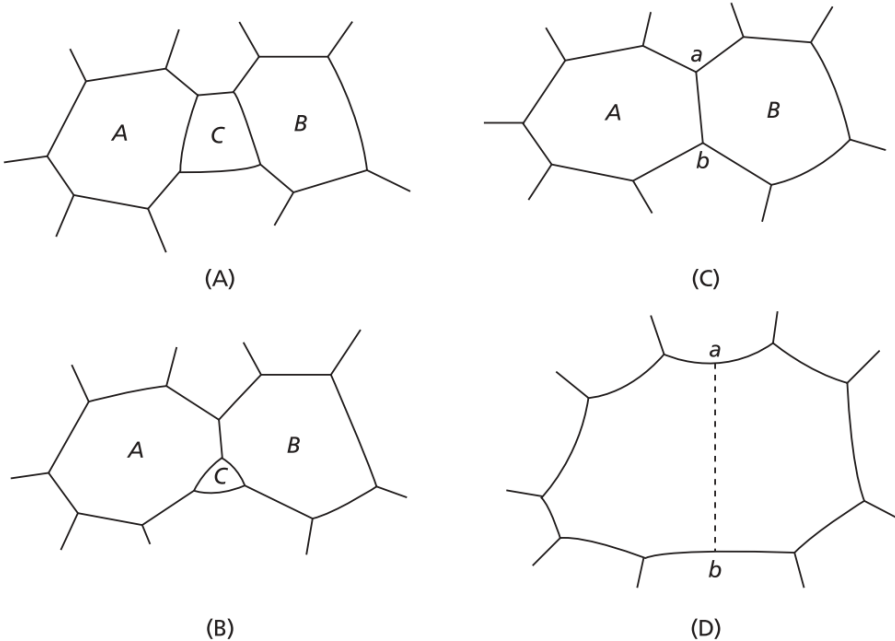
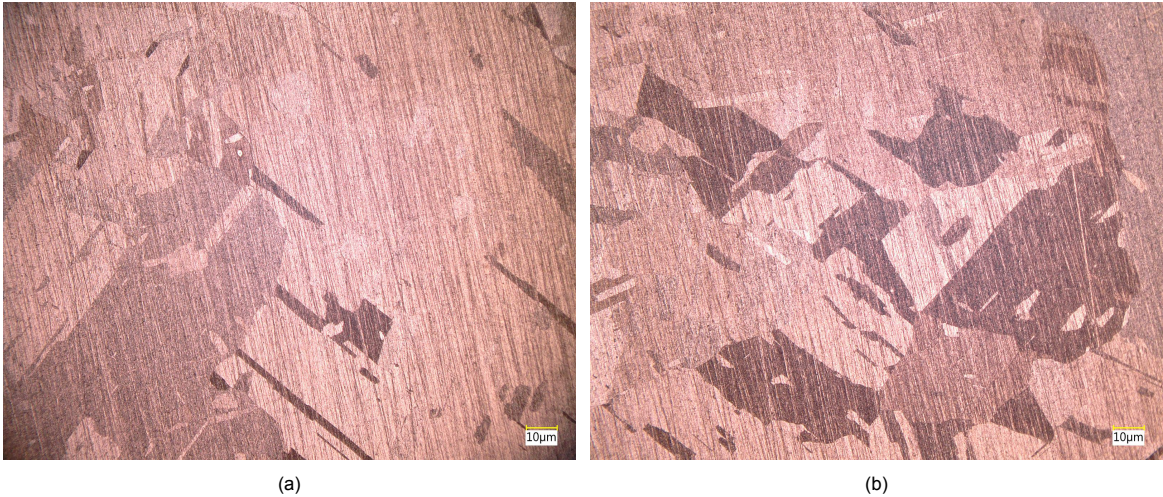Figure 4.6: Mechanism of Grain Coalescence.[2]

Figure 4.7: Microscopic pictures of sample annealed for 500 degrees for 3 hours

(a)   (b)
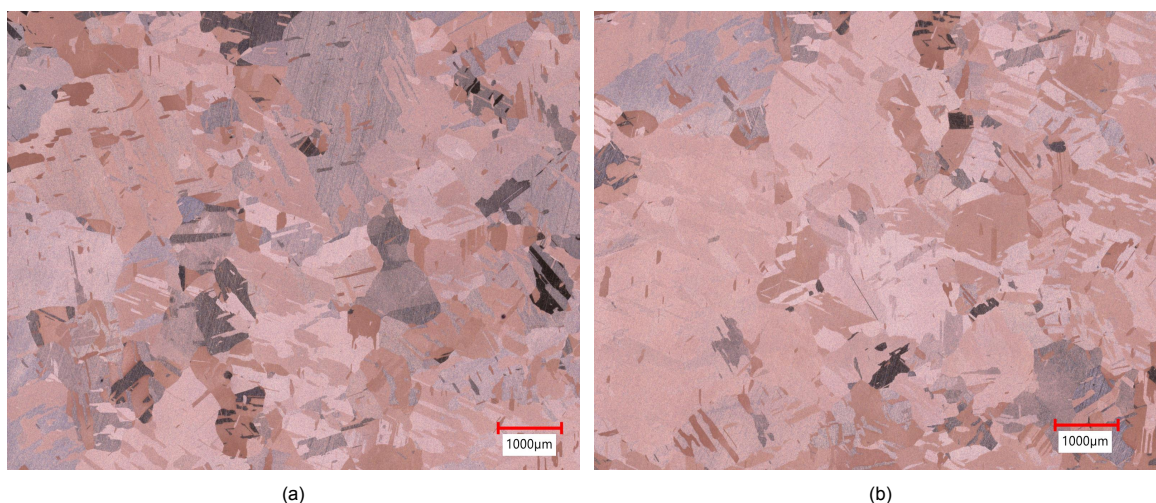
Figure 4.8: Microscopic pictures of sample annealed for 500 degrees for 9 hours

and 450°C annealed sample were further studied. The selection of the sample was made to highlight the effect of increased grain size and electropolishing on electrochemical and CO_2 reduction properties of Cu samples.

4.1.2. XRD results

This section discusses the XRD results obtained for the Cu samples.

Phase identification

XRD phase identification was done to analyze the composition of the as-received and annealed copper samples. As-received copper sample only showed peaks corresponding to copper, and no other peaks in the XRD spectrum. The results were expected as copper with a purity of 99.999% was acquired from Sigma Aldrich. There were four high-intensity peaks identified related to different orientations in the sample. No presence of copper oxides was detected in XRD measurements for pure copper.

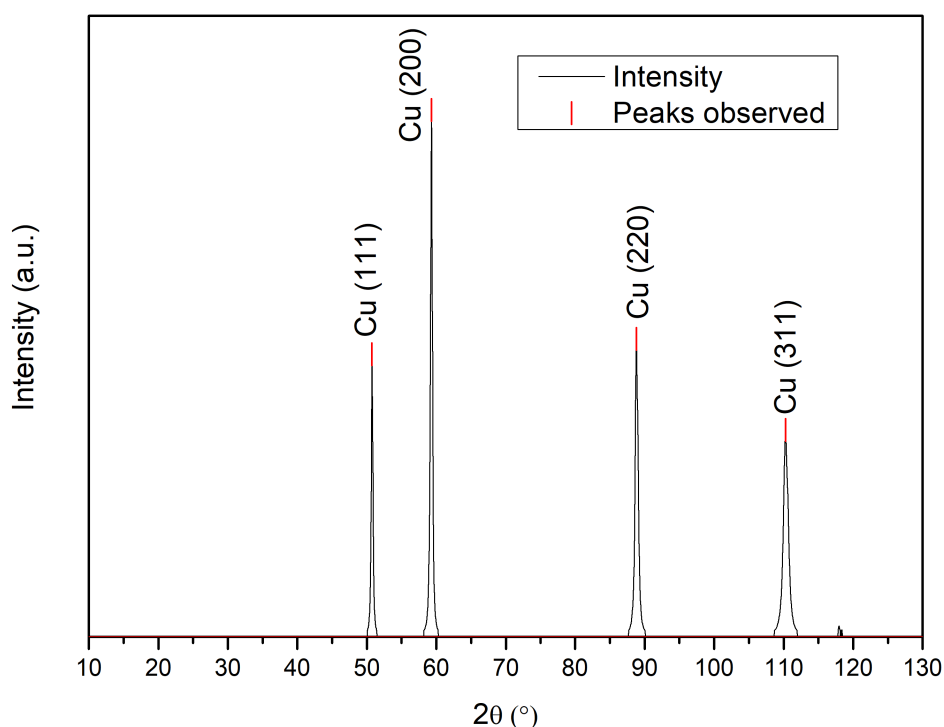Figure 4.9: XRD measurement of as received sample

In the Figure 4.9 the peaks at 50°corresponds to Cu(111), 59°to Cu(200), 88°to Cu(220) and Cu(311) at 110°respectively. Figure 4.10 is the XRD plot for the 350°C annealed copper sample. The sample showed some CuO and Cu_2O peaks along with Cu peaks. 350°C annealed sample had one distinct difference of the absence of more than one high-intensity peak of
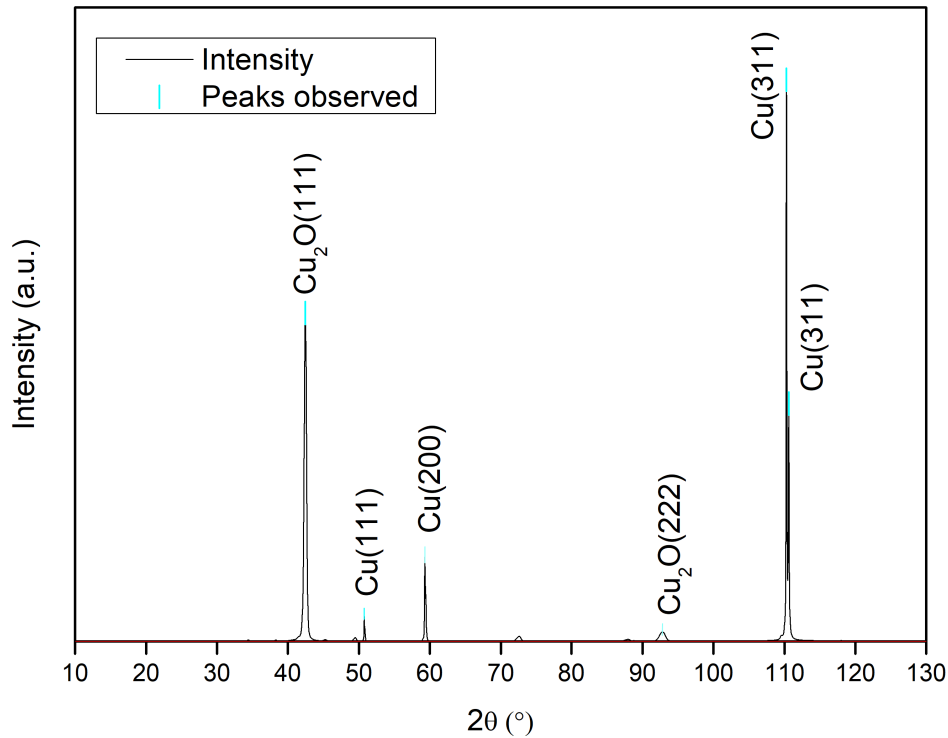
Figure 4.10: XRD measurement of 350 °C sample

pure copper. One high-intensity peak of Cu_2O was observed at 42°, and the other peak of Cu_2O and copper were present with intermediate intensity. Cu(311) had the highest intensity peak for pure copper at 110°.

Figure 4.11 is the XRD plot for the 450°C annealed copper sample. The sample only had peaks of pure copper. The sample had a high-intensity Cu(311) peak at 110°, and others were present with intermediate and small intensity.

Peak analysis for annealed sample revealed that the dominant copper peaks corresponded to {311} family of planes. XRD analysis confirmed the re-crystallization of copper samples due to annealing as high intensity peaks of copper samples before and after annealing changed. The copper samples became more directional and favoured the formation of {311} family of planes.

Texture analysis

Texture analysis was performed on annealed samples to explore the impact on copper samples further. It focused on recording the signals of various planes on specific angles, and their maximum and minimum values before and after annealing were reported. The minimum and maximum values listed in Table 4.2 and Table 4.3 are the average intensity observed on the overall sample times the numerical values listed on the sample.

Sample 1 and Sample 2 were the as-received samples which were annealed at 350°C and Sample 450°C respectively.

Table 4.2: Result of texture analysis of samples before annealing

	(111) 2θ=50.7°		(200) 2θ =59.3°		(220) 2θ =88.8°	
	Min	Max	Min	Max	Min	Max
Sample 1	0.25	7.24	0.18	32.83	0.18	5.42
Sample 2	0.27	6.9	0.22	7.85	0.2	7.53

Table 4.3: Result of texture analysis of samples after annealing

	(111) 2θ=50.7°		(200) 2θ =59.3°		(220) 2θ =88.8°	
	Min	Max	Min	Max	Min	Max
Sample 1 at 350°C	0.0	346.5	0.0	374.5	0.01	307.99
Sample 2 at 450°C	0.09	51.97	0.08	159.89	0.08	75.19

Figure 4.12 shows the result of texture analysis of 350°C annealed sample for Cu(111) plane. For the 350°C annealed sample, there was an overall increase in the maximum values for all the planes considered. The most significant increase was found for the maximum of (200) planes whose value increased from 32.83 times to 374.5 times the average concentration of the plane. Interestingly, the minimum decreased to 0 for (111) and (200) planar orientations. The variation in average intensity
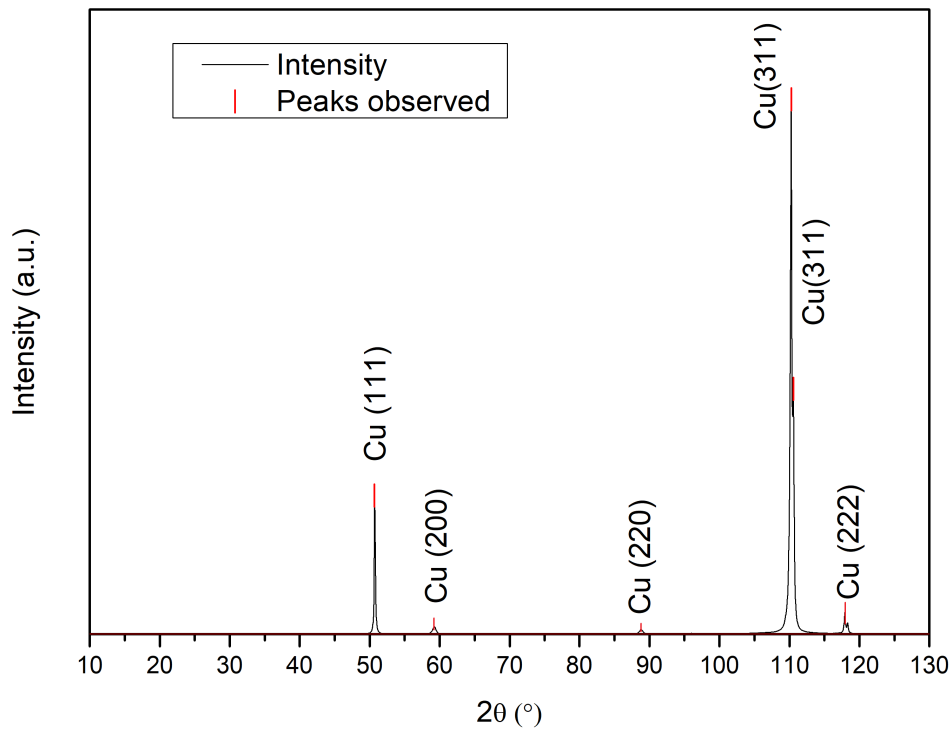
Figure 4.11: XRD measurement of 450 °C sample

values of grain orientation in annealed samples supported the microscopy results of re-crystallization. Complete results of texture analysis have been attached in Appendix B.

Figure 4.13 shows the result of texture analysis of 450°C annealed sample for Cu(111) plane. For the 450°C annealed sample, there was an increase in the maximum values for all the planes. The most considerable increase was found to be for (200) planes whose maximum value increased from 7.85 times to 159.89 times the average concentration of the plane. Unlike the 350°C annealed sample, none of the minimum values reached zero for this sample.

(a) Before annealing   (b) After annealing

Figure 4.12: Texture results for 350°C at 50.7°

XRD results of 350°C and 450°C annealed samples showed that Cu{311} set of planes were found in abundance after annealing. As XRD peak identification showed the highest peak intensity for Cu(111), Cu(200) and Cu(220) peaks for the as-received copper samples, texture analysis was performed only on three orientations. Quantitative data was obtained, which

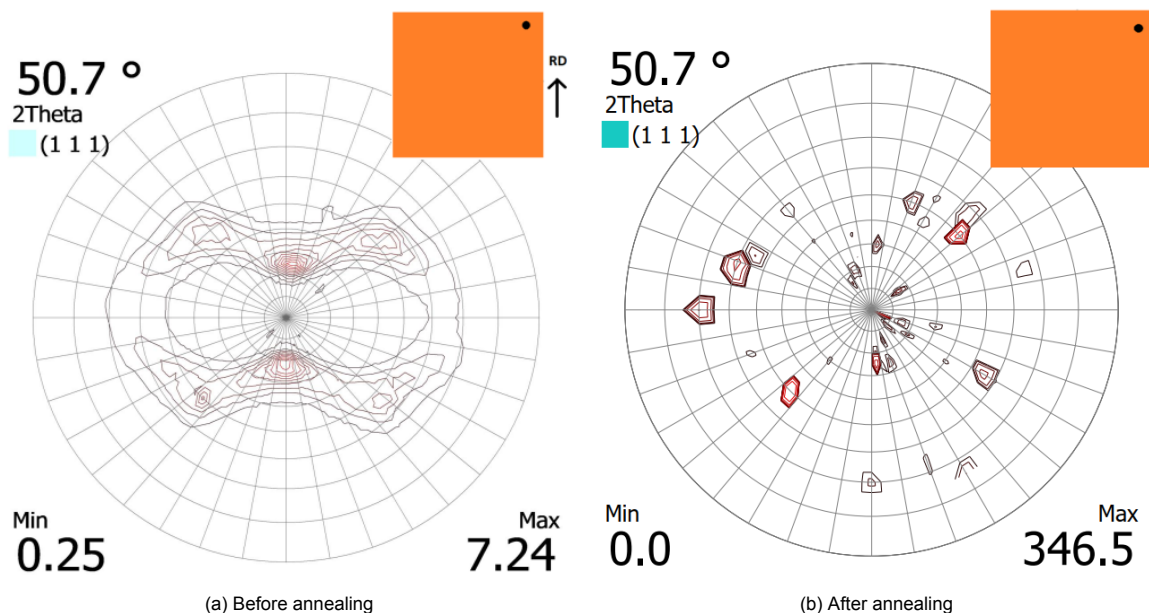further cemented the notion of re-crystallization as the average minimum, and maximum concentration of (100), (200) and (220) crystal planes changed drastically in annealed samples.

From the texture analysis, it can be concluded that the as-received copper samples go through a re-crystallization process and change their grain orientation after annealing. This effect could be explained through the concept of free surface energy. When annealing is done, the grain boundaries gain energy to reorient themselves in a pattern with the least surface energy.The increased free surface energy gave the copper crystals the kinetic energy to move from their original positions and reorient themselves. Another prominent feature to observe was the loss of rolling direction, as the grains coalesced together and arranged themselves in a more energetically stable orientation. [24].
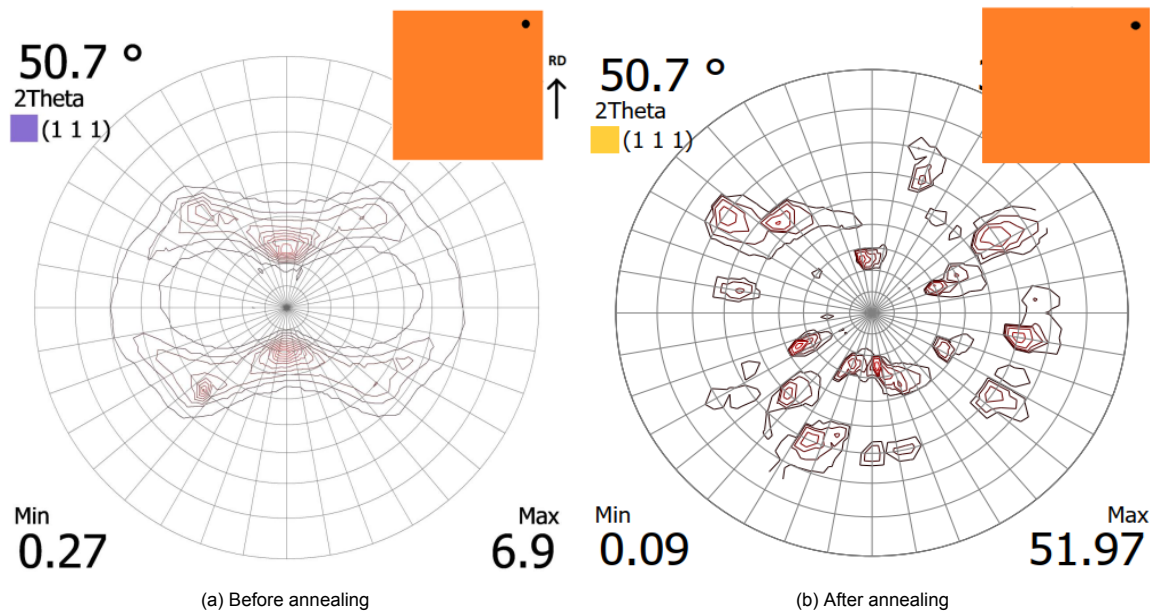

(a) Before annealing   (b) After annealing

Figure 4.13: Texture results for 450°C at 50.7°

4.2. Electrochemical Measurements

Cyclic Voltammetry and Electrochemical Impedance Spectroscopy results have been summarized below.

4.2.1. Cyclic Voltammetry

Table 4.4 summarizes the possible reactions occurring during cyclic voltammetry experiments. The table has been compiled with reference to the work of *Sanchez et al.* and *Nishikata et al.*[32, 43] The authors proposed the possible products when copper reacts to a solution with presence of HCO_3^- ions. *Sanchez et al.* used Pourbaix diagram and thermodynamics to hypothesize the formation of possible products which this report utilizes (Table 4.4) to analyse the CV results.

Table 4.4: Product formation during CV experiments

Oxidation	Symbol	Reduction	Symbol
$2Cu + H_2O \rightarrow Cu_2O + H^+ + 2e^-$	I(a)	$Cu_2O + H^+ + 2e- \rightarrow 2\ Cu + H_2O$	I(b)
$Cu_2O + H_2O \rightarrow 2CuO + 2H^+ + 2e^-$	II(a)	$2CuO + 2H^+ + 2e^- \rightarrow Cu_2O + H_2O$	II(b)
$Cu_2O + 2H_2O \rightarrow 2CuO*H_2O + 2H^+ + 2e^-$	III(a)	$2CuO*H_2O + 2H^+ + 2e^- \rightarrow Cu_2O + 2H_2O$	III(b)

As Received Sample

Figure 4.14 shows the CV result for the as-received sample from the third run of trial three. All the CV measurements have been taken from the third run as it is assumed that at the third run, electrodes will form a stable interface with the electrolyte and respond accurately to potential variation in the system. Two clear peaks, **I(a)** and **III(a)** were seen during the oxidation cycle. All the samples had a common feature of a flat line after complete oxidation of copper into Cu^{+2} (CuO and $Cu(OH)_2$) state. The **I(a)** peak was observed at -0.082 V vs RHE represented the formation of Cu_2O. The **III(a)** peak was broad compared to other samples possibly due to the formation of a single peak for formation of $Cu_2O \rightarrow CuO$ and $Cu_2O \rightarrow Cu(OH)_2$.

During the reduction sweep, there were more than two peaks. The increase in the number of peaks can be attributed to the slow reduction of oxidized products in the reverse cycle, which led to the observation of three clear peaks. The **III(b)** peak could be attributed to conversion of $Cu(OH)_2$ into Cu_2O and the **II(b)** peak can be attributed to conversion of CuO into Cu_2O. The sharp peak **I(b)** corresponds to the conversion of Cu_2O into Cu. The sharp **I(b)** is observed in all the trials, and it is because of the energetically favourable conversion of Cu^{+1} (Cu_2O) into Cu neutral state. [43]

I(a) and **III(a)** showed a current intensity of 0.02369 mA/cm^2 and 0.04268 mA/cm^2 respectively. A higher current intensity for formation of **III(a)** suggests that a higher amount of Cu^{1+} species were oxidized at **III(a)** than Cu at **I(a)**. The current intensity
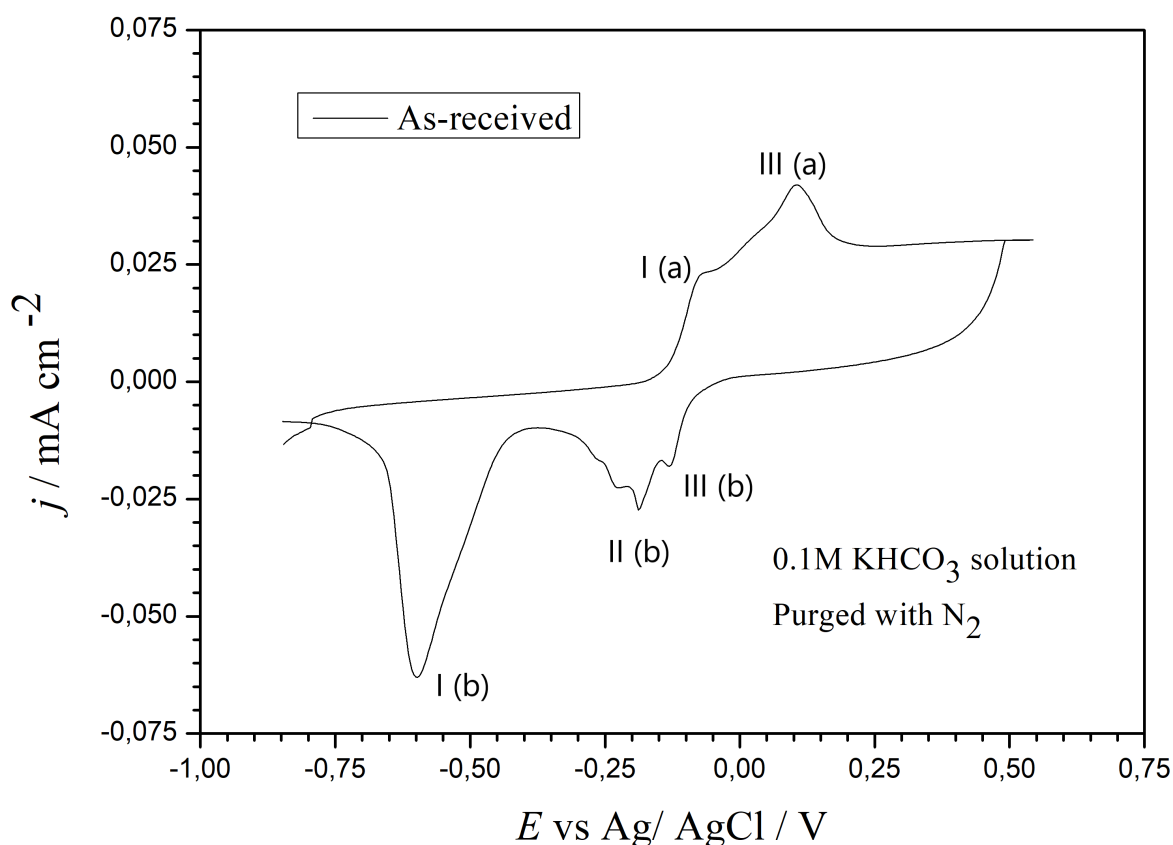
Figure 4.14: CV result of as-received copper sample

observed for **III(b)** and **II(b)** are -0.017 mA/cm^2 and -0,0263 mA/cm^2 respectively. These values are not very far from each other. The peak current value observed for **I(b)** was -0.0624 mA/cm^2. A high current intensity gives the information that a high number of Cu^{+1} ions were reduced at **I(b)**. It should be noted that all the current intensity values recorded by the system are for the geometrical surface area which was considered to equal to 0.436 cm^2.

Electropolished sample

Figure 4.15 shows the CV result for electropolished sample from trial 2. In the case of electropolished copper samples, a slight difference was observed in terms of peak positions and the number of peaks identified. Two voltagramms showed three peaks during the oxidation cycle, and one voltagramm showed two peaks in the forward sweep. The first peak, **I(a)**, was attributed to the formation of the Cu$_2$O product. The average value of formation of Cu^{+1} state was -0.137 V vs Ag/AgCl. The average peak potential values of **II(a)** and **III(a)** were found to be -0.023 V and 0.055 V vs Ag/AgCl. Compared to pure Cu samples, Cu^{+2} products (Cu(OH)$_2$ and CuO) formed at a smaller potential for electropolished samples. The peaks were also sharper compared to **III(a)** peak of the pure copper sample.

While during the reduction sweep, there were three peaks. The **III(b)** and **II(b)** peaks had an average potential value of -0.064 V vs Ag/AgCl and -0.113 V vs Ag/AgCl. Again, these values were different from the average peaks observed for pure copper samples. The peak **I(b)** was observed at an average value of -0.492 V vs Ag/AgCl, and it represented the conversion of Cu^{+1} into neutral state of copper. (Cu$_2$O → Cu)

I(a), **II(a)** and **III(a)** showed a current intensity of 0.034 mA/cm^2, 0.047 mA/cm^2 and 0.049 mA/cm^2 respectively. The average current values of the product formation were higher by about 0.01 mA/cm^2 when compared to the pure copper sample, but the Cu^{+2} product formation current was similar. The current intensity observed for **III(b)** and **II(b)** were -0.016 mA/cm^2 and -0.031 mA/cm^2 respectively. These values were also comparable to the values of the pure copper sample. The peak current value observed for **I(b)** was -0.323 mA/cm^2 instead. At **I(b)**, the current intensity was comparatively more negative compared to pure Cu sample. It meant for electropolished sample, a higher number of Cu^{+1} ions were available to be reduced at **I(b)**.

350°C annealed sample

Figure 4.16 shows the CV result for 350°C annealed sample from trial 2. In the positive direction sweep, three distinct peaks were observed. The first peak was attributed to the formation of the Cu$_2$O product. The average value of formation of Cu^{+1} (Cu$_2$O) state was -0.130 V vs Ag/AgCl. The average peak potential values of **II(a)** and **III(a)** were found to be -0.044 V vs Ag/AgCl and 0.052 V vs Ag/AgCl. Compared to pure Cu samples, Cu^{+2} products (CuO and Cu(OH)$_2$) formed at a more negative potential for 350°C annealed sample.

During the reduction sweep three peaks were identified, similar to pure Cu and electropolished sample. The **III(b)** and **II(b)** peaks had an average potential value of -0.091 V vs Ag/AgCl and -0.179 V vs Ag/AgCl. These values again were different from average peaks observed for electropolished samples. The peak **I(b)** was observed at an average value of -0.507 V vs Ag/AgCl,
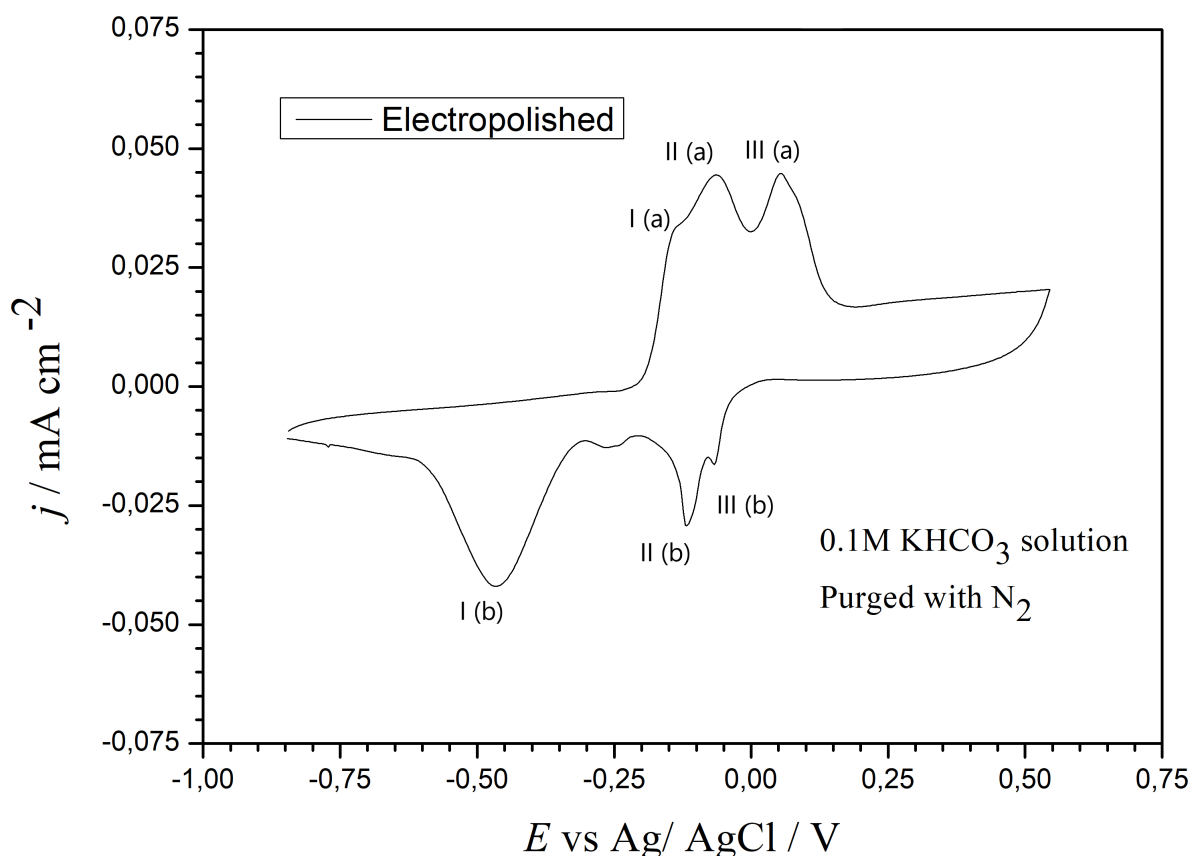
Figure 4.15: CV result of electropolished copper sample

and it represented the conversion of Cu^{+1} into a Cu neutral ($Cu_2O \rightarrow Cu$) state. Thus, CV results showed that pure Cu and 350°C annealed samples behaved similarly in terms of peak positions. [43]

I(a), **II(a)** and **III(a)** showed a current density of 0.0331 mA/cm², 0.046 mA/cm² and 0.05 mA/cm² respectively. The current density observed for **III(b)** and **II(b)** were -0.019 mA/cm² and -0.030 mA/cm² respectively. These values were comparable to the values of pure copper and electropolished sample. The peak current value observed for **I(b)** was -0.058 mA/cm².

450°C annealed sample

Figure 4.17 shows the CV results for 450°C annealed sample. Three distinct peaks were observed in the positive direction sweep, similar to the electropolished and 350°C annealed sample. The peak **I(a)** was attributed to the formation of the Cu_2O product. The average value of formation of Cu^{+1} state was -0.123 V vs Ag/AgCl. The average peak potential values of **II(a)** and **III(a)** were found to be -0.051 V vs Ag/AgCl and 0.057 V vs Ag/AgCl. Thus, the peak positions were similar to the 350°C annealed sample. The peak **I(a)** was very small. The peaks **II(a)** and **III(a)** were sharp like 350°C annealed and electropolished sample.

During the reduction peak, three peaks were identified. The **III(b)** and **II(b)** peaks had an average potential value of -0.083 V and -0.123 V vs Ag/AgCl. The **I(b)** was observed at an average value of -0.507 V vs Ag/AgCl, and it represented the conversion of Cu^{+1} into a Cu neutral state ($Cu_2O \rightarrow Cu$). Thus, CV results showed that pure 450°C and 350°C annealed samples behaved similarly.

I(a), **II(a)** and **III(a)** showed a current density of 0.03 mA/cm², 0.044 mA/cm² and 0.052 mA/cm² respectively. The current density was similar to the 350°C annealed sample. The current density observed for **III(b)** and **II(b)** were -0.018 mA/cm² and -0.034 mA/cm² respectively. These values were comparable to the values of pure copper and electropolished sample. The peak current value observed for **I(b)** was -0.06 mA/cm². The current intensity at **I(b)** was comparable to pure copper and 350°C annealed sample.

Table 4.5: Average potential values for all samples

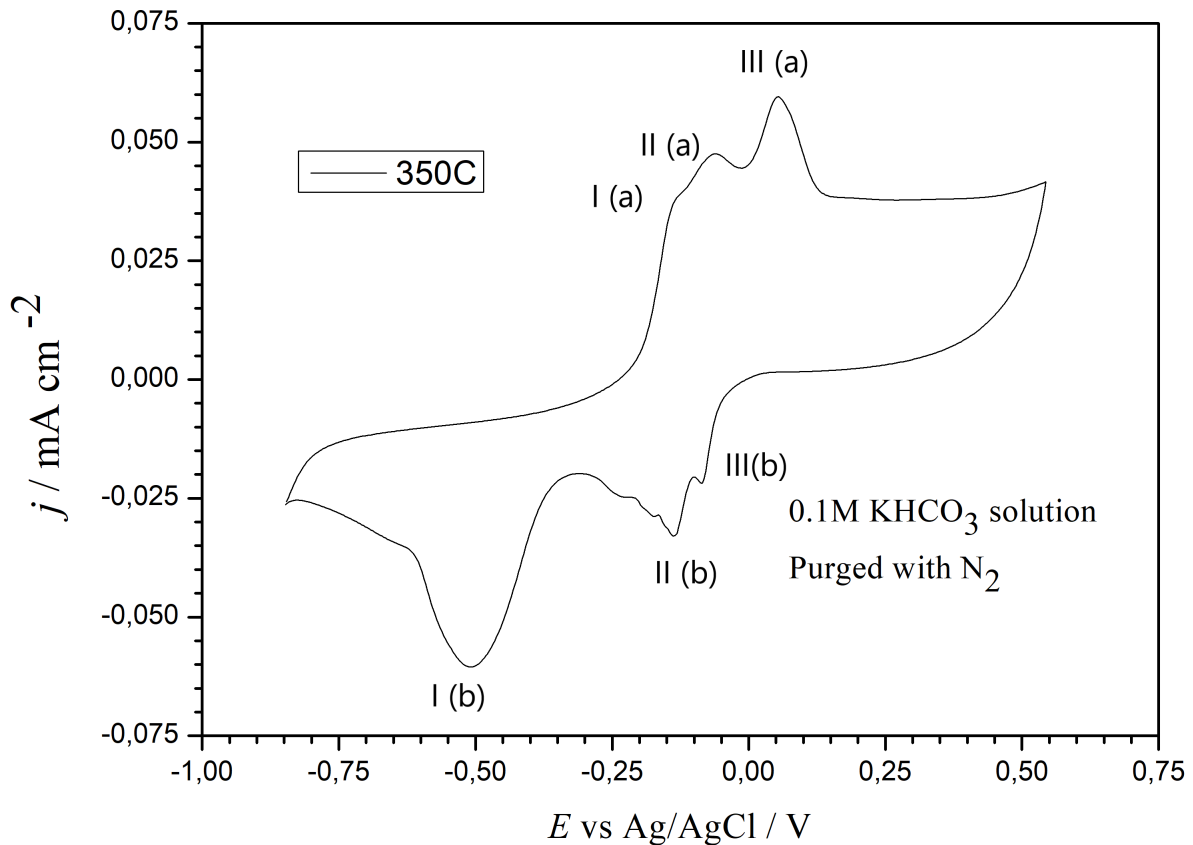|	Potential vs Ag/AgCl / (V)					
	I(a)	II(a)	III(a)	I(b)	II(b)	III(b)
As received	-0.082 ± 0.004		0.102 ± 0.003	-0.607 ± 0.006	-0.185 ± 0.01	-0.131± 0.001
Electropolished	-0.137 ± 0.000	-0.023 ± 0.052	0.055 ± 0.002	-0.492 ± 0.017	-0.113 ± 0.010	-0.064 ± 0.005
350C	-0.130 ± 0.015	-0.044 ± 0.016	0.052 ± 0.003	-0.507 ± 0.021	-0.179 ± 0.050	-0.091 ± 0.001
450C	-0.123 ± 0.009	-0.051 ± 0.000	0.056 ± 0.001	-0.507 ± 0.012	-0.123 ± 0.005	-0.083 ± 0.009

Figure 4.16: CV result of 350°C annealed copper sample

Table 4.6: Average current density values for all samples

	Current density / (mA / cm^2)					
	I(a)	II(a)	III(a)	I(b)	II(b)	III(b)
As received	0.028 ± 0.003		0.050 ± 0.005	-0.063 ± 0.003	-0.029 ± 0.002	-0.020± 0.002
Electropolished	0.034 ± 0.001	0.047 ± 0.007	0.0493 ± 0.005	-0.322 ± 0.192	-0.031 ± 0.005	-0.016 ± 0.012
350C	0.031 ± 0.005	0.046 ± 0.006	0.050 ± 0.008	-0.058 ± 0.003	-0.030 ± 0.002	-0.019 ± 0.002
450C	0.03 ± 0.006	0.044 ± 0.006	0.052 ± 0.007	-0.06 ± 0.004	-0.034 ± 0.003	-0.018 ± 0.003

The data obtained through CV experiments, pointed at a clear formation of Cu_2O product at a potential -0.13V vs Ag/AgCl. Similarly, the reduction of Cu_2O to Cu was observed at a potential around -0.50V vs Ag/AgCl during reverse cycle. These values resembled closely to the values obtained in experiments conducted by *Drogowska et al.* and *Sanchez et al.*[8, 36] The standard deviation calculated in Table 4.5 showed that there was no significant change in the oxidation and reduction potentials of different samples.

From the literature present on cyclic voltammetry on copper in bicarbonate solution, it can be deduced that copper can form three layers on its surface. Study conducted by *Kaluzhina et al.*[19] on copper with 0.1 M $NaHCO_3$ found that in presence of bicarbonate ions and with a pH value of 8, three layered passive structure was obtained for copper. XPS experiments conducted by *Kaluzhina et al.* showed presence of Cu_2O, $Cu(OH)_2$ and CuO layers. Relating the experiments performed in this study to study conducted by *Kaluzhina et al.*[19], the three peaks were interpreted as the products discussed in this section. It is noteworthy that there are other possible reactions that might have occurred during the CV experiments but they are not visible on the voltagramms as the valency of copper ion does not change

Two such possible reactions are

• $2CuO + CO_2 + H_2O \rightarrow CuO*Cu(OH)_2$

• $Cu(OH)_2 + CO_3{}^{2-} \rightarrow CuCO_3 + 2OH^-$

These reactions were not visible on the CV graph but they play a role during the formation of passive layers. Again, the nature of passivity is very complex and based on the literature available related to this research, only informed estimations can be made within the scope of this research. Additional studies might explain the specific reaction mechanisms.

From the experimental results it was observed that the all the copper samples had similar potentials for oxidation and reduction peaks. No major difference was identified between the products formed by each sample. Another interesting phenomenon observed during cyclic voltammetry was the presence of shoulders in the voltagramms. One key aspect which was not highlighted in CV graphs is time. Figure 4.18 shows a part of the CV graph extrapolated on a three-axis curve to explain the concept
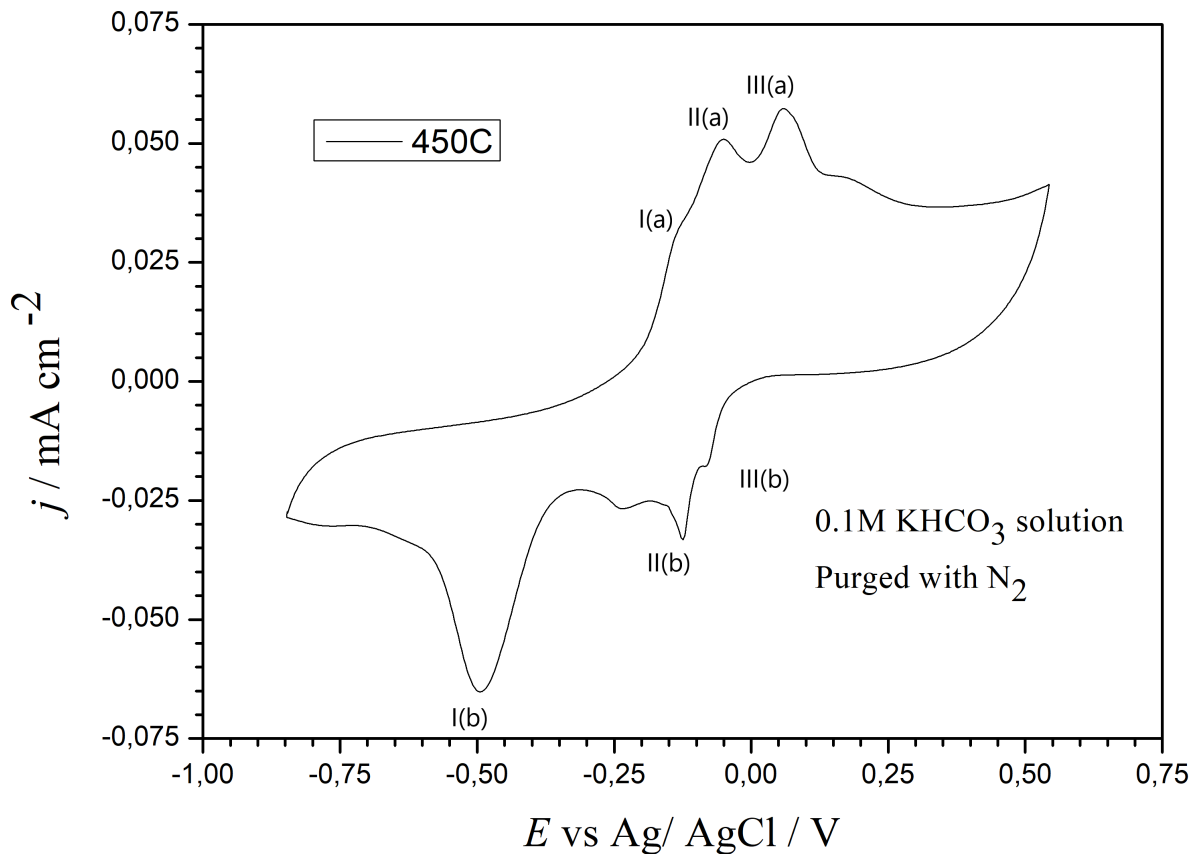
Figure 4.17: CV result of 450°C annealed copper sample

better. From the graph, it can be understood that during a CV experiment when there is a potential increase or decrease, the potentiostat recorded data for a specific moment of time. So, when a peak occurred in the CV graph, it is possible that a significant amount of copper atoms transitioned from a Cu^{1+} state to a Cu^{2+} state which resulted in a peak. Subsequently, when the remaining atoms transitioned after a small time gap, there was a shoulder to indicate the same transition. Hence, CV results should be interpreted with the understanding of this concept that apart from peaks there is a possibility of formation of shoulders in a CV graph, especially at slow scan rates. Figure 4.17 shows the presence of a shoulder after the **III(a)** peak on 450°annealed sample.
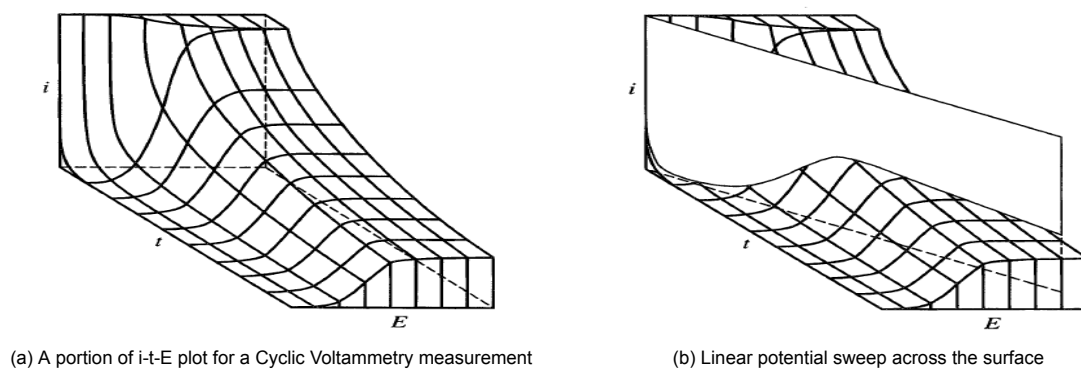
(a) A portion of i-t-E plot for a Cyclic Voltammetry measurement

(b) Linear potential sweep across the surface

Figure 4.18: Section of Cyclic Voltammetry plotted in a three-axis plot. [4]

4.2.2. Electrochemical Impedance Spectroscopy

EIS experiments were performed on samples at OCP (Open Circuit Potential), and the various representative plots for each sample are shown here. For interpreting the data, an equivalent circuit was proposed for each sample. In the equivalent circuit, constant phase element was used to model the circuit instead of a capacitor as the layers were porous, and hence they could not be modelled as an ideal capacitor. Figure 4.20 demonstrates the circuit used for data fitting. Figure 4.19 shows bode plots

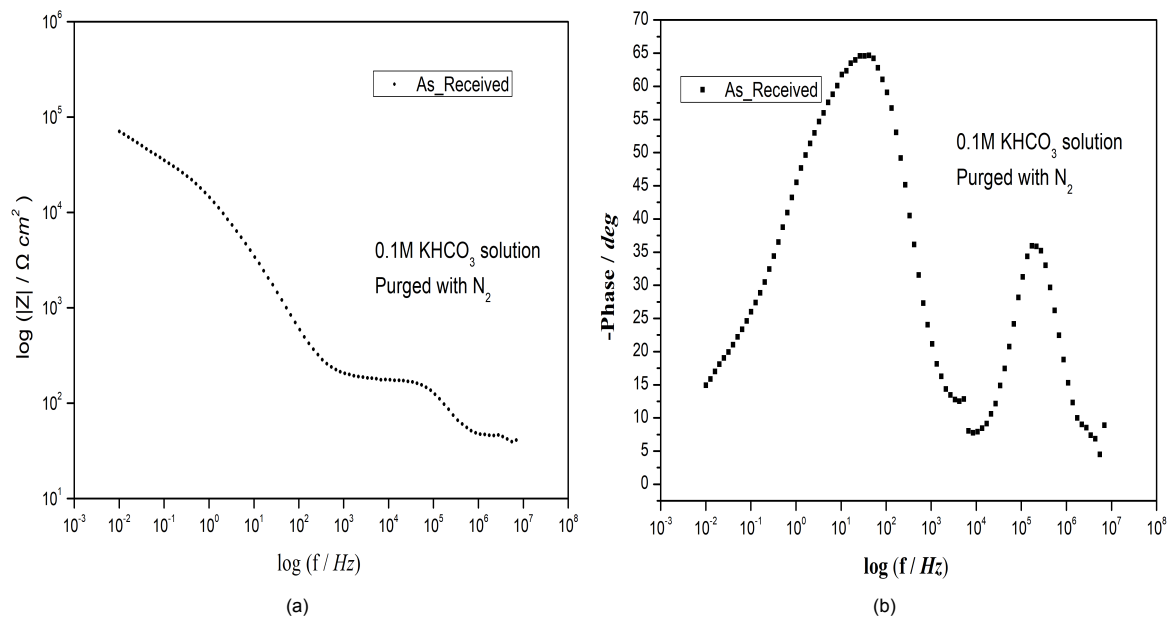obtained for as-received sample. The bode plots for other samples have been demonstrated in Appendix D.

Figure 4.19: Bode plots for as received sample

The circuit consists of resistor **R1** to represent the solution resistance. The constant phase element **CPE1** and its respective resistance **R2** represented the top oxide layer of Cu(OH)$_2$ formed on the copper surface. **CPE2** and resistance **R3** represented the middle oxide layer of CuO. **CPE3** and **R4** represented the innermost and most resistant layer of Cu$_2$O. It should be noted that Cu$_2$O is mentioned as the innermost layer as it is the first product formed when copper is oxidized in a KHCO$_3$ solution. Order of CuO and Cu(OH)$_2$ can not be ascertained with certainty as they form the second oxide and form very close to each other. CV results obtained in this thesis work observed a formation of two Cu^{+2} products but were not sufficient to identify the order of product formation. An exact layer composition has not been determined in the previous studies [19, 43] and is beyond the scope of this research. For the interpretation of EIS results, an equivalent capacitance value was calculated from **CPE** and corresponding impedance values, and were denoted as capacitance **C**. Table 4.7.

The formula used for the calculation of capacitance values is

$$C = (Q * R)^{(1/n)}/(R) \tag{4.1}$$

Here, Q represents the conductivity of the **CPE**, n represents the exponential factor ranging from 0 to 1, describing the behaviour of the capacitor. If the value tends towards 1, the capacitor behaves like an ideal capacitor.[23] Three **R** values represent the impedance value of different resistors associated with different **CPEs**.
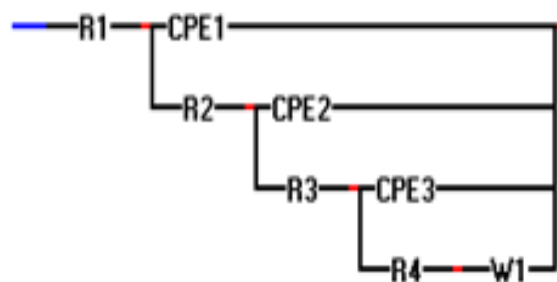
Figure 4.20: Equivalent circuit used for interpretation of EIS results

The Warburg element, **Aw1**, was introduced in the circuit as through data fitting and literature review [50], it was found that Cu reaction in KHCO$_3$ was a diffusion-controlled process, and warburg element helps in simulating the process. In the Nyquist plots (Figure 4.21), around 10,000 Ω cm², a sharp increase in values of **Z''** (the imaginary portion of the impedance), was
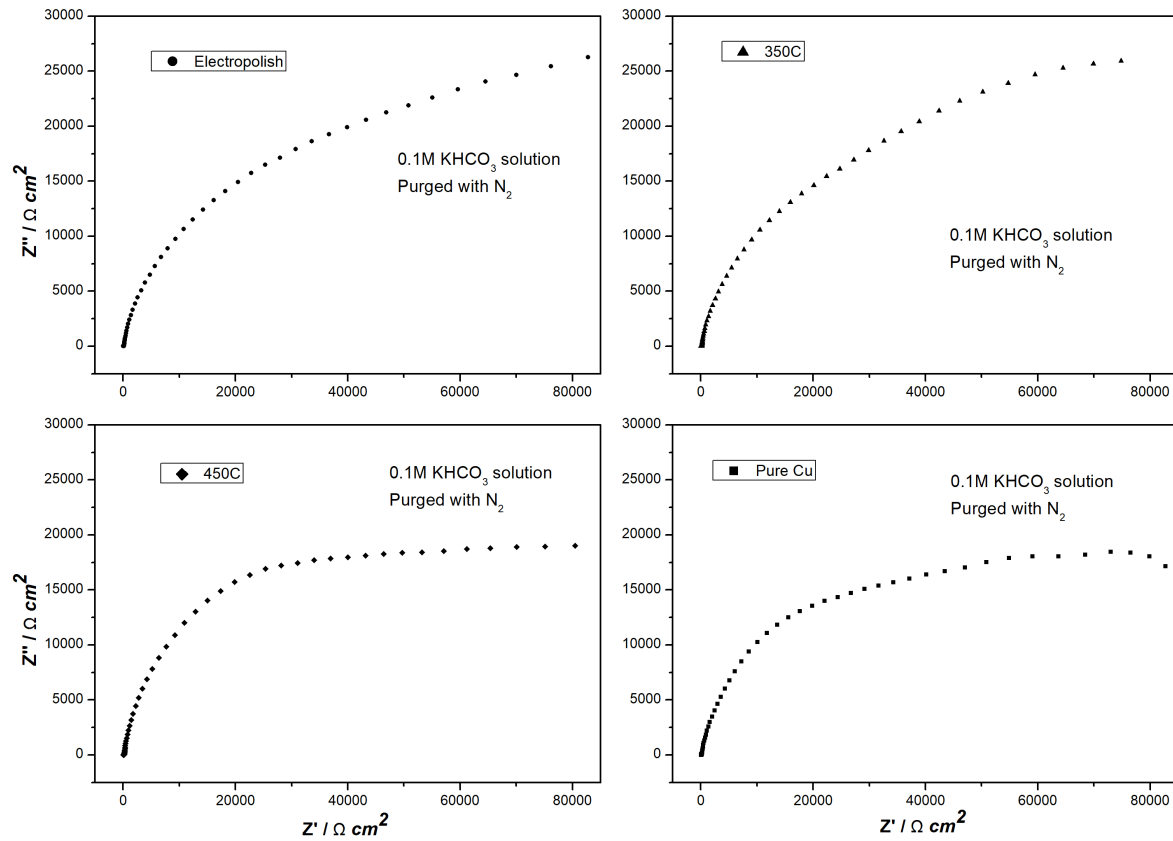
Figure 4.21: Nyquist plots of different samples

observed. Since this increase in slope was around 45°, it indicated the presence of a diffusion-controlled process taking place. This sharp increase in values of **Z''** was more dominant in the electropolished and 350°C annealed sample. Diffusion control in the system meant that the transport in the bulk of the sample was lower than the charge transport at the electrode-electrolyte interface. [41]

Table 4.7: Averaged circuit values for EIS

	R1	R2	R3	R4	Aw1	C1	C2	C3
	Ω cm^2	kΩ cm^2	kΩ cm^2	kΩ cm^2	μF/cm^2	μF/cm^2	μF/cm^2	μF/cm^2
As Received	40.9 ± 1.70	0.14 ± 0.006	7.56 ± 1.18	119 ± 11.62	1.22 E-06	1.28E-02 ± 6 E-04	1.81 ± 0.04	128 ± 7.84
Electropolished	38.5 ± 0.96	0.13 ± 0.004	14.9 ± 0.86	146 ± 10.32	4.92E-07	1.27E-02 ± 3.7 E-04	1.87 ± 0.03	93.8 ± 4.36
350°C	39.2 ± 1.21	0.14 ± 0.004	7.14 ± 2.28	129 ± 7.35	6.09 E-06	1.24E-02 ± 4.2 E-04	1.54 ± 0.02	77.1 ± 4.36
450°C	39.7 ± 1.23	0.14 ± 0.004	17.5 ± 5.40	108 ± 9.61	1.65E-06	7E-03 ± 2.4 E -04	1.67 ± 0.03	42.4 ± 2.80

From the Table 4.7, it can be observed that the average solution resistance (**R1**) was 39.58 Ω cm^2. The (**R1**) values were similar for all the samples as it is a characteristic of the setup. The second resistance **R2** also had an average value of 0.14 kΩ cm^2. The standard deviation amongst the sample was significantly less, and it suggested that the first layer of Cu(OH)$_2$ showed a similar impedance for all samples. Numerical values suggested that the resistance offered by the Cu(OH)$_2$ layer was small and alike for all the samples. Combining the **R2** values with **C1** values offered more insight into the uniformity of the layer. Low **R2** values suggested the top layer offered no insulation to the reaction of copper with the ions present in the solution. 450°C annealed sample had the smallest value for **C1**. Thus, the Cu(OH)$_2$ layer formed on a 450°C annealed sample had the smallest charge buildup across its surface and hence offered the maximum insulation towards reactivity with ions present in the solution.

The **R3** values represented the passive layer of CuO. The average value for **R3** was 11.77 kΩ cm^2 which meant that the second oxide layer formed was more resistant than the top layer. 450°C annealed sample had the highest **R3** value amongst all the samples of 17.4 kΩ cm^2. It also had the highest error value in data fitting of ± 5.40 kΩ cm^2 which meant the value could be even higher or close to 12 kΩ cm^2. Going further with original calculated data and considering **C2** values, it was seen that 450°C showed the most negligible capacitance value of 7E-03 μF/cm2 which meant that charge build-up across the oxide layer was least for **C2**, and it provided maximum insulation. **R3** values for 350°C annealed sample was the least. It means CuO or theCuO layer formed on 350°C annealed sample had the least resistance from corrosion. The **C2** value was 1.24E-02 μF/cm^2 for the 350°C annealed sample. It was higher than the 450°C samples, and thus the **C2** and **R3** values were in harmony with each other. From the high values of **R3** it could also be deduced that it had a more uniform structure than Cu(OH)$_2$ layer.

The **R4** values represented the innermost oxide layer of Cu$_2$O. The average value for **R4** was 125.42 kΩ cm^2. Thus, the innermost layer had higher reactivity insulation compared to other oxide layers. It meant that the layer was most uniform and

had higher charge resistance. The average capacitance value, **C3**, associated with this layer was 85.32 $\mu F/cm^2$, which was the highest amongst all the three oxide layers. It meant that the charge formation across this layer was very high too. This layer was closest to the metal surface, and as copper tends to react with oxygen, hydroxide and carbonate ions in the solution, it reacted closely with the metal surface and the subsequent layer formed on it, creating a high charge across the double layer. It also hinted about the layer's porosity and suggested a porous stacked-layer formation. Among different samples, the electropolished sample had the highest value of 146 $k\Omega$ cm^2 for **R4**, indicating the Cu_2O layer formed on the electropolished sample was most stable and insulating. The calculated **C3** values did not entirely support this reasoning as the electropolished sample had the second-highest **C3** value of 93.8 $\mu F/cm^2$. It meant that even though the electropolished sample had a uniform and stable Cu_2O layer , the charge build-up across the layer was very high. The 450°C annealed sample had the lowest value of **R4** amongst all the samples, which meant that its uniformity was low compared to other samples. However, the C3 value associated with the 450°C sample was 42.4 $\mu F/cm^2$, which was the lowest value. It meant that even though the Cu_2O layer offered the least protection from external ions for 450°C annealed sample, the charge build-up across this layer was the least too. It hinted that the 450°C annealed sample showed less inclination towards being reactive at this layer.

Finally, **Aw1** values associated with the samples were calculated too. **Aw1** was found to be the least for the electropolished sample with a value of 4.92E-07 $\mu s^{-1/2}$. It meant that the electropolished sample had the most negligible affinity towards oxygen, carbonate and hydroxide ion diffusion on its surface. It was because of the strong oxide layers formed on the surface of electropolished sample. As all the oxides formed on Cu samples had oxygen element in them and, it can be concluded that the sample which showed higher reactivity to oxygen was the most reactive. The EIS experiments conducted found that 350°C annealed sample showed the highest affinity towards oxygen diffusion as it had the highest **Aw1** value of 6.09 E-06 $\mu s^{-1/2}$.

EIS gave a good insight into the electrochemical behaviour of different copper samples and how they interacted with 0.1 M KHCO$_3$ solution. From the EIS results, it was observed that there was a clear formation of three oxide layers on copper surface. It confirmed the observation of CV results, where there was a clear formation of three products. On further analysis it was found that, different layers of different samples behaved in a contrasting manner. The CuO layer and Cu(OH)$_2$ layers offered maximum resistance for 450°C annealed sample and the capacitance values were found to be low on them too. On the other hand, for the electropolished sample, the Cu_2O layer had the highest **R4** values which suggested the formation of a strong resistant layer. Though, this observation was challenged with high **C3**, the associated capacitance of the layer, which meant that even though, the electropolished sample had the most resistive Cu_2O layer, the charge build-up across its surface was high. Finally, the **Aw1** component of the circuit was found to be common across all the samples and it signified that all the reactions were dominated by oxygen diffusion on the on the sample surfaces. It should be noted that diffusing ions can not be ascertained with conviction as the KHCO$_3$ solution has many dissolved ions and further studies would be needed for clarification.
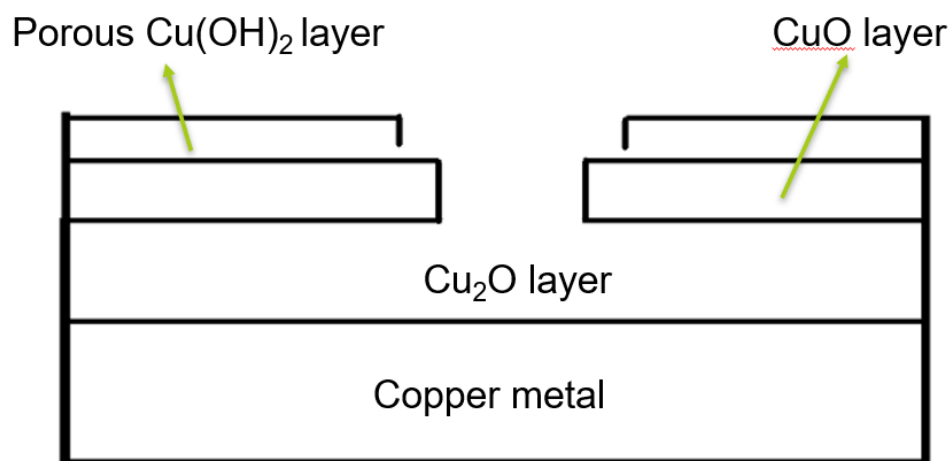

Figure 4.22: Schematic for oxide layer formation on Copper

The most important inference from EIS experiments was the tentative model that came out due to interpretation of EIS results. In practice, the EIS results are fitted to a simple model but this was not the case of reaction of copper with KHCO$_3$ solution. Many circuits were used and in the end a circuit with three passive layers was finalized. Work done by *Kaluzinha et al.* and *Drogowska et al.* [8, 19] showed that interaction of copper with NaHCO$_3$ formed a complex layer structure with presence of oxide, carbonate, hydroxide and carbon ions on the surface of copper metal. Figure 4.22 shows the proposed schematic for the interaction of copper with KHCO$_3$. The layers formed on the copper were concluded to be porous as EIS results pointed out towards a diffusion based passivation. O_2 and CO_3^{2-} could be proposed to be the primary diffusing ion on the copper surface. As presence of oxygen was scarce, it was considered to be the limiting atom for the diffusion process. Though, the model circuit(Figure 4.20) emerged as a product of result fitting, XPS would be required to verify the exact composition of the layers. Figure 4.22 represents a schematic for different oxide layers formed due to Cu-electrolyte interface. Originally, the layers are intertwined amongst each other and are not this uniform. Furthermore, as layers are porous, they will have micro-pores throughout their structure instead of just a big opening in the centre. Moreover, EIS results showed that the nature of passivation films varied amongst different samples. **R4** values were found to be the highest, 146 $k\Omega cm^2$ for electropolished sample. Due to flat surface of electropolished sample the fist layer formed on sample was more uniform. Though, a single reason can not be attributed to the high values of **R4** as electropolished sample had second highest **C3** value of 93.8μF which meant that they had a high porosity as well. As the chemical insulation of thin films depends on factors like thickness, uniformity and porosity of the layer, it is tough to pinpoint a single reason for this behaviour of **R4** values. The passive layers have a complex morphology

which need further analysis to be completely understood.

4.3. CO$_2$ reduction

CO$_2$ reduction was performed on two independently prepared samples, and their averaged production yield for different samples have been tabulated in Table 4.8.

For the as-received sample, the total faradic efficiency (F.E.) was reported to be 84.15%. The maximum F.E. was observed for hydrogen. The F.E. for hydrogen production was 49.5%, and a standard deviation of 9.5% was observed between the two trials. The second most produced product was formate with an F.E. of 21.15%. As received sample yielded only ethene (C$_2$H$_4$) as 2e$^-$ product with a faradic efficiency of 5.5%. Apart from these products, carbon monoxide (CO) with an F.E. of 6% and methane (CH$_4$) with an F.E. of 2% were recorded.

Table 4.8: CO$_2$ reduction results

Product distribution (%)	As Received Averaged	As Received Std. Deviation	Electropolished Averaged	Electropolished Std deviation	350°C Averaged	350°C Std. Deviation	450°C Averaged	450°C Std. Deviation
H$_2$	49.5	9.5	37.5	1.5	44	4	55.5	5.5
CO	6	0	6,5	0.5	5	0	4	0
CH$_4$	2	1	4.5	2.5	4.5	0.5	1.5	0.5
C$_2$H$_4$	5.5	3.5	11	2	8.5	0.5	4.5	1.5
Formate	21.15	3.55	19.75	2.05	19.2	0.1	16.6	0.5
Ethanol	0	0	3,15	0.65	0.95	0	0	0
Acetone	0	0	0	0	0	0	1.35	0.05
1-propanol	0	0	1.4	1.4	0	0	0	0
Total F.E. %	84.15	1.45	83.8	2.5	82.15	3.85	83.45	2.95

For the electropolished sample, the total F.E. was observed to be 83.8%. Again, hydrogen had a maximum F.E. of 37.5%, which was a 12% reduction compared to the as-received sample. Like the as-received copper sample, formate had the second-highest F.E. of 19.75%. The third highest F.E. of 11% was observed for C$_2$H$_4$. The electropolished sample also had yields of ethanol 3.15% and 1-propanol 1,4%. CO and CH$_4$ showed yields of 6.5% and 4.5%, respectively. Ethanol and 1-propanol were unique to the electropolished sample. Another thing that should be noted was that the electropolished samples had the highest F.E. devoted directly to the production of hydrocarbons. Thus, it can be concluded that electropolished samples were more efficient in suppressing hydrogen evolution reactions than other samples at -1.0 V vs RHE.

Experiments performed on electropolished sample by *Kuhl et al.*[22] at -1.01 V vs RHE yielded similar results with hydrogen, methane, formate, carbon monoxide and ethylene as major product. Exact F.E. at this potential was not provided, but the major products identified were similar to the results obtained by *Kuhl et al.*.

For the 350°C annealed sample, total faradic efficiency of 82.15% was observed. H$_2$ again had the maximum F.E. of 44%. Formate had the second-highest F.E. of 19.2%, and the third-highest was C$_2$H$_4$ with an F.E. of 8.5%. Other products observed were CO with an F.E. of 5%, CH$_4$ with an F.E. of 4.5% and ethanol with the smallest F.E. of 0.95%. 350°C annealed sample had the smallest F.E. amongst the four samples considered. It was probably because of the low **R4** values observed in EIS values which meant that the Cu$_2$O layer was the weakest for 350C annealed sample. A less chemically insulating layer meant that the sample had the weakest protection against poisoning by oxygen, carbonate and hydroxide ions.

For the 450°C annealed sample, a total F.E. of 83.45% was observed. The F.E. of H$_2$ was found to be 55.5% which was the maximum amongst all the samples. The second highest yield was for formate with F.E. of 16.6%, and the third-highest was C$_2$H$_4$ with an F.E. of 4.5%. Acetone was also observed with an F.E. of 1.35%, and it was found to be unique to this sample. Other products observed were CO with an F.E. of 4%, CH$_4$ with an F.E. of 1.5%.

From the results obtained, it can be inferred that electropolished samples had the best ability to suppress hydrogen evolution reaction as they gave the best results in terms of hydrocarbon production. It can be due to the favour of efficient CO production in the electropolished sample as CO acts as an intermediate for many hydrocarbon products via CO$_2$ reduction.[5, 30] Another significant observation was the highest hydrogen evolution F.E. of 55.5%. on 450°C annealed sample.

The CO$_2$ reduction results obtained during this thesis gave an insight into the working of copper catalyst and how electropolishing affected CO$_2$ reduction. Work done by *Shibata*[45] highlighted the impact electropolishing has on the surface of copper. *Shibata*[45] found that electropolishing decreased the interaction of hydroxide ions on the surface as electropolished samples already had a strong passive oxide layer. The non-electropolished copper surface on the other hand were more susceptible to interaction with hydroxide ions which leads to poisoning of catalyst sites on interaction of KHCO$_3$ purged with CO$_2$. EIS experiments conducted during this thesis work, also indicated a similar result, as electropolished sample had the highest **R4** values for Cu$_2$O. This possibly led to better interaction of CO$_2$ with oxide surface and resulted in higher hydrocarbon production.

As hydrocarbon formation and HER (Hydrogen Evolution reaction) are competitive reactions during CO$_2$ reduction it can be concluded that electropolished copper surface suppressed hydrogen evolution more effectively and gave priority to hydrocarbon formation. Figure 4.24 gives an idea of difference between the interaction of hydroxide ion on electropolished and non-electropolished copper sample. As the copper used for this thesis was 99.999% pure, Figure 4.24 gives a good estimate of hydroxide formation on the samples.

The reasoning given by *Shibata*[45] was in conformity with the impact of electropolishing explained by *Palmieri et al.* [35] Electropolishing created a strong passive layer on the Cu sample, therefore the poisoning of the copper sample due to impurities in the solution might be delayed. This led to availability of more catalytic copper sites during the CO$_2$ reduction which in turn increased yield of hydrocarbons. *Lee et al.*[25] found that presence of Cu$_2$O layers on the copper surface decreased the graphite adsorption on copper surface which poisoned the copper surface and reduced the hydrocarbon formation F.E. of copper. Decrease in active number of copper sites for CO$_2$ reduction could be a major reason why non-electropolished sample produced more hydrogen than hydrocarbons during the experiments conducted for this thesis.

Verdaguer-Casadevall et al.[51] found that copper samples with a strong oxide layers on their surface reduced CO$_2$ into hydrocarbons better as the CO molecules bonded better with the oxide layers. As CO is an intermediate product during the formation of hydrocarbons, better binding led to more time for further hydrogen and CO$_2$ to react with the CO molecules bonded
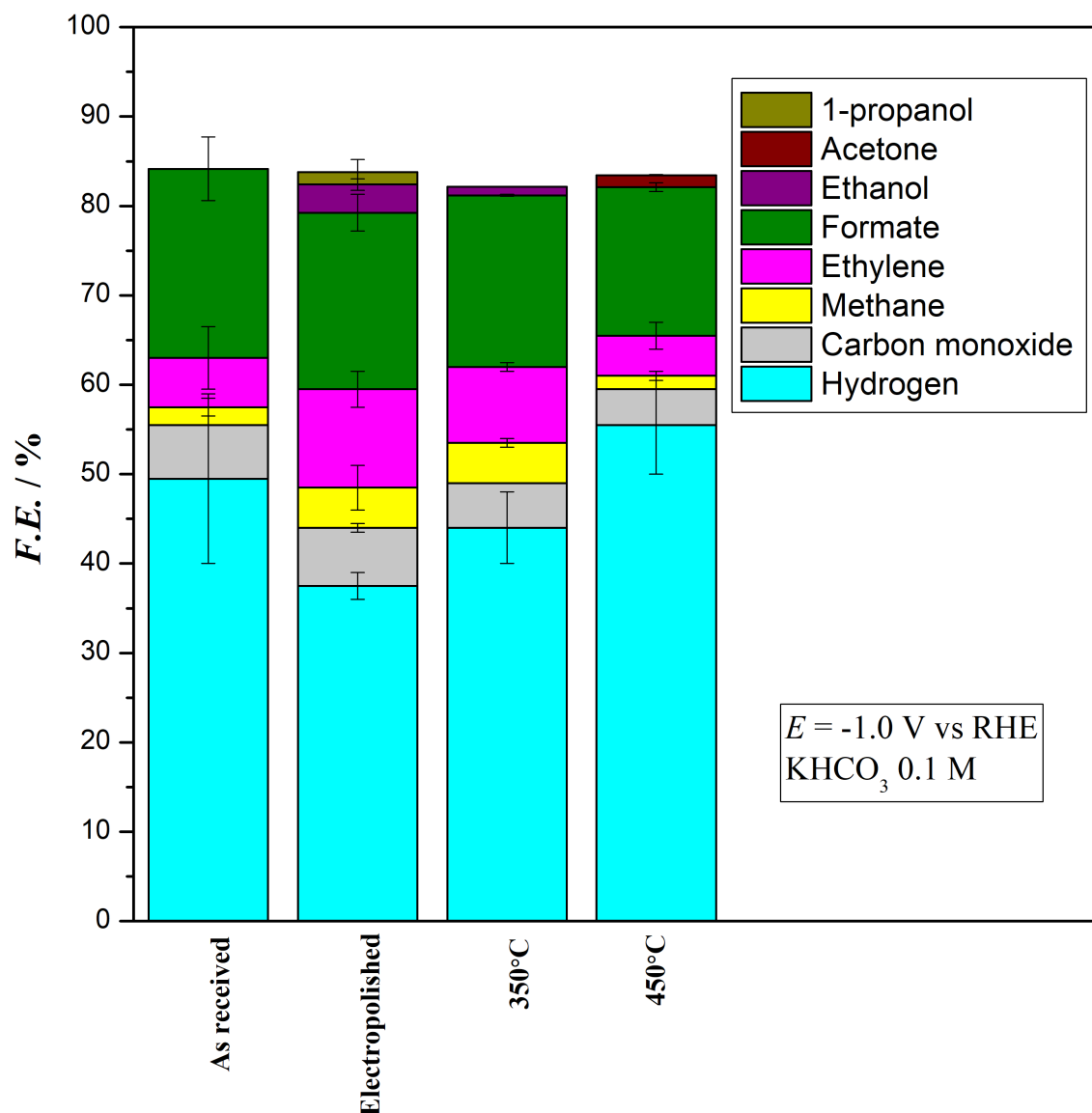
Figure 4.23: Result of CO_2 reduction experiment

on the surface. *Ooka et al.*[34] concluded in their study that HER and hydrocarbon formation were competing reactions which occurred simultaneously on the copper sample. Adsorption of CO on the sample surface was found to be the major reason for the inhibition of competing HER reaction. This supported the findings of the study done by *Lee et al.*[25] and *Shibata* [45] which followed the findings of the experimental work done for this thesis. EIS results from this thesis work also pointed towards the evidence that electropolished samples formed the most resistant oxide layer.

Another interesting feature observed was the production of acetone in 450°annealed sample. This could be because of the change in dominant planar orientation due to annealing of copper sample. *Hori et al.*[13] found that when CO_2RR was performed on differently orientated single crystal electrodes of copper under same experimental conditions the products varied significantly. As acetone was not produced by any other sample, it is highly probable that 450°annealed sample had a different dominant planar orientation than the rest of the samples. XRD results showed that after annealing the Cu samples had a high intensity peak of Cu(311) planar orientation and varied average concentration of Cu(100), Cu(220) and Cu(200). This gave a hint towards change in planar orientation due to annealing. EBSD measurements would be required to graph the overall planar orientations and verify the hypothesis.

In general, the increase in grain size of copper samples did not have a major impact on CO_2 reduction products and their faradic efficiencies. It is possible that the impact of grain size could not be properly investigated as the annealed samples were not electropolished. Work done by *Li et al.*[26] suggested that annealing the copper samples reduced the reduction potential of certain hydrocarbons and it is possible that products like ethanol and 1-propanol which were not present for 350°and 450°annealed sample could be observed at a lower potential. Thus, it is an interesting avenue of research for future work.

The overall change of electrodes and their subsequent impact on CO_2 reduction can not be entirely estimated from this study. As the CO_2 reduction experiments were carried on a fixed potential of -1.0 vs RHE, to get a better idea, CO_2 reduction needs to be performed on a broad range of potentials and for a more extended amount of time. It would also be interesting to

(a) Electropolished sample   (b) Non-electropolished sample
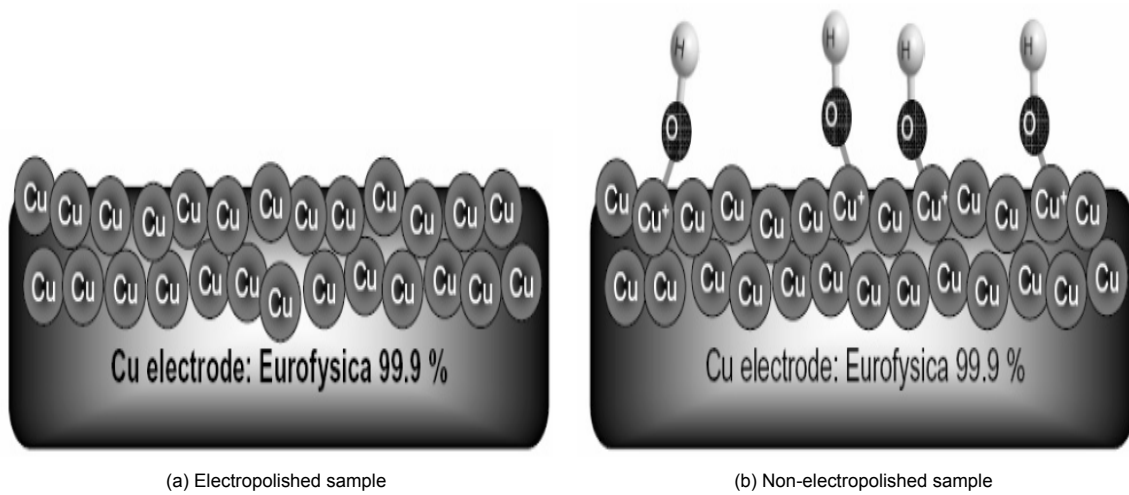
Figure 4.24: Difference in oxide layer formation due to electropolishing[45]

electropolish the annealed samples and study the impact of grain size increase as it has not been studied extensively before.

5

Conclusions

Copper has shown a promising quality to reduce CO_2 into useful products electrochemically. However, some pitfalls as a catalyst hindered its progress from being used at an industrial scale. The major problems with copper are its high over-potential, low deactivation time, and uncontrollably varying product selectivity. From the literature study, it was found that the interaction of polycrystalline copper with $KHCO_3$ has not been studied extensively. This thesis tried to bridge the gap between the microstructural changes on copper and its subsequent effect on CO_2 reduction.

From the thesis work, the following conclusions can be drawn.

- Annealing the copper samples increased the grain sizes linearly. Grain coalescence was observed on the annealed samples. Copper samples annealed at 350°C and 450°C with grain sizes of 2943μm and 3794μm were considered for further analysis.

- XRD results indicated the loss of rolling direction and grain growth based on surface energy on the 350°C and 450°C annealed samples.

- Cyclic voltammetry results demonstrated the formation of three oxidation and reduction products. All the samples had similar redox reaction products and potentials.

- EIS results concluded the formation of a three passivation layer model on all the copper samples with Cu_2O the innermost layer, CuO the middle layer and $Cu(OH)_2$ the topmost layer. The layers were porous, and the reaction of copper was diffusion controlled by oxygen.

- Electropolished sample had the highest Cu_2O layer resistance of 146 kΩcm^2 compared to other samples. The smooth surface of the electropolished sample seemingly helped form a more robust Cu_2O layer as the bonding of copper and oxygen is better on smooth surfaces.

- As-received copper sample was found to have the highest F.E. of 84.15% amongst all the samples. The electropolished sample had the highest F.E. for production of hydrocarbons of 46.3% while 450°C annealed sample had the lowest with 27.95%.

- The electropolished sample was found to have a higher F.E. for hydrocarbon production because of its ability to suppress the competing hydrogen evolution reactions. The non-electropolished samples, on the other hand, were susceptible to promoting hydrogen evolution reaction over hydrocarbon production due to catalyst poisoning with $Cu(OH)_2$.

- The results were inconclusive to comment on the overall impact of microstructural changes on CO_2RR as the experiments were carried on a fixed potential of -1.0 vs RHE. Nevertheless, the study established an excellent premise for further study as the formation of acetone on 450°C annealed sample and high F.E. for H_2 on non-electropolished sample open up exciting avenues for further research.

6

Future Recommendations

The thesis work undertaken covered the impact of microstructural changes in copper and its effect on CO_2 reduction. The experimental results gave insight into the behaviour of copper in $KHCO_3$ and how different samples performed differently under these conditions. As such, the results opened up avenues that can prove to be of vital importance in understanding the behaviour of copper in $KHCO_3$ and the interaction of various samples with CO_2 reduction. A few facets of the research were uncovered from work undertaken that were not worked on during this thesis, and this chapter enlists them for future considerations. Following are the areas where further work can be done.

- To better understand the impact of annealing and supplement the knowledge obtained from annealing, EBSD should be performed on the copper samples. EBSD would help quantify planar orientations and better understand how planar orientations changed with annealing. EBSD would also help relate the CO_2RR products to specific samples as it is known from literature study that planar orientation impacts CO_2RR products.

- Microstrain and ECSA of the different samples should be calculated and considered to study the copper samples' electrochemical behaviour differences.

- XPS measurements should be performed on the samples which underwent EIS measurements to verify the formation of products proposed from this study. Low and high-resolution XPS measurement can help in understanding the layer composition and help quantify the presence of different products on copper samples exposed to $KHCO_3$.

- CO_2 reduction experiments should be performed on voltages other than -1.0 vs RHE to understand the consequences of annealing and electropolishing of copper samples better. Different potentials would help generate a more varied product distribution and might help paint a better picture of how products vary with microstructural changes.

- Lastly, electropolishing the annealed samples and performing CO_2 reduction on annealed samples could result in exciting results as increased grain sizes might impact the formation of subsequent Cu_2O layers on the copper sample and result in interesting findings.
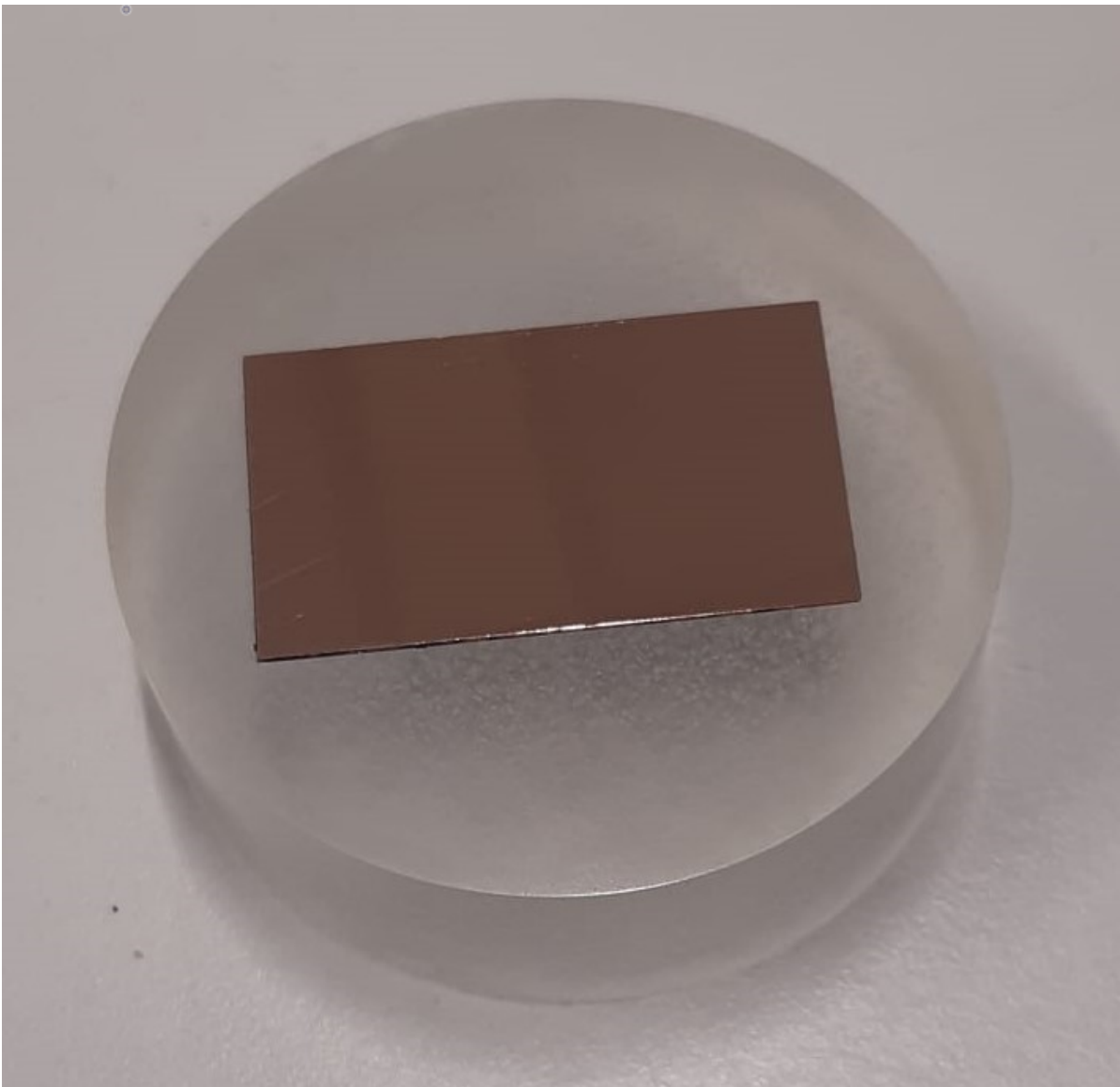
A

Appendix:Experimental setup

Figure A.1: Copper sample prepared in cold mounting resin

Figure A.2: Electrochemical cell used for CV and EIS measurement

B

Appendix:XRD results

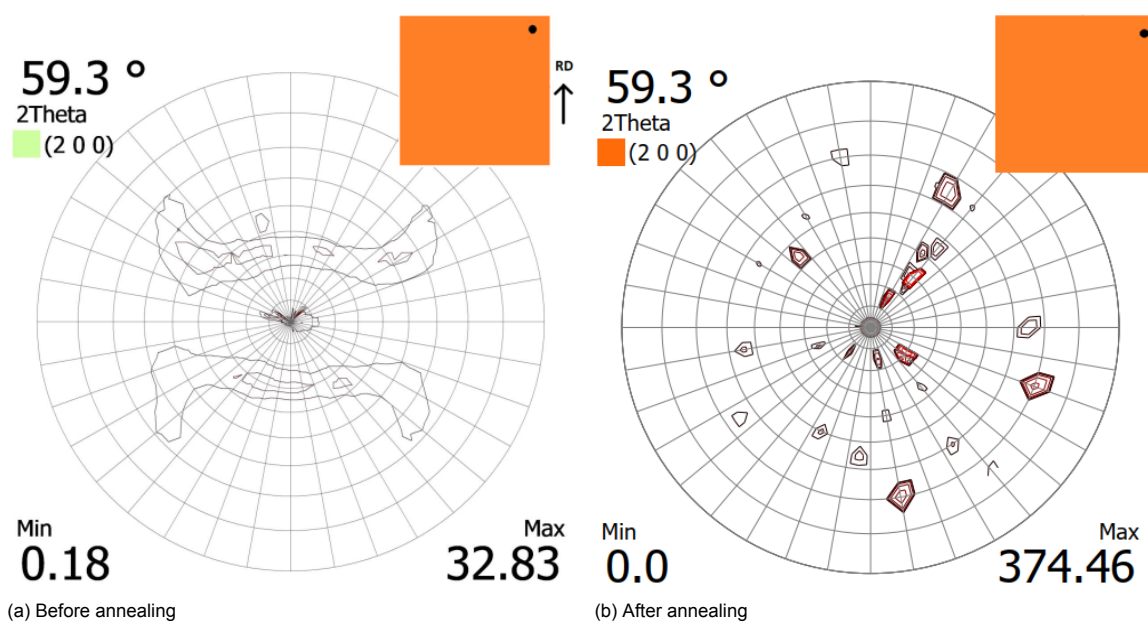The results of texture measurements have been attached in this section.

(a) Before annealing

(b) After annealing

Figure B.1: Texture results for 350°C at 59.3°.

88.8 °
2Theta
■ (2 2 0)

RD
↑

Min
0.18

Max
5.42

(a) Before annealing

88.8 °
2Theta
■ (2 2 0)

Figure 3 (220) pole plot sample "Cu 2a annealed 350C "

Min
0.01

Max
307.99

(b) After annealing
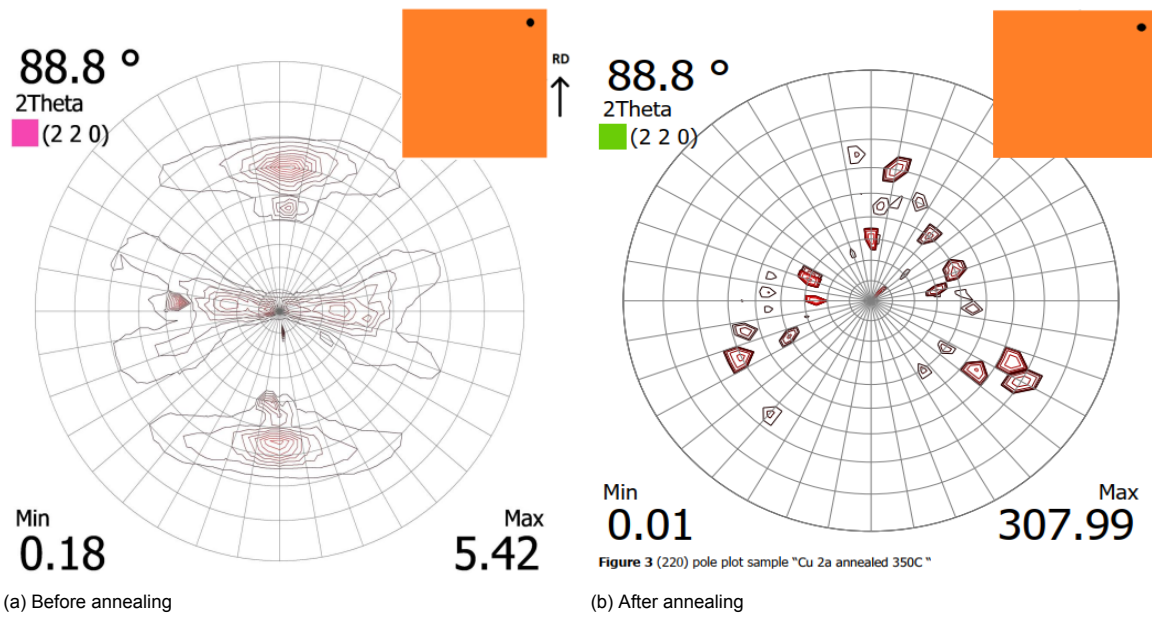
Figure B.2: Texture results for 350°C at 88.8°.

59.3 °
2Theta
■ (2 0 0)

RD
↑

Min
0.22

Max
7.85

(a) Before annealing

59.3 °
2Theta
■ (2 0 0)

Min
0.08

Max
159.89

(b) After annealing
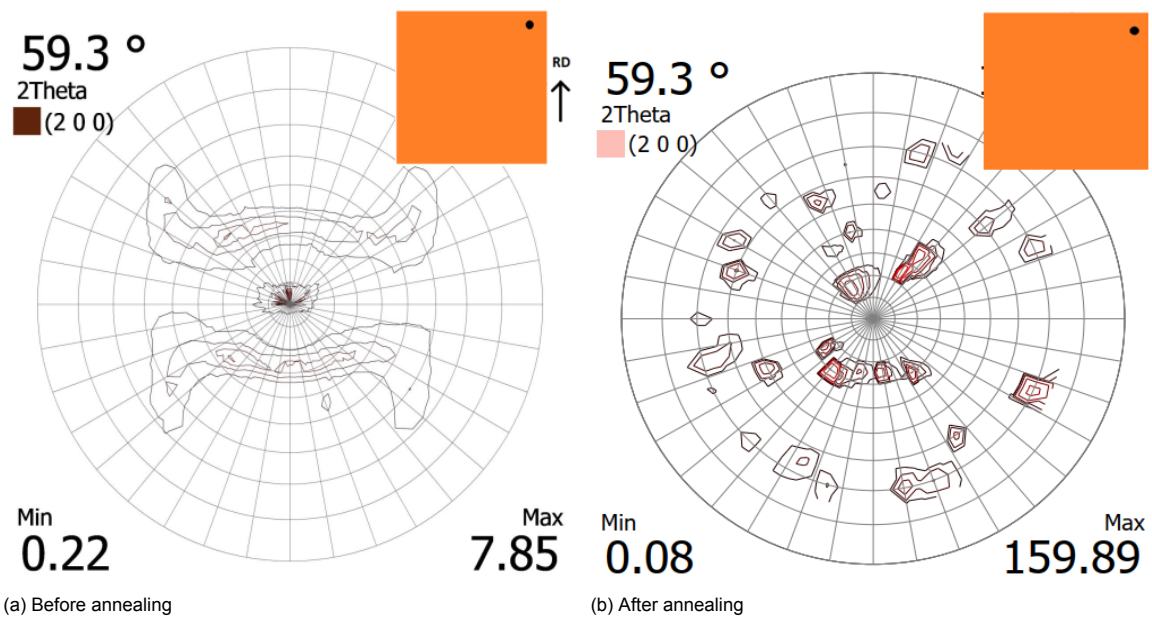
Figure B.3: Texture results for 450°C at 59.3°.

88.8 °
2Theta
(2 2 0)

RD

Min
0.2

Max
7.53

(a) Before annealing

88.8 °
2Theta
(2 2 0)

RD

Min
0.2

Max
7.53

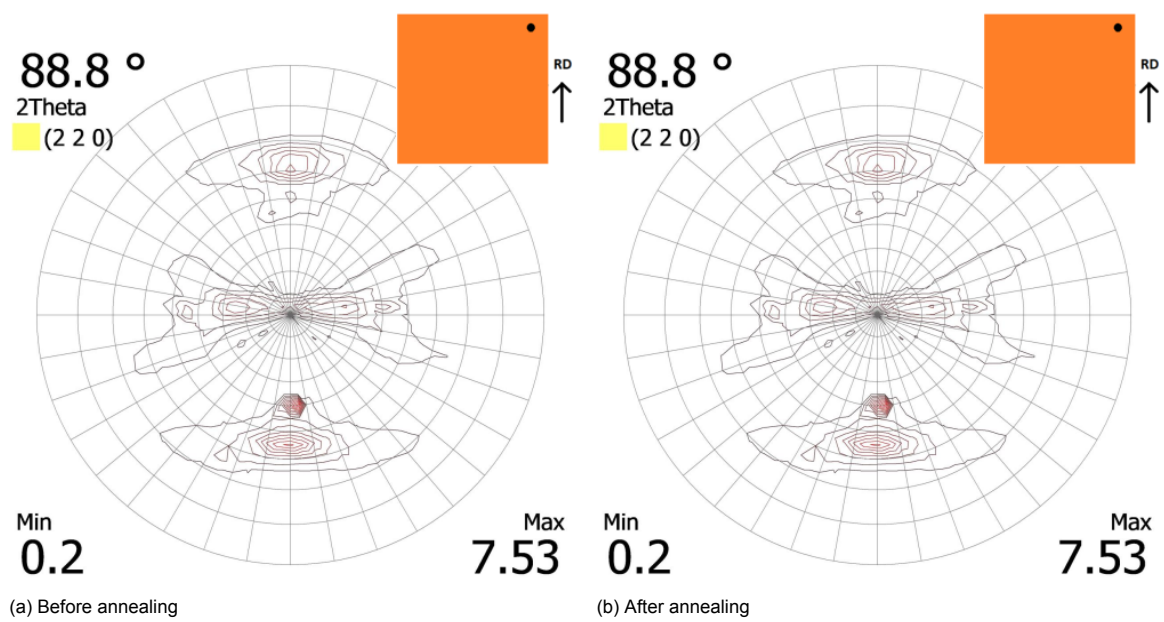(b) After annealing

Figure B.4: Texture results for 450°C at 88.8°.

Appendix:CV results

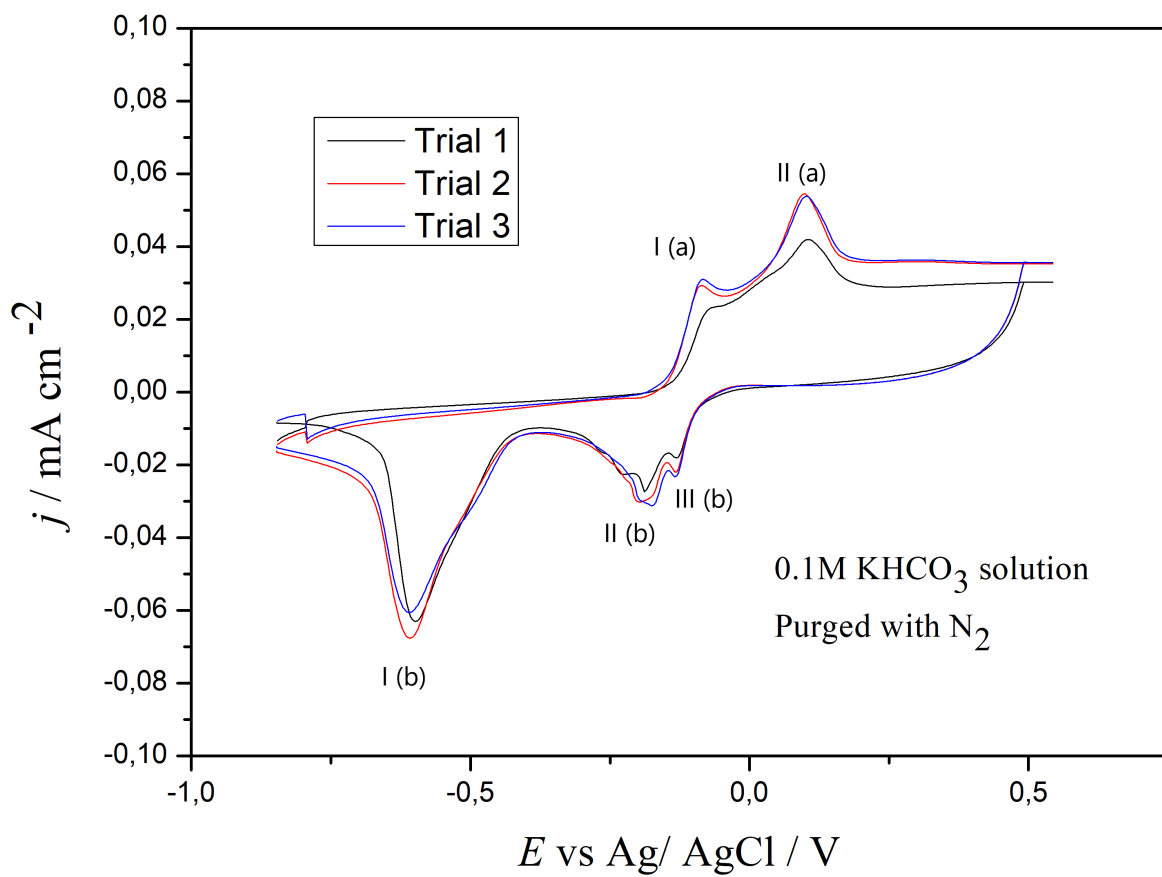The combined results of all the trials have been given here.

Figure C.1: Combined CV results of as-received copper sample
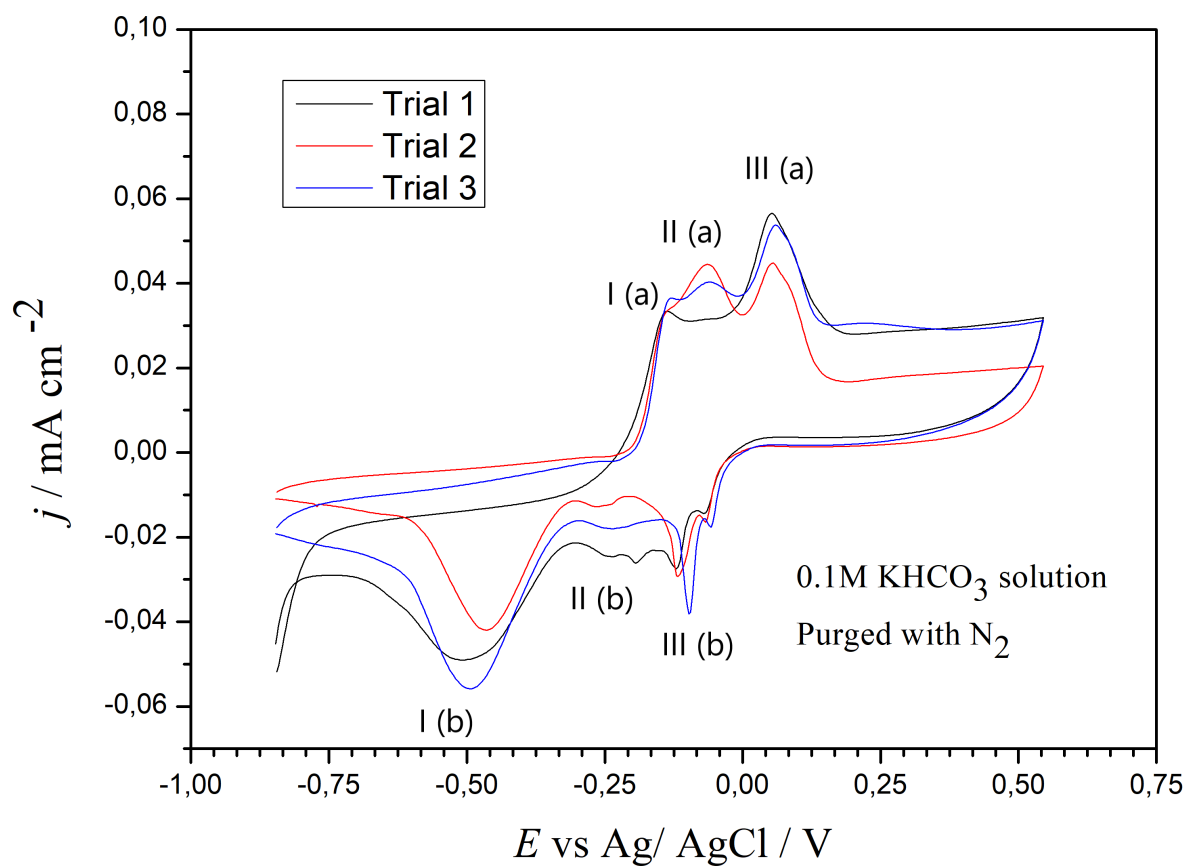
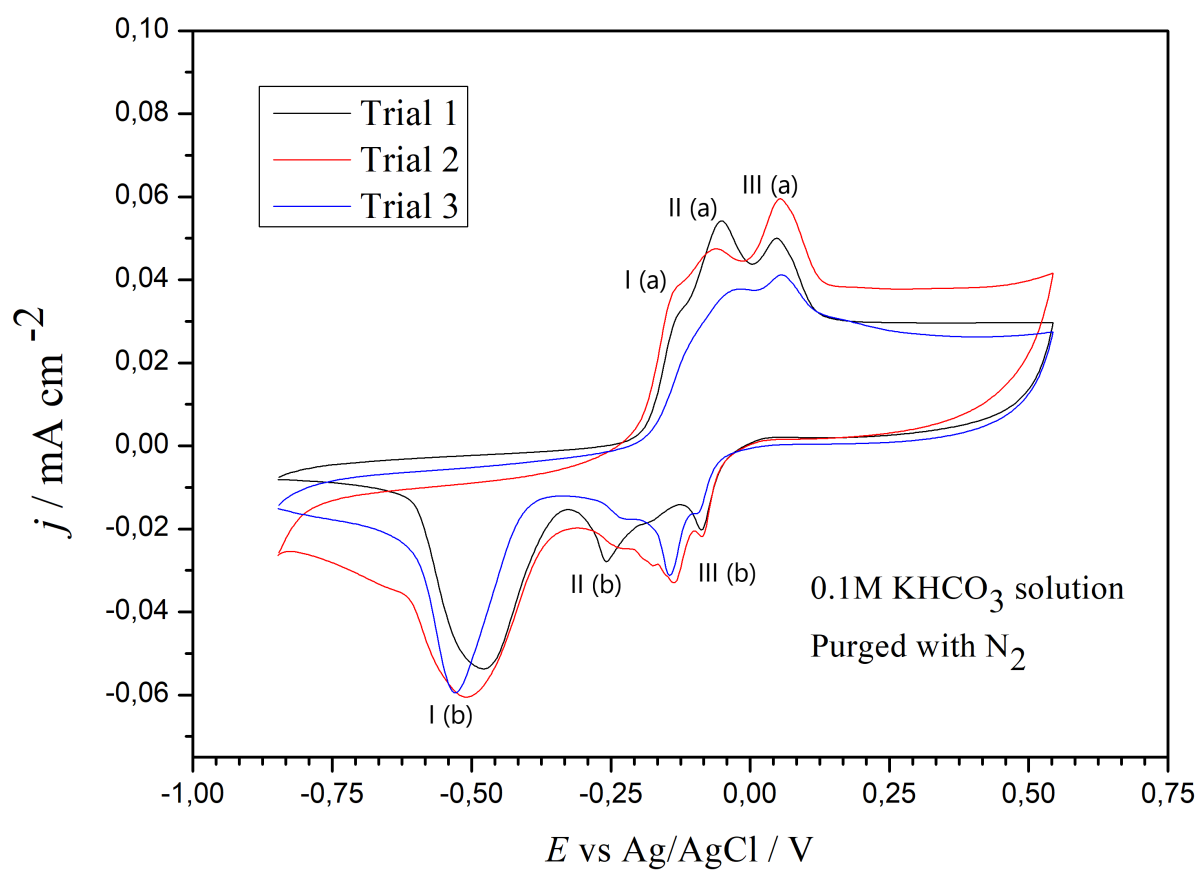Figure C.2: Combined CV results of electropolished copper sample

Figure C.3: Combined CV results of 350°C annealed copper sample

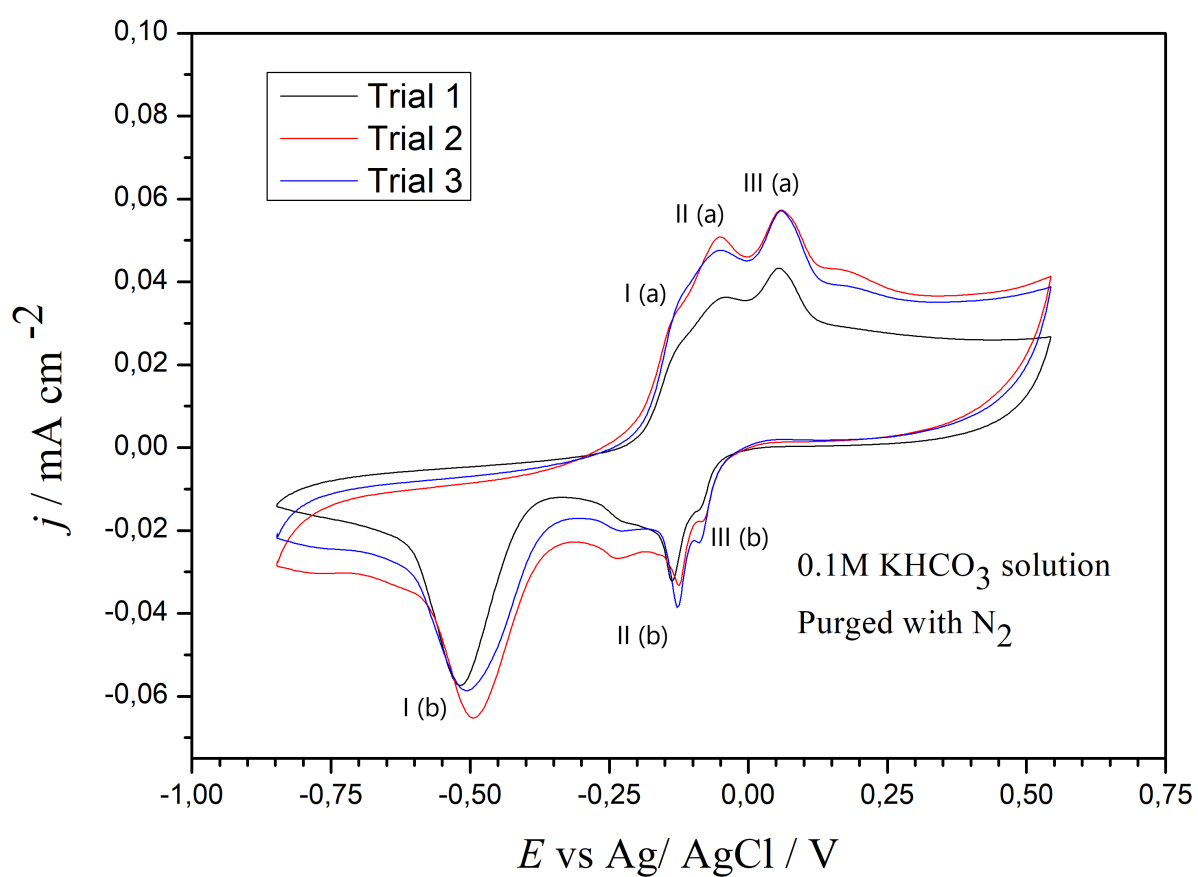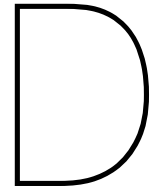Figure C.4: Combined CV results of 450°C annealed copper sample

D

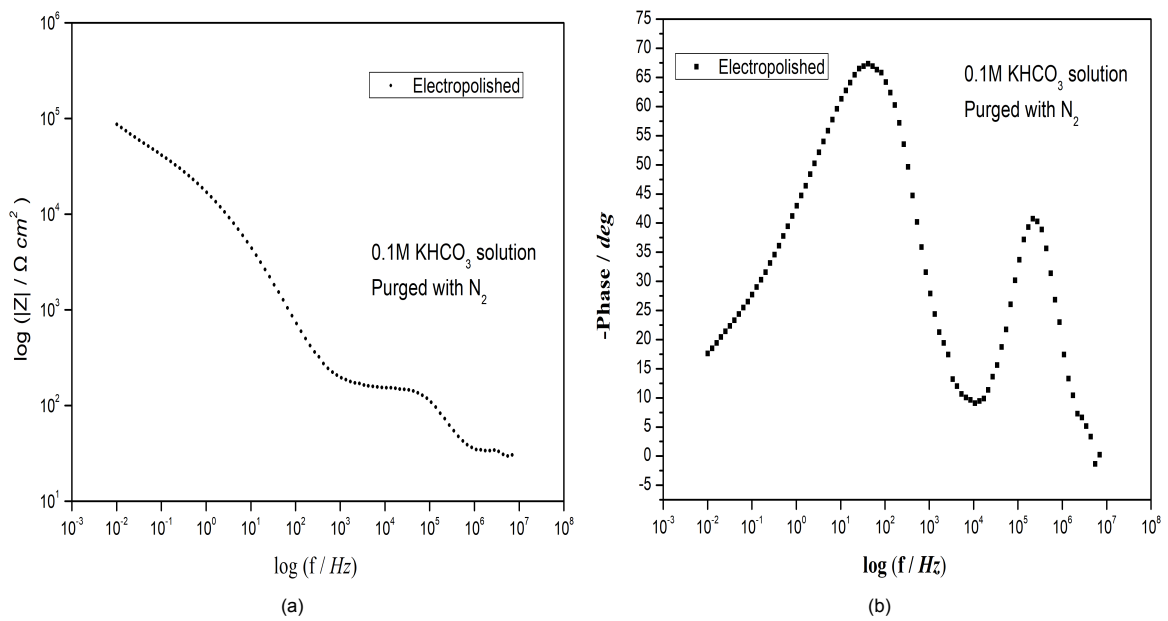## Appendix:EIS results

(a)

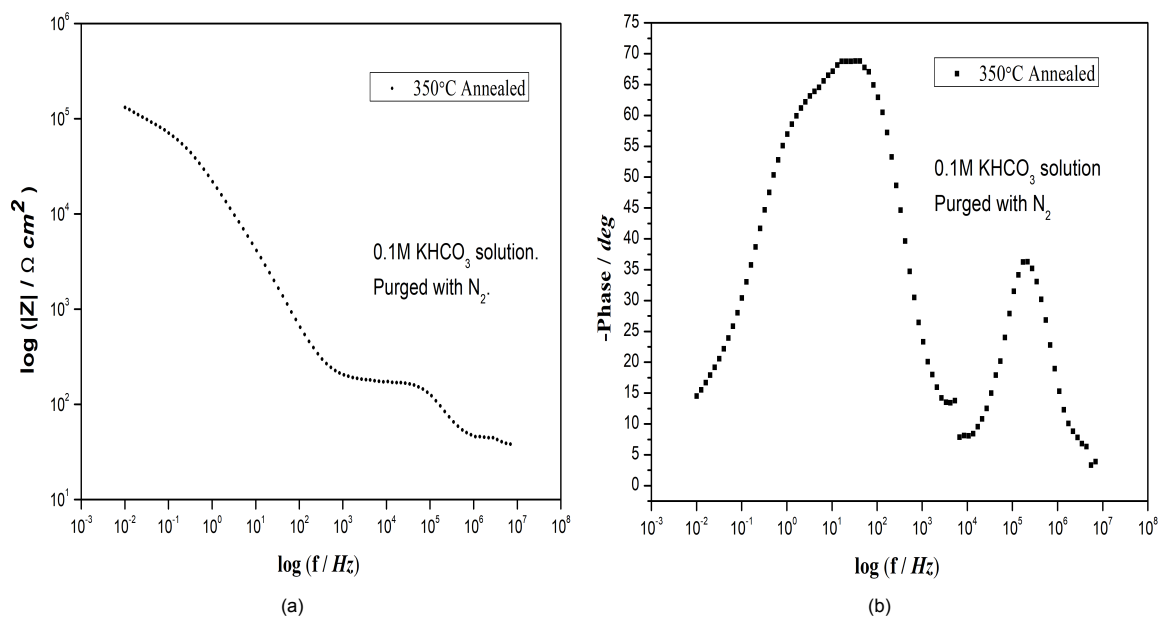(b)

Figure D.1: Bode plots for electropolished sample
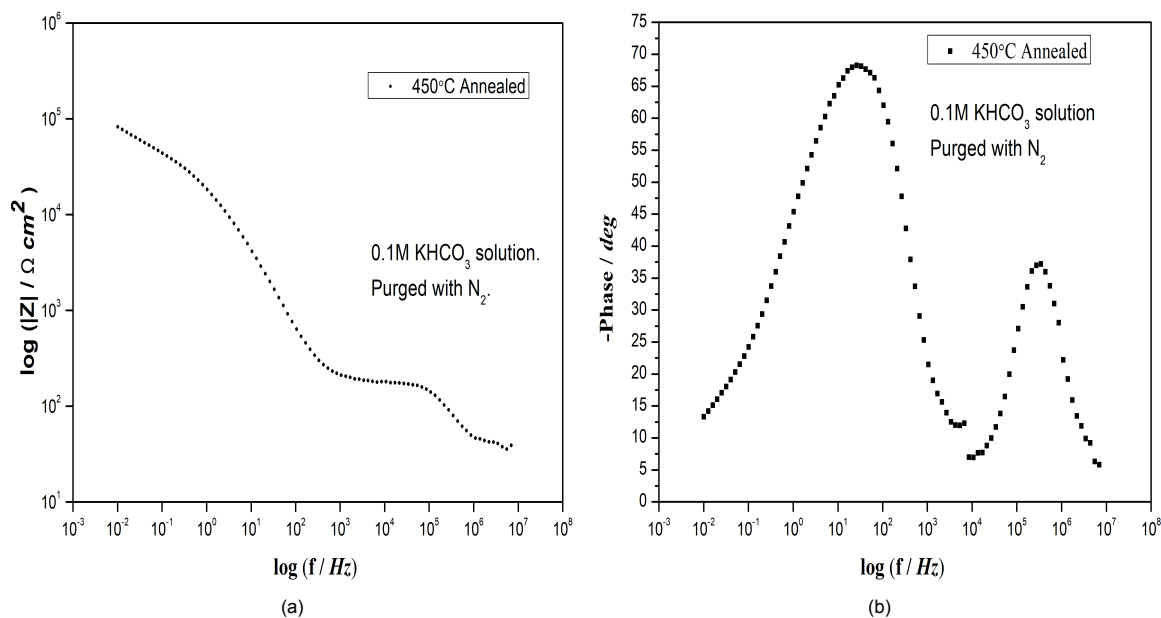
Figure D.2: Bode plots for 350°C annealed sample

Figure D.3: Bode plots for 450°C annealed sample

Bibliography

[1] CAIT , Climate Watch, 2018. URL https://www.climatewatchdata.org/ghg-emissions?end_year=2017&source=CAIT&start_year=1990.

[2] Reza Abbaschian, Lara Abbaschian, and Robert E. Reed-Hill. *Physical metallurgy principles*. Cengage Learning, fourth edi edition, 2009. ISBN 13: 978-0-495-08254-5. URL www.ichapters.com.

[3] Anton Paar. Anton Paar. URL https://wiki.anton-paar.com/hu-hu/roentgendiffrakcio-xrd/.

[4] Allen J. Bard and Larry R. Faulkner. *ELECTROCHEMICAL METHODS Fundamentals and Applications Allen*, volume 2. John Wiley Sons, second edition, 2001. ISBN 0471043729. doi: 10.1038/s41929-019-0277-8.

[5] Federico Calle-Vallejo and Marc T.M. Koper. Theoretical considerations on the electroreduction of CO to C2 Species on Cu(100) electrodes. *Angewandte Chemie - International Edition*, 52(28):7282–7285, 2013. ISSN 14337851. doi: 10.1002/anie.201301470.

[6] David W. DeWulf, Tuo Jin, and Allen J. Bard. Electrochemical and surface studies of carbon dioxide reduction to methane and ethylene at copper electrodes in aqueous solutions. *Journal of The Electrochemical Society*, 136(6):1686–1691, jun 1989. doi: 10.1149/1.2096993. URL https://doi.org/10.1149/1.2096993.

[7] Cao Thang Dinh, Thomas Burdyny, Golam Kibria, Ali Seifitokaldani, Christine M. Gabardo, F. Pelayo García De Arquer, Amirreza Kiani, Jonathan P. Edwards, Phil De Luna, Oleksandr S. Bushuyev, Chengqin Zou, Rafael Quintero-Bermudez, Yuanjie Pang, David Sinton, and Edward H. Sargent. CO2 electroreduction to ethylene via hydroxide-mediated copper catalysis at an abrupt interface. *Science*, 360(6390):783–787, 2018. ISSN 10959203. doi: 10.1126/science.aas9100.

[8] M. Drogowska, L. Brossard, and H. Ménard. Comparative study of copper behaviour in bicarbonate and phosphate aqueous solutions and effect of chloride ions. *Journal of Applied Electrochemistry*, 24(4):344–349, 1994. ISSN 0021891X. doi: 10.1007/BF00242064.

[9] Hamid El Bilali, Imaël Henri Nestor Bassole, Lawali Dambo, and Sinisa Berjan. Climate change and food security. *Agriculture and Forestry*, 66(3):197–210, 2020. ISSN 18009492. doi: 10.17707/AgricultForest.66.3.16.

[10] Sahil Garg, Mengran Li, Adam Z. Weber, Lei Ge, Liye Li, Victor Rudolph, Guoxiong Wang, and Thomas E. Rufford. Advances and challenges in electrochemical CO2 reduction processes: An engineering and design perspective looking beyond new catalyst materials. *Journal of Materials Chemistry A*, 8(4):1511–1544, 2020. ISSN 20507496. doi: 10.1039/c9ta13298h.

[11] M. Gattrell, N. Gupta, and A. Co. A review of the aqueous electrochemical reduction of CO2 to hydrocarbons at copper. *Journal of Electroanalytical Chemistry*, 594(1):1–19, 2006. ISSN 15726657. doi: 10.1016/j.jelechem.2006.05.013.

[12] Y Hori. Electrochemical CO 2 Reduction on Metal Electrodes. (42):89–189.

[13] Y. Hori, H. Konishi, T. Futamura, A. Murata, O. Koga, H. Sakurai, and K. Oguma. "deactivation of copper electrode" in electrochemical reduction of CO2. *Electrochimica Acta*, 50(27):5354–5369, 2005. ISSN 00134686. doi: 10.1016/j.electacta.2005.03.015.

[14] Yoshio Hori, Hidetoshi H I Wakebe, Toshio Tsukamoto, and Osamu Koga. 堀先生：金属電極における二酸化炭素還元 2 . *Electrochimica Acta*, 39(11-12):1833–1839, 1994. ISSN 00134686.

[15] Yoshio Hori, Ichiro Takahashi, Osamu Koga, and Nagahiro Hoshi. + Electrochemical Reduction of CO 2 at a Series of Copper Single Crystal Electrodes. *The Journal of Physical Chemistry B*, 106(1):15–17, 2002. ISSN 1520-6106. URL https://pubs.acs.org/doi/10.1021/jp013478d.

[16] Peng Huang, Jinxi Chen, Peilin Deng, Fan Yang, Jing Pan, Kai Qi, Hongfang Liu, and Bao Yu Xia. Grain refinement of self-supported copper electrode by multiple-redox treatment for enhanced carbon dioxide electroreduction towards carbon monoxide generation. *Journal of Catalysis*, 381:608–614, 2020. ISSN 10902694. doi: 10.1016/j.jcat.2019.12.008. URL https://doi.org/10.1016/j.jcat.2019.12.008.

[17] IPCC. IPCC Special Report on Global Warming of 1.5°C. Technical Report 5813, IPCC, 2018. URL https://www.ipcc.ch/site/assets/uploads/sites/2/2019/06/SR15_Full_Report_High_Res.pdf.

[18] Pigewh Isa, Hitler Louis, Kayode Adesina, and Ededet Akpan. Review article Understanding the Mechanism of Electrochemical Reduction of CO 2 Using Cu / Cu-Based Electrodes. 1(4):183–224, 2018.

[19] S. A. Kaluzhina and I. V. Sieber. Copper passivity and its breakdown in sodium bicarbonate solutions: A scanning electron microscopy and x-ray photoelectron and auger spectroscopy study. *Russian Journal of Electrochemistry*, 42(12):1352–1357, 2006. ISSN 10231935. doi: 10.1134/S1023193506120135.

[20] Recep Kas, Ruud Kortlever, Alexander Milbrat, Marc T.M. Koper, Guido Mul, and Jonas Baltrusaitis. Electrochemical CO2 reduction on Cu2O-derived copper nanoparticles: Controlling the catalytic selectivity of hydrocarbons. *Physical Chemistry Chemical Physics*, 16(24):12194–12201, 2014. ISSN 14639076. doi: 10.1039/c4cp01520g.

[21] Gopalram Keerthiga, Balasubramanian Viswanathan, and Raghuram Chetty. Electrochemical reduction of CO2 on electrodeposited Cu electrodes crystalline phase sensitivity on selectivity. *Catalysis Today*, 245:68–73, 2015. ISSN 09205861. doi: 10.1016/j.cattod.2014.08.008. URL http://dx.doi.org/10.1016/j.cattod.2014.08.008.

[22] Kendra P. Kuhl, Etosha R. Cave, David N. Abram, and Thomas F. Jaramillo. New insights into the electrochemical reduction of carbon dioxide on metallic copper surfaces. *Energy and Environmental Science*, 5(5):7050–7059, 2012. ISSN 17545692. doi: 10.1039/c2ee21234j.

[23] Matt Lacey. The constant phase element. URL http://lacey.se/science/eis/constant-phase-element/.

[24] L. Lapeire, J. Sidor, E. Martinez Lombardia, K. Verbeken, I. De Graeve, H. Terryn, and L. A.I. Kestens. Texture comparison between cold rolled and cryogenically rolled pure copper. *IOP Conference Series: Materials Science and Engineering*, 82 (1), 2015. ISSN 1757899X. doi: 10.1088/1757-899X/82/1/012016.

[25] Jaeyoung Lee and Yongsug Tak. Electrocatalytic activity of Cu electrode in electroreduction of CO2. *Electrochimica Acta*, 46(19):3015–3022, 2001. ISSN 00134686. doi: 10.1016/S0013-4686(01)00527-8.

[26] Christina W Li and Matthew W Kanan. Supporting Information CO 2 Reduction at Low Overpotential on Cu Electrodes Resulting from the Reduction of Thick Cu 2 O Films.

[27] Christina W. Li and Matthew W. Kanan. CO 2 reduction at low overpotential on Cu electrodes resulting from the reduction of thick Cu 2O films. *Journal of the American Chemical Society*, 134(17):7231–7234, 2012. ISSN 00027863. doi: 10.1021/ja3010978.

[28] Peter Lobaccaro, Meenesh R. Singh, Ezra Lee Clark, Youngkook Kwon, Alexis T. Bell, and Joel W. Ager. Effects of temperature and gas-liquid mass transfer on the operation of small electrochemical cells for the quantitative evaluation of CO2 reduction electrocatalysts. *Physical Chemistry Chemical Physics*, 18(38):26777–26785, 2016. ISSN 14639076. doi: 10.1039/c6cp05287h.

[29] Osmando F. Lopes and Hamilton Varela. Effect of Annealing Treatment on Electrocatalytic Properties of Copper Electrodes toward Enhanced CO2 Reduction. *ChemistrySelect*, 3(31):9046–9055, 2018. ISSN 23656549. doi: 10.1002/slct.201802102.

[30] Wenjia Luo, Xiaowa Nie, Michael J. Janik, and Aravind Asthagiri. Facet Dependence of CO2 Reduction Paths on Cu Electrodes. *ACS Catalysis*, 6(1):219–229, 2016. ISSN 21555435. doi: 10.1021/acscatal.5b01967.

[31] E. Martinez-Lombardia, Y. Gonzalez-Garcia, L. Lapeire, I. De Graeve, K. Verbeken, L. Kestens, J. M.C. Mol, and H. Terryn. Scanning electrochemical microscopy to study the effect of crystallographic orientation on the electrochemical activity of pure copper. *Electrochimica Acta*, 116:89–96, 2014. ISSN 00134686. doi: 10.1016/j.electacta.2013.11.048. URL http://dx.doi.org/10.1016/j.electacta.2013.11.048.

[32] Atsushi NISHIKATA, Masayuki ITAGAKI, Tooru TSURU, and Shiro HARUYAMA. Corroswn Science,. *Corrosion Science*, 31:287–292, 1990. doi: https://doi.org/10.1016/0010-938X(90)90121-K. URL https://www.sciencedirect.com/science/article/pii/0010938X9090121K.

[33] Stephanie Nitopi, Erlend Bertheussen, Soren B Scott, Xinyan Liu, Albert K Engstfeld, Sebastian Horch, Brian Seger, Ifan E L Stephens, Karen Chan, Christopher Hahn, Jens K Nørskov, Thomas F Jaramillo, and Ib Chorkendor. Progress and Perspectives of Electrochemical CO 2 Reduction on Copper in Aqueous Electrolyte. 2019. doi: 10.1021/acs.chemrev.8b00705.

[34] Hideshi Ooka, Marta C. Figueiredo, and Marc T.M. Koper. Competition between Hydrogen Evolution and Carbon Dioxide Reduction on Copper Electrodes in Mildly Acidic Media. *Langmuir*, 33(37):9307–9313, 2017. ISSN 15205827. doi: 10.1021/acs.langmuir.7b00696.

[35] V Palmieri. The Electrolytic Polishing of metals . Application to Copper and Niobium. *11th workshop on Superconductivity*, 0:579–587, 2003.

[36] M. Pérez Sánchez, M. Barrera, S. González, R. M. Souto, R. C. Salvarezza, and A. J. Arvia. Electrochemical behaviour of copper in aqueous moderate alkaline media, containing sodium carbonate and bicarbonate, and sodium perchlorate. *Electrochimica Acta*, 35(9):1337–1343, 1990. ISSN 00134686. doi: 10.1016/0013-4686(90)85004-7.

[37] Andrew A. Peterson, Frank Abild-Pedersen, Felix Studt, Jan Rossmeisl, and Jens K. Nørskov. How copper catalyzes the electroreduction of carbon dioxide into hydrocarbon fuels. *Energy and Environmental Science*, 3(9):1311–1315, 2010. ISSN 17545692. doi: 10.1039/c0ee00071j.

[38] Ilia Platzman, Reuven Brener, Hossam Haick, and Rina Tannenbaum. Oxidation of polycrystalline copper thin films at ambient conditions. *Journal of Physical Chemistry C*, 112(4):1101–1108, 2008. ISSN 19327447. doi: 10.1021/jp076981k.

[39] Stefan Popović, Milutin Smiljanić, Primož Jovanovič, Jan Vavra, Raffaella Buonsanti, and Nejc Hodnik. Stability and Degradation Mechanisms of Copper-Based Catalysts for Electrochemical CO2 Reduction. *Angewandte Chemie - International Edition*, 59(35):14736–14746, 2020. ISSN 15213773. doi: 10.1002/anie.202000617.

[40] Anže Prašnikar, Andraž Pavlišič, Francisco Ruiz-Zepeda, Janez Kovač, and Blaž Likozar. Mechanisms of Copper-Based Catalyst Deactivation during CO2 Reduction to Methanol. *Industrial and Engineering Chemistry Research*, 58(29):13021–13029, 2019. ISSN 15205045. doi: 10.1021/acs.iecr.9b01898.

[41] Tien Quang, Cornelia Breitkopf, and J Electrochem Soc. Determination of Diffusion Coefficients Using Impedance Spectroscopy Data. *Journal of The Electrochemical Society*, 165(14):826–831, 2018. doi: 10.1149/2.1151814jes. URL https://iopscience.iop.org/article/10.1149/2.1151814jes/pdf.

[42] Sh Ranjbar Bahadori, K. Dehghani, and F. Bakhshandeh. Microstructure, texture and mechanical properties of pure copper processed by ECAP and subsequent cold rolling. *Materials Science and Engineering A*, 583:36–42, 2013. ISSN 09215093. doi: 10.1016/j.msea.2013.06.061.

[43] M Perez Sanchez, M Barrera, S Gonzalez, and R M Soutot. ELECTROCHEMICAL BEHAVIOUR OF COPPER IN AQUEOUS MODERATE ALKALINE MEDIA , CONTAINING SODIUM CARBONATE AND BICARBONATE , AND SODIUM PERCHLORATE. *Electrochimica Acta*, 35(9):1337–1343, 1990. URL https://core.ac.uk/download/pdf/301094738.pdf.

[44] K. J.P. Schouten, Y. Kwon, C. J.M. Van Der Ham, Z. Qin, and M. T.M. Koper. A new mechanism for the selectivity to C1 and C2 species in the electrochemical reduction of carbon dioxide on copper electrodes. *Chemical Science*, 2(10):1902–1909, 2011. ISSN 20416520. doi: 10.1039/c1sc00277e.

[45] Hirokazu Shibata. *Electrocatalytic CO 2 Reduction*. Doctoral thesis, Delft University of Technology, 2009. URL http://resolver.tudelft.nl/uuid:6bfda384-d6b4-4641-9ad6-318e2c4fdeb2.

[46] Ke Bin Sun, Yan Feng Li, Ye Xin Jiang, Guo Jie Huang, Xue Shuai Li, Qing An Sun, and Xiang Qian Yin. Effect of annealing treatment on the properties of cold rolled copper foil. *Materials Science Forum*, 921 MSF:231–235, 2018. ISSN 16629752. doi: 10.4028/www.scientific.net/MSF.921.231.

[47] Wei Tang, Andrew A. Peterson, Ana Sofia Varela, Zarko P. Jovanov, Lone Bech, William J. Durand, Søren Dahl, Jens K. Nørskov, and Ib Chorkendorff. The importance of surface morphology in controlling the selectivity of polycrystalline copper for CO2 electroreduction. *Physical Chemistry Chemical Physics*, 14(1):76–81, 2012. ISSN 14639076. doi: 10.1039/c1cp22700a.

[48] Pragya Tiwari, Himanshu Srivastava, Sanjay Rai, and S. K. Deb. Recrystallization, grain growth in copper foil at high temperature studied by electron back scatter diffraction. *AIP Conference Proceedings*, 1349(PART A):705–706, 2011. ISSN 0094243X. doi: 10.1063/1.3606053.

[49] Karin Beaussant Törne. EIS for determination of corrosion mechanisms. URL https://www.ri.se/en/what-we-do/services/eis-for-determination-of-corrosion-mechanisms.

[50] Ana Sofia Varela, Matthias Kroschel, Tobias Reier, and Peter Strasser. Controlling the selectivity of CO2 electroreduction on copper: The effect of the electrolyte concentration and the importance of the local pH. *Catalysis Today*, 260:8–13, 2016. ISSN 09205861. doi: 10.1016/j.cattod.2015.06.009. URL http://dx.doi.org/10.1016/j.cattod.2015.06.009.

[51] Arnau Verdaguer-Casadevall, Christina W. Li, Tobias P. Johansson, Soren B. Scott, Joseph T. McKeown, Mukul Kumar, Ifan E.L. Stephens, Matthew W. Kanan, and Ib Chorkendorff. Probing the Active Surface Sites for CO Reduction on Oxide-Derived Copper Electrocatalysts. *Journal of the American Chemical Society*, 137(31):9808–9811, 2015. ISSN 15205126. doi: 10.1021/jacs.5b06227.

[52] Yu Wang, Dengyao Yang, Shaozhong Li, Lingxia Zhang, Guanyu Zheng, and Limin Guo. Layered copper manganese oxide for the efficient catalytic CO and VOCs oxidation. *Chemical Engineering Journal*, 357:258–268, 2019. ISSN 13858947. doi: 10.1016/j.cej.2018.09.156.

[53] Ming xing GUO, Ming pu WANG, Kun SHEN, Ling fei CAO, Ruo shan LEI, and Shu mei LI. Effect of cold rolling on properties and microstructures of dispersion strengthened copper alloys. *Transactions of Nonferrous Metals Society of China (English Edition)*, 18(2):333–339, 2008. ISSN 10036326. doi: 10.1016/S1003-6326(08)60058-8.

[54] Xiao yan Zhang, Ming hua Wang, Zhong yi Chen, P. Xiao, P. Webley, and Yu chun Zhai. Preparation, characterization and catalytic performance of Cu nanowire catalyst for CO2 hydrogenation. *Journal of Central South University*, 25(4):691–700, 2018. ISSN 22275223. doi: 10.1007/s11771-018-3773-0.

[55] Chao Yang, Hanchen Shen, Anxiang Guan, Junlang Liu, Tengfei Li, Yali Ji, Abdullah M. Al-Enizi, Lijuan Zhang, Linping Qian, and Gengfeng Zheng. Fast cooling induced grain-boundary-rich copper oxide for electrocatalytic carbon dioxide reduction to ethanol. *Journal of Colloid and Interface Science*, 570:375–381, 2020. ISSN 10957103. doi: 10.1016/j.jcis.2020.03.017. URL https://doi.org/10.1016/j.jcis.2020.03.017.

[56] Heng Zhong, Katsushi Fujii, and Yoshiaki Nakano. Effect of KHCO 3 Concentration on Electrochemical Reduction of CO 2 on Copper Electrode . *Journal of The Electrochemical Society*, 164(9):F923–F927, 2017. ISSN 0013-4651. doi: 10.1149/2.0601709jes.